An Investigation of the Concentration Dependence of the Interdiffusion Coefficient in the Binary Liquid Aluminum-Copper System

by

By C. Brock Porth

A Thesis submitted to the Faculty of Graduate Studies of

The University of Manitoba

in partial fulfillment of the requirements of the degree of

DOCTOR OF PHILOSOPHY

Department of Mechanical Engineering

University of Manitoba

Winnipeg, Manitoba, Canada

ABSTRACT

Challenges continue to exist in developing a comprehensive theory of diffusion in liquid metals, despite the advancement of several semi-empirical and theoretical models. One major difficulty in developing a theory is that experimental data are not available for many pure metals and binary metal systems, and when they do exist, data are often inaccurate. In addition to challenges with data quality, where deemed reliable, existing data are typically reported over limited temperature and concentration intervals. In this thesis research, interdiffusion data was obtained for the binary Al-Cu system using the solid wire long capillary technique (SWLC), and molecular dynamics (MD) simulation with a concentration-dependent embedded atom method (CD-EAM) interatomic potential.

In the SWLC experiments the interdiffusion coefficient was determined at temperatures of 993 K, 1023 K, 1073 K, 1123 K, and 1193 K, over an Al-rich concentration range limited by the liquidus of the binary phase diagram at the given temperature. For liquid $Al_{\sim 100}Cu_{\sim 0}$ (tracer), $Al_{80}Cu_{20}$, and $Al_{60}Cu_{40}$, the interdiffusion coefficient is well described by the Arrhenius relationship $D_{AlCu} = D_0 \exp(-Q_0/RT)$ over the temperature range, with best fit parameter values of

Q_0 = 20.85 $\pm$ 4.49 kJ/mol, D_0 = 8.21 (+5.4, -3.26) x 10^{-8} m^2/s,
Q_0 = 34.41 $\pm$ 3.71 kJ/mol, D_0 = 2.84 (+1.47, -0.97) x 10^{-7} m^2/s,
Q_0 = 38.74 $\pm$ 8.01 kJ/mol, D_0 = 4.03 (+5.89, -2.39) x 10^{-7} m^2/s,

respectively. For the MD simulations, a new Al-Cu CD-EAM interatomic potential was developed that is suitable for the study of diffusion phenomena in the liquid state. Self- and interdiffusion coefficients were determined over a temperature interval of 993-1493 K. Simulations are performed for liquid $Al_{99.999}Cu_{0.001}$ (tracer), $Al_{80}Cu_{20}$, and $Al_{60}Cu_{40}$, and interdiffusion is described by

Q_0 = 22.81 $\pm$ 0.27 kJ/mol, D_0 = 1.04 (+0.03, -0.03) x 10^{-7} m^2/s
Q_0 = 30.15 $\pm$ 0.49 kJ/mol, D_0 = 1.78 (+0.08, -0.08) x 10^{-7} m^2/s,
Q_0 = 37.01 $\pm$ 1.48 kJ/mol, D_0 = 3.29 (+0.52, -0.45) x 10^{-7} m^2/s,

respectively. The calculated values of the interdiffusion coefficients from the MD simulation are in good agreement with those obtained using the SWLC technique, supporting the accuracy of these new experimental findings.

Keywords: Al-Cu; liquid metal; self-diffusion; interdiffusion; long capillary method; reactive diffusion; molecular dynamics simulation; concentration-dependent EAM.

ACKNOWLEDGEMENTS

I would like to thank my advisor Dr. Cahoon. Your expertise, understanding, and teaching added considerably to my graduate experience. I appreciate your vast knowledge, guidance, and mentorship, and you have provided me with an invaluable learning opportunity. As well, I would like to extend my appreciation to the other members of my committee, Dr. Richards and Dr. Polyzois. Your valuable comments have greatly contributed to the quality of this thesis. I would also like to extend my gratitude to Mike Boskwick, Don Mardis, and Irwin Penner for technical assistance and guidance in the laboratory.

I am grateful for the encouragement and support of my family.

TABLE OF CONTENTS

LIST OF FIGURES

LIST OF TABLES

1. INTRODUCTION

The study of diffusion in liquid metals is of scientific interest and technological significance, offering insight into a fundamental physical phenomenon that is critical in materials science. Knowledge of diffusion coefficients is a key factor in the design of materials [1] and is required for quantitative modelling of microstructure evolution [2, 3] in processes that involve solidification such as casting, and semiconductor manufacturing [4, 5]. However, challenges continue to exist in developing a comprehensive theory of diffusion in liquid metals, despite the advancement of several semi-empirical and theoretical models for self- [6, 7] and solute diffusion [8, 7, 9, 10]. Without adequate theory, the relationships that describe the temperature and/or concentration dependence of diffusion must be determined empirically through experimentation, a practice that is time consuming and requires specialized equipment.

One major difficulty in developing a theory is that experimental data are not available for many pure metals and binary metal systems, and when they do exist, data are often inaccurate [11, 12, 13, 14, 3, 2]. The long capillary method and its variations are commonly used to measure self- and interdiffusion coefficients in liquid metals. However, this technique has noted limitations that can lead to considerable systematic error in the measured value of the diffusion coefficient [11, 3, 14, 12, 15]. Primarily, this is due to the presence of buoyancy driven convective flow within the capillary [16, 17, 18], and the axial translation of the concentration profile upon solidification from the liquid state due to changes in volume [12, 3]. For example, Meyer and Kargl [3] report that the value of the diffusion coefficient is overstated by 10 – 100% in terrestrial-based long capillary experiments, as compared to results obtained in microgravity where buoyancy driven convection is suppressed. Similarly, Geng et al. [12] estimate diffusion coefficient errors of approximately 50 – 100 %, in part due to a failure to account for the effect of solidification. Additionally, Klassen

and Cahoon [11] discuss problems with data obtained using the capillary reservoir technique, where lid-driven flow inflates diffusion coefficient measurements.

In addition to challenges with data quality, where deemed reliable, existing data are typically reported over limited temperature intervals. Further, diffusion is not well studied beyond low solute concentrations in most liquid metal systems. Of current interest in diffusion literature [1, 19, 20, 21, 22, 23] is the relationship between concentration X (mol fraction units), temperature T, and the self- $D_{A\ or\ B}$ and interdiffusion D_{AB} coefficients in binary A-B type liquid metal mixtures. As no definitive theoretical model for liquid metal diffusion exists, Darken's phenomenological equation is used [19] to describe diffusion phenomena at solute levels beyond low (tracer) concentrations. The Darken equation describes interdiffusion such that $D_{AB}(X,T) = D_{AB}^{0}(X,T) \cdot \Phi(X,T)$, where $D_{AB}^{0}(X,T)$ is the purely kinetic Maxwell-Stefan (MS) diffusivity coefficient that is taken as a linear combination of the self-diffusion coefficients $D_{AB}^{0}(X,T) = (1-X) \cdot D_{A}(X,T) + X \cdot D_{B}(X,T)$, and $\Phi(X,T)$ is a thermodynamic enhancement factor that is proportional to the second derivative of Gibbs free energy [19]. The thermodynamic enhancement factor is related to the structure of the liquid, and quantitatively reflects the degree of ordering or dissociation between atoms in the mixture. For an ideal A-B type mixture the thermodynamic enhancement factor does not affect the value of the interdiffusion coefficient ($\Phi(X,T) = 1$), and only assumes a scalar value different than unity for non-ideal mixtures. More recently attempts have been made to explore this relationship in the binary metallic Al-Ni [20, 19], Zr-Ni [1], Ni-Cu [23], and Al-Cu systems [21, 22, 23] using a variety of approaches including molecular dynamics simulation, quasi-elastic neutron scattering, and long capillary methods. However, further study is required over wider temperature and concentration intervals to validate existing data, and

explore the Darken equation with the intent of providing additional data and insight for the development of theory in future.

In this thesis research, diffusion in the binary liquid Al-Cu system is chosen for investigation. There are several reasons for this choice of system, and they are briefly outlined below. This system exemplifies the problem of data accuracy, and while the system has been the focus of past investigations [15, 24, 25, 26], there is a considerable disagreement between the published values of the interdiffusion coefficient. For example, within the concentration range of 0 to 40 at% Cu, Tanaka et al. [24, 25] calculate a constant (non-concentration dependent) interdiffusion coefficient of 1.24×10^{-9} m^2/s at T = 973 K. However, in Lee and Cahoon [15] although the interdiffusion coefficient is again assumed to be constant, the reported value is considerably higher at 8.11×10^{-9} m^2/s at the same temperature. It is also interesting to note that both experiments use variations of a similar method, the solid wire long capillary technique. In contrast to these findings, Cheng et al. [23] find the interdiffusion coefficient is concentration-dependent within this concentration range. Using molecular dynamics simulation with an embedded atom method (EAM) interatomic potential, they determine a value of the interdiffusion coefficient of 1.12×10^{-8} m^2/s at T = 973 K at a concentration of 40 at% Cu. This is an order of magnitude higher than Tanaka et al. [24, 25]. A possible problem in the work of Cheng et al. [23] though is they use an EAM interatomic potential that was developed by Cai and Ye [27] for the binary Al-Cu system in the solid state. Becker et al. [28] have recently commented on the necessity of using interatomic potentials that are optimized for the conditions of the system under investigation. In this case, using an EAM interatomic potential developed for the solid versus a potential optimized for the liquid may result in a failure to correctly model the energetics of the interacting atoms, and by virtue, the associated properties such as transport phenomena. Further

to specific data accuracy concerns, self- and interdiffusion experimental results for this system are primarily only available for limited temperature and concentration intervals.

Beyond questions of data accuracy and data shortage, further motivation for study the liquid Al-Cu binary system is to explore the concentration dependence of the interdiffusion coefficient, if it exists. The Al-Cu binary system is characterized by several intermetallic phases in the Cu rich portion of the phase diagram that persist to high temperature, and their presence suggests that energetically favorable configurations of atoms may exist within the liquid state [29]. Thermodynamic data also supports the possibility of an associative (non-ideal) structured liquid, where the excess Gibbs free energy of solution is reported to be negative and concentration-dependent [30, 31, 32]. The negative value of the excess Gibbs free energy results in positive scalar value of the thermodynamic enhancement factor $\Phi(X,T)$. The effect of the liquid structure, through $\Phi(X,T)$, can be further explored in the context of Darken's equation.

Therefore, the objective of this thesis research is: 1. To obtain accurate interdiffusion coefficients for the binary liquid Al-Cu system over a range of temperature and concentrations, and 2. To investigate the concentration dependence of the interdiffusion coefficient in the binary liquid Al-Cu system and the effect of liquid structure on the interdiffusion coefficient. In determining these objectives, the outline of this thesis is as follows. Chapter 2 provides the theoretical and experimental background necessary to support the work presented in Chapters 3 and 4. This chapter also includes a review of the pertinent thermodynamics and diffusion theory for binary liquid mixtures, followed by a literature review specific to the Al-Cu system. In Chapter 3, reactive diffusion is used to obtain interdiffusion coefficients in the liquid Al-Cu melt, utilizing the solid wire long capillary (SWLC) technique. In the experiments, a reduced long capillary diameter of 1 mm is used to suppress convective flow within the capillary as discussed in Lee et

al. [18] and Porth and Cahoon [17]. The existing mathematical framework of the variable space network method [33, 34, 35] is extended to model a concentration-dependent interdiffusion coefficient, and concentration profiles are corrected for the volume change accompanying solidification. Interdiffusion coefficients are reported over a temperature range of 993 K to 1193 K in 50 K increments, for concentrations of $Al_{\sim 100}Cu_{\sim 0}$ (tracer), $Al_{80}Cu_{20,}$ and $Al_{60}Cu_{40}$. The concentration dependence of the interdiffusion coefficient is determined, and the experimental results are compared to the data presented in Chapter 2. In Chapter 4, interdiffusion is further investigated using molecular dynamic (MD) computer simulation. A new concentration-dependent embedded atom method (CD-EAM) interatomic potential [36] is developed in this thesis that is optimized for the liquid Al-Cu system. Using the CD-EAM interatomic potential, MD simulation is performed using the LAMMPS (Large-scale Atomic/Molecular Massively Parallel Simulator) supercomputing code [37], and self-diffusion coefficients are determined from the statistical averages of the ensemble fluctuations. The interdiffusion coefficients are calculated using Darken's equation, and are reported over a temperature range of 993 K to 1493 K in 100 K increments for liquid $Al_{99.999}Cu_{0.001}$ (tracer), $Al_{80}Cu_{20,}$ and $Al_{60}Cu_{40}$. Further, the liquid structure is examined in terms of coordination number and nearest neighbor distance, and the effect of the liquid structure on the interdiffusion coefficient is discussed. The results from the simulation are then compared to those experimentally obtained in Chapter 4 and the benchmark data from Chapter 2. Chapter 5 provides a summary of the research, and discusses limitations of the current work and recommendations for future research.

2. THEORY OF DIFFUSION IN LIQUID METALS AND A REVIEW OF THE AL-CU SYSTEM

2.1. THE DIFFUSION EQUATION

The mathematical theory of diffusion [38] was formulated by Adolf Fick in 1855, by direct analogy with the equations of heat conduction first derived by Joseph Fourier in 1822. In an isotropic medium, Fick's first law states that the flux **j** is proportional to the concentration gradient such that

$$\mathbf{j}(\boldsymbol{r}, t) = -D \cdot \nabla \cdot C(\boldsymbol{r}, t) \tag{1}$$

where D is the diffusion coefficient, ∇ is the gradient operator with respect to position $\boldsymbol{r}$, and C is defined as the mass density concentration field. The mass continuity equation relates the change in C with respect to time t to the gradient of the flux field

$$\frac{\partial C(\boldsymbol{r}, t)}{\partial t} + \nabla \cdot \mathbf{j}(\boldsymbol{r}, t) = 0, \tag{2}$$

and combining Equations (1) and (2) yields the diffusion equation

$$\frac{\partial C(\boldsymbol{r}, t)}{\partial t} = \nabla \cdot \big(D \cdot \nabla C(\boldsymbol{r}, t)\big). \tag{3}$$

If the diffusion coefficient is constant Equation (3) is simplified and written

$$\frac{\partial C(\boldsymbol{r}, t)}{\partial t} = D \cdot \nabla^2 C(\boldsymbol{r}, t) \tag{4}$$

where ∇^2 is the Laplace operator. If the diffusion coefficient is not constant and varies as a function of concentration such that $D = f\big(C(\boldsymbol{r}, t)\big)$, Equation (3) is expanded and becomes

$$\frac{\partial C(\boldsymbol{r}, t)}{\partial t} = \nabla D\big(C(\boldsymbol{r}, t)\big) \cdot \nabla C(\boldsymbol{r}, t) + D\big(C(\boldsymbol{r}, t)\big) \cdot \nabla^2 C(\boldsymbol{r}, t). \tag{5}$$

2.2. THERMODYNAMICS OF BINARY MIXTURES

2.2.1. THE RANDOM SOLUTION MODEL

For a binary alloy with A- and B-type atoms the Gibbs free energy of the solution G_{AB}^{rs} in the liquid state is commonly described using the random solution model with [30]

$$G_{AB}^{rs}(T,X) = X_A G_A^0(T) + X_B G_B^0(T) + RT(X_A lnX_A + X_B lnX_B) + G_{AB}^{ex}(T,X) \quad (6)$$

where G_A^0 and G_B^0 are the reference Gibbs free energies of the pure metals, $RT(X_A lnX_A + X_B lnX_B)$ is the contribution to the solution stemming from the change in entropy due to ideal mixing where R is the universal gas constant, and G_{AB}^{ex} is the excess Gibbs free energy. The excess Gibbs free energy describes the deviation of the system from the ideal liquid, quantifying the thermodynamic propensity of atoms to order or disorder in solution. G_{AB}^{ex} is usually fit to experimental data using a Redlich-Kister polynomial

$$G_{AB}^{ex}(T,X) = X_A X_B \left(\sum_v L_G^v(T) \, (X_A - X_B)^v \right), \qquad v = 0, 1, 2, \dots, N_v \quad (7)$$

where L_G^v is defined as the binary interaction energy parameter

$$L_G^v(T) = a_0^v + a_1^v T + a_2^v T ln(a_2^v) \quad (8)$$

that is a temperature dependent function that is fit to experimental data by optimizing the parameters a_0^v, a_1^v, and a_2^v for N_v sets of L_G^v.

The excess enthalpy of mixing H_{AB}^{ex} can also be expressed in terms of Redlich-Kister polynomial function of similar form such that

$$H_{AB}^{ex}(T,X) = X_A X_B \left(\sum_v L_H^v(T) \, (X_A - X_B)^v \right), \qquad v = 0, 1, 2, \dots, N_v \quad (9)$$

where L_H^v is defined as the binary interaction energy parameter for the excess enthalpy of mixing. The Gibbs-Helmholtz equation can be used to relate the excess Gibbs free energy to the excess

enthalpy of mixing, where the binary interaction parameter L_H^v can be expressed in terms of the constants defined in Equation (8) from the L_G^v [31] such that

$$L_H^v(T) = a_0^v - a_2^v T. \tag{10}$$

It should be noted that for $a_2^v = 0$, the value of L_H^v is constant, and the excess enthalpy is independent of temperature $H_{AB}^{ex}(X)$.

2.3. PARTICLE DISTRIBUTION FUNCTIONS

The structure of liquids is characterized by the absence of long-range order, which defines crystalline materials. However, liquids do possess a rich and varied array of short to medium range order, which originates from chemical bonding and related interactions. The relative arrangement of molecules in space is referred to as the liquid structure, where statistical distribution functions give the time-averaged spatial configuration of the molecules in the liquid.

The underlying structural relationships in the liquid are often described in terms of the radial distribution function (or pair correlation function) $\mathrm{g}(r)$, which is a measure of the probability of finding two particles a distance r apart averaged over all particles within the system. The definition of the radial distribution function is derived by considering the n-particle correlation function that describes the deviation from a random distribution. In a material that is homogeneous and isotropic on a macroscopic scale, the radial distribution function can be defined as [39]

$$\mathrm{g}(r) = \frac{1}{\rho_0} \sum_{\alpha \neq 0} \langle \delta(\boldsymbol{r} - \boldsymbol{r_\alpha}) \rangle, \tag{11}$$

where $\boldsymbol{r_\alpha}$ is a vector from the particle 0 at the origin to another particle with label α, and ρ_0 is the homogenous density. Further, the probability for a particle being present in a spherical shell of width dr around a central particle at the origin with distance r is given by $\rho_0 4\pi r^2 \mathrm{g}(r) dr$. The

mean number of particles around the central particle within a sphere of radius R is defined as the coordination number

$$Z(R) = \rho_0 4\pi \int_0^R r^2 \mathrm{g}(r)\, dr, \tag{12}$$

where the first, second, and third, etc. coordination numbers are taken at the value of R corresponding to the minimum values of $\mathrm{g}(r)$ after the first, second, third, etc. peaks.

The radial pair correlation function $\mathrm{g}(r)$ can be determined experimentally from the scattering of X-rays or neutrons from a liquid sample via the structure factor

$$S(q) = 1 + \frac{4\pi\rho_0}{q} \int_0^\infty \mathbf{r} \sin(q\mathbf{r})\, [\mathrm{g}(r) - 1]\, dr, \tag{13}$$

where q is the modulus of the exchanged momentum. In the low q limit ($q \to 0$), Equation (13) reduces to

$$S(q = 0) = 1 + 4\pi\rho_0 \int_0^\infty \boldsymbol{r}^2 [\mathrm{g}(r) - 1]\, dr. \tag{14}$$

Alternatively, analytical solutions that approximate $\mathrm{g}(r)$ can be obtained by solving the Ornstein-Zernike equation, such as the Percus-Yevick approximation for hard spheres [9].

2.3.1. PARTIAL PAIR CORRELATION FUNCTIONS

Additional structural insight is provided by the partial pair correlation functions (PPCFs), which express the spatial correlations among different types of atoms. It is difficult to obtain PPCFs from experiment, however, they can be readily calculated via molecular dynamics or Monte Carlo simulations. For a mixture of A- or B-type atoms three unique the partial structure factors, i.e. S_{AA}, S_{BB}, and $S_{AB} = S_{BA}$, are defined [39]

$$S_{\alpha\beta}(q) = 1 + \frac{\rho_0 V}{N_\alpha N_\beta} \underbrace{\sum_{j=1}^{N_\alpha} \sum_{k=1}^{N_\beta}}_{j \neq k} e^{i\mathbf{q}\cdot[\mathbf{r}_j - \mathbf{r}_k]}, \qquad \alpha, \beta = A \; or \; B \tag{15}$$

where i denotes the imaginary unit. Taking the Fourier transform of $S_{\alpha\beta}(q)$ then gives the partial radial distribution function $g_{\alpha\beta}(r)$ as defined by

$$g_{\alpha\beta}(r) = 1 + \frac{1}{2\pi^2 r} \int_0^\infty q \, \sin(q) \, h(q) \, \mathrm{d}q \tag{16}$$

where $h(q) = (1/\rho_0)(S(q) - 1)$ is the distinct correlation function, and $\rho_0 4\pi r^2 g_{\alpha\beta}(r)\mathrm{d}r$ gives the probability for the presence a particle species β inside a spherical shell of thickness dr given a central particle of species α at the origin. The mean number of β particles around a given central particle α within a sphere of radius R is defined as the partial coordination number

$$Z_{\alpha\beta}(R) = \rho_0 4\pi \int_0^R r^2 \, g_{\alpha\beta}(r) \, dr. \tag{17}$$

2.4. MOLECULAR DYNAMICS AND THE CLASSICAL DESCRIPTION OF THE LIQUID STATE

The classical hypothesis is used to describe the properties of metals in the liquid state, where quantum effects are assumed negligible. This assumption leads to an important simplification where the contributions to thermodynamic properties can be separated into those due to thermal motion and those resulting from the force interactions between particles. For an isolated, macroscopic system of N spherical particles, of mass m, within in a closed volume V, the dynamical state of the system at each instant in time t is defined in Cartesian coordinates by the $3N$ positions $\boldsymbol{r}_i = (x_1, y_1, z_1, x_2, \dots, y_N, z_N)$ and the $3N$ momenta $\boldsymbol{p}_i = \left(p_{x,1}, p_{y,1}, p_{z,1}, p_{x,2}, \dots, p_{y,N}, p_{z,N}\right)$ of the particles. Combined, this defines a $6N$ dimensional

phase space, with an axis for the position and conjugate momentum of each particle, and where every point on the multidimensional manifold corresponds to a single microstate of the system. A microstate is simply one possible configuration of the system, and for any microstate the total energy of the system is calculated using the classical Hamiltonian function

$$H(\boldsymbol{p}^N, \boldsymbol{r}^N) = K(\boldsymbol{p}^N) + U(\boldsymbol{r}^N), \tag{18}$$

where the potential energy U is a function of all particle positions $\boldsymbol{r}^N$ only, and the kinetic energy K is a function of the the particle momenta $\boldsymbol{p}^N$ only with

$$K(\boldsymbol{p}^N) = \sum_{i=1}^{N} \frac{|\boldsymbol{p}_i|^2}{2m_i}. \tag{19}$$

In the classical description, the time evolution of the system of particles follows the Newtonian equations of motion

$$\frac{d\boldsymbol{p}_i}{dt} = -\frac{dU(\boldsymbol{r}^N)}{d\boldsymbol{r}_i}, \qquad i = 1, 2, 3 \ldots N \tag{20}$$

where the time derivative of each particle's momenta is equal to the negative spatial derivative of potential energy function. Equivalently, Newton's second law can be formulated as

$$m_i \frac{d^2\boldsymbol{r}_i}{dt^2} = -\frac{dU(\boldsymbol{r}^N)}{d\boldsymbol{r}_i}, \qquad i = 1, 2, 3 \ldots N \tag{21}$$

where m_i is the mass of particle i, forming a set of $3N$, nonlinear, coupled differential equations that must be solved for all atomic coordinates in the system. It can be shown by taking time derivative of the Hamiltonian that Newton's equations of motion conserve total energy, net linear momentum, net angular momentum, and are time reversible.

The time evolution of a classical system of particles in equilibrium obeys the ergodic hypothesis, visiting all points in phase space (microstates) with equal probability that exist on the constant energy hypersurface for a specified total energy E. With the condition of equilibrium and

constant total energy E, the isolated macroscopic system of N particles at constant volume V defines the microcanonical ensemble of statistical mechanics [40]. The function $\Omega(E,V,N)$ is termed the density of states or the microcanonical partition function, and effectively counts the number of microstates accessible to the system by integrating the Hamiltonian

$$\begin{aligned}\Omega(E,V,N) &= \frac{1}{h^{3N}N!}\iint \dots \int \delta\left[H(\boldsymbol{p}^N,\boldsymbol{r}^N)-E\right]d\boldsymbol{p_1}d\boldsymbol{p_1}\dots d\boldsymbol{p_N}d\boldsymbol{r_1}d\boldsymbol{r_2}\dots d\boldsymbol{r_N} \\ &= \frac{1}{h^{3N}N!}\int \delta\left[H(\boldsymbol{p}^N,\boldsymbol{r}^N)-E\right]\, d\boldsymbol{p}^N d\boldsymbol{r}^N\end{aligned} \tag{22}$$

where the total number of integrals is $6N$. In the equation, the δ denotes the Dirac delta function and it "filters" those configurations in phase space that are of the specified constant total energy.

The macroscopic thermodynamic properties of the system can be calculated using the relationship between the microcanonical partition function and entropy

$$S = k_B ln\Omega(E,V,N), \tag{23}$$

via the energy version of the fundamental equation

$$dE = TdS - PdV + \mu dN \tag{24}$$

where T, P, and μ are the temperature, pressure, and chemical potential of the system, respectively. The fluctuating macroscopic properties (T,P,μ) of the system appear constant as the system size $N \to \infty$.

The most important aspect of simulation of systems is the forces interacting between atoms, which are usually derived from interatomic potentials. The interatomic potential takes in a set of positions of all atoms and returns an energy due to the interatomic interactions. This energy approximates what would be obtained by solving the many-body Schrödinger equation for all electrons in the multi-atom system, for given fixed positions of the nuclei. The simplest model of the interatomic potential is the hard-sphere (HS) potential, which assumes the potential is zero

except when the two molecules collide. It has been widely used as a first approximation in theoretical investigations where some form of interatomic potential is necessary and where quantitative accuracy is of secondary importance to a conceptual view of the phenomenon under study.

2.5. LIQUID METAL DIFFUSION THEORY

2.5.1. INTERDIFFUSION IN DILUTE SOLUTIONS

Several theories of solvent self-diffusion have been developed for liquid metals, some of which have been extended to consider solute diffusion. In this section the "modified" hole theory of Cahoon [7], the fluctuation theory of Swalin [8, 6], the Stokes-Einstein and Sutherland viscosity based theories [10, 41], and Enskog's theory of hard spheres [42, 43] are discussed. Each theory proposes a unique description of the liquid state, and approaches the problem of solute diffusion in the liquid metal from a different theoretical perspective. However, the application of theory is typically limited to specific binary systems, while no theory broadly predicts the interdiffusion phenomena [16].

2.5.1.1. MODIFIED "HOLE" THEORY

The "Hole" Theory for liquid metals is analogous to the Lazarus-LeClaire hole or vacancy theory of impurity diffusion solids [44, 45], where atoms are in constant motion (oscillating about their equilibrium positions) and migrate in a stepwise manner through vacant sites within the lattice. In the theory, diffusion is controlled by a thermally activated process following the Arrhenius relationship,

$$D = D_0 \exp(-Q_0/RT) \tag{25}$$

where Q_0 is the activation energy, D_0 the frequency factor, and R is the the universal gas constant.

In Cahoon's [7] Modified "Hole" Theory, it is postulated that impurity diffusion D_2 is described by

$$D_2 = D_0 \exp(-(\Delta Q^L + Q_0^L)/RT), \tag{26}$$

where D_0 and Q_0^L are the frequency factor and activation energy for solvent self-diffusion, R the universal gas constant, T is the temperature, and ΔQ^L is the difference in the activation energies between solute impurity diffusion and solvent self-diffusion.

Expanding Equation 26, the value of D_0 is taken as a unique value from independent studies specific to each liquid metal, as no underlying relationship for this parameter is apparent. However, the value of Q_0^L can be determined from the phenomenological relationship between the experimental solvent self-diffusion activation energy and melting temperature, $Q_{0\,experimental}^L \; vs \; RT_m$, which is a good approximation for several liquid metals. This linear equation is given as

$$Q_0^L = 0.17RT_m(16 + V_0) \tag{27}$$

where V_0 is the Engel-Brewer valence of the solvent taken as integer values: 1 for body-centered cubic (bcc), 2 for close-packed hexagonal (cph), 3 for face-centered cubic (fcc) structures, and for metals with other crystal structures, the number of $s + p$ electrons in the outermost shell is used [46]. The value of Q_0^L predicted by Equation 27 is approximately 17 percent of that in the solid [47], and correspondingly, it is assumed that ΔQ^L is 17 percent of that for the solid [48], written as

$$\Delta Q^L = -\frac{0.17 Z_2 V_0 e^2 \alpha}{11a/17} e^{-\frac{11qa}{16}} \tag{28}$$

where Z_2 the relative valence between solute and solute atoms, a is the jump distance, and α is a constant dependent upon the solvent and the value of Z_2. In Equation 28, the screening parameter q is given by

$$q^2 = \frac{16m\pi^2\bar{e}^2}{h^2}\left(\frac{3\mathbb{V}}{\pi}\right)^{1/3} \tag{29}$$

where m is the electron mass, $\bar{e}$ is the electronic charge, $\mathbb{V}$ is the number of valence electrons per unit volume, and h is Planck's constant.

In Equation 29, the relative valence Z_2 of the solute impurity atom is calculated using

$$\mathrm{Z}_2 = V_{solute}^{effective\ valence} - V_0 = (V_2 + V_{ZP}) - V_0 \tag{30}$$

where V_2 is the Engle-Brewer valence of the solute impurity atom (the ground state), and V_{ZP} is the contribution to the effective valence due to differences in zero-point energy (considered to be 0.33 electrons for every 1 eV difference in zero-point energy). The value of V_{ZP} can then be calculated using the equation

$$V_{ZP} = 0.33\left(P_{0\,adj.}^{solute} - P_0^{solvent}\right) \equiv 0.33\left(E_f^{solvent} - E_f^{solute}\right) \tag{31}$$

where the zero-point energy level of the impurity atom P_0^{solute}, adjusts such that it assumes a Fermi energy level P_{max} equal to the Fermi energy level of the solvent (i.e. $P_{max} = P_{0\,adj.}^{solute} + E_f^{solvent} = P_0^{solvent} + E_f^{solute}$). Rephrasing this concept for clarity, during the adjustment, only the value of the solute zero-point energy changes, while the Fermi energy of the solute E_f^{solute}remains unchanged (Figure 1).

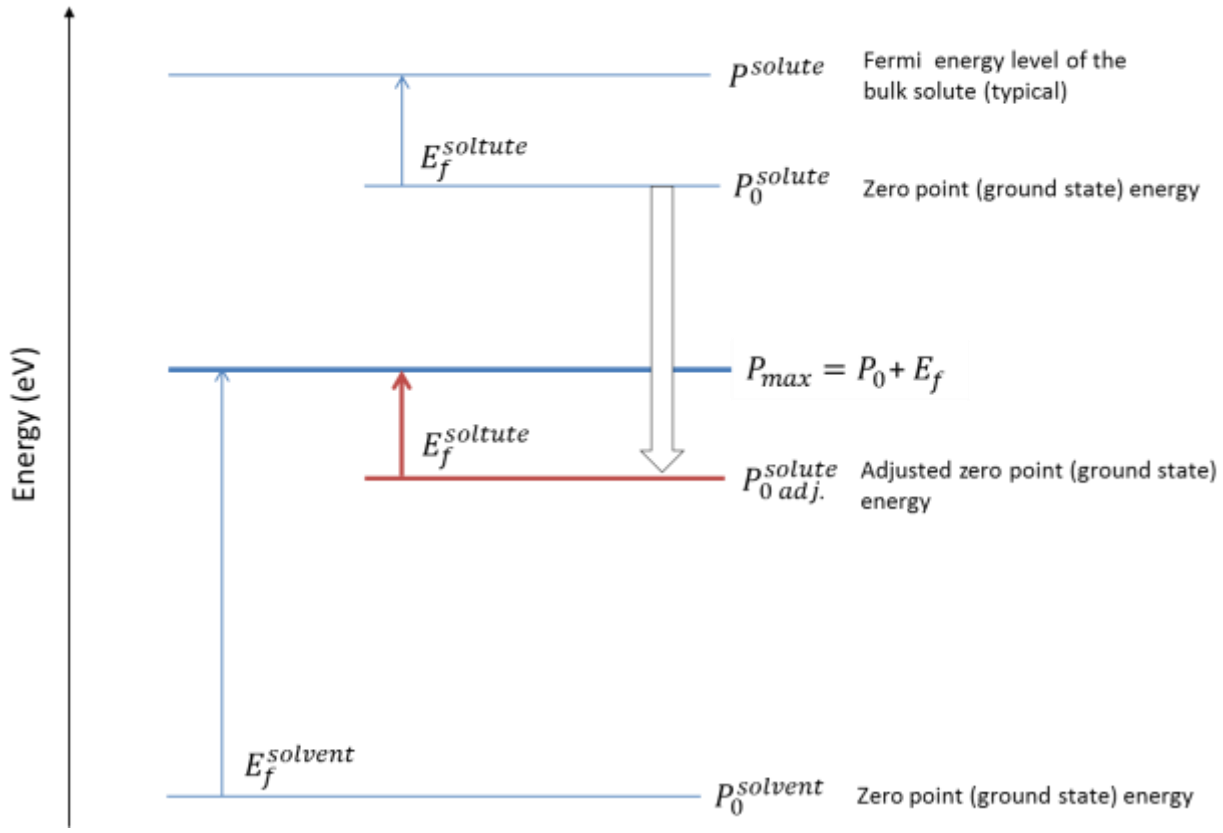

Figure 1 – Graphical representation of the adjustment in the zero point energy level of the solute, aligning the Fermi energy levels of the solute and solvent.

2.5.1.2. FLUCTUATION THEORY

The Fluctuation Theory of liquid diffusion was proposed by Swalin [6] for solvent self-diffusion in liquid metals. It considers that diffusion occurs through the movement of groups of atoms by small, variable distances, in contrast to "Hole" Theory where diffusion occurs through the movement of single atoms by fixed distanced jumps. The derivation of the theory begins with the Einstein random walk equation, where diffusion is related to the mean square jump distance $\bar{j}^2$ and the average time an atom stays at a particular site $\tilde{\tau}$ by

$$D = \frac{\bar{j}^2}{6\tilde{\tau}}. \tag{32}$$

In the theory, statistical fluctuations within the liquid cause the separation of atoms, and with a given probability, variable sized voids are formed which depend on the range of permissible jump distances. The energy ϵ_s needed to separate two nearest neighbor atoms a small distance j from their equilibrium spacing in the pure metal is given by the Morse function

$$\epsilon_s(j) = \epsilon_D\left[1 + e^{-2\alpha j} + 2e^{-\alpha j}\right] \tag{33}$$

where the α term is related to the ϵ vs. j curve. In Equation (33), the dissociation energy of a bond for a pair of ions ϵ_D is taken from quasi-chemical theory as

$$\epsilon_D = \frac{2\Delta H_v}{N_{CN}N_A} \tag{34}$$

where ΔH_v is the heat of vaporization, N_{CN} is the coordination number of the liquid metal, and N_A is Avogadro's number. The energy of the fluctuation in the pure liquid metal required to form a void is considered in terms of an elongation of the four nearest neighbor pair bonds $E_s(j) = 4\epsilon_s$, which is proven to be related to the mean squared jump distance by the equation

$$\bar{J_s}^2 = \frac{3}{4kT}\left[\frac{d^2E_s(j)}{dj^2}\right]_{j=0} = \frac{3ZN_AkT}{16\Delta H_v\alpha^2}. \tag{35}$$

From absolute reaction rate theory, $\tilde{\tau}$ is then determined to be approximately equal to $\tilde{\tau} \cong h/kTZ$, resulting in an expression for solvent self-diffusion given as

$$D_s = \frac{3Z^2N_Ak^2T^2}{16h\Delta H_v\alpha^2}. \tag{36}$$

For solute diffusion in liquid metals, Swalin and Leak [8] present a modified version of the Fluctuation model, which similar to "Hole" Theory, makes use of Thomas-Fermi screening – the concept that solute-ions behave like solvent-ions within the solvent, with the exception that the solute possesses a valence relative to the solvent [44].

When a solute is introduced to the solution a coulombic repulsion occurs between the ions, and this increases the probability for local density fluctuations in the vicinity of the solute ion. For electropositive solutes (relative to the solvent), it is postulated that the increased occurrence of fluctuations increases the diffusivity of the solute. The Thomas-Fermi model is used to express this effect quantitatively, where the coulombic repulsive energy ϵ_i is given by

$$\epsilon_i = \frac{\beta Z \bar{e}^2}{d_0} e^{-q d_0} \tag{37}$$

In the above equation Z is the valence of the solute relative to the solvent, $\bar{e}$ is the electronic charge, d_0 is the distance between solvent-ion/solute-ion centers, q is the screening constant, and β is a parameter which is a function of Z. When a fluctuation occurs where the distance between the ions is increased a distance $d_0 + j$, the coulombic energy becomes

$$\epsilon_i(j) = \frac{\beta Z \bar{e}^2}{(d_0 + j)} e^{-q(d_0 + j)}. \tag{38}$$

The energy of a fluctuation involving the impurity atom $E_i(j)$ in the solution is then taken to be the energy of a fluctuation in the pure solvent, less the energy of the perturbing solute-ions,

$$E_i(j) = 4[\epsilon_s(j) - \epsilon_i(j)] = \frac{8\Delta H_v}{N_{CN} N_0}\left[1 + e^{-2\alpha j} + 2e^{-\alpha j}\right] - \frac{4\beta Z \bar{e}^2}{(d_0 + j)} e^{-q(d_0 + j)} \tag{39}$$

where again the void in the solvent is formed through the elongation of the four nearest neighbor atomic bonds. The average jump distance for the solute ion is calculated in terms of $E_i(j)$,

$$\bar{J_i}^2 = \frac{3}{4kT}\left[\frac{d^2 E_i(j)}{dj^2}\right]_{j=0} = \frac{16\alpha^2 H_v}{Z N_0} - 4q^2\epsilon_i - \frac{8q\epsilon_i}{d_0} - \frac{8\epsilon_i}{{d_0}^2} \tag{40}$$

where ϵ_i is equal to Equation (37), and the impurity diffusion coefficient D_i can then be assessed as the ratio to solvent self-diffusion D_s, given as

$$\frac{D_i}{D_s} = \frac{\bar{j}_i^2}{6t}\frac{6t}{\bar{j}_s^2} = \left[1 - \frac{q^2\epsilon_i}{k_f} - \frac{2q\epsilon_i}{d_0 k_f} - \frac{2\epsilon_i}{d_0^2 k_f}\right]^{-1}, \qquad where\ k_f = \frac{N_{CN}N_A}{4\Delta H_v \alpha^2}. \tag{41}$$

2.5.1.3. STOKES-EINSTEIN AND SUTHERLAND THEORIES

The Stokes-Einstein theory [41] relates atomic diffusion and the viscosity of the liquid using Stokes' law, which predicts the drag force F_D acting on a large, hard, dense sphere moving through a viscous medium. Stokes' law is given as

$$F_D = 3\pi d\eta v \tag{42}$$

where d is the sphere diameter, η is the absolute viscosity, and v the terminal velocity of the diffusing particle. Einstein's equation relates the self-diffusion coefficient to the average velocity of the diffusing particle per unit force acting on the particle, a parameter termed the mobility M, through the expression

$$D = k_B T M \tag{43}$$

where k_B is Boltzmann's constant, and T is the temperature. Combining Equations (42) and (43) and making use of the fact that the mobility of the sphere can be determined from Stokes' law as v/F_D, an expression for the self-diffusion coefficient is derived

$$D = \frac{k_B T}{6r\pi\eta} \tag{44}$$

where r is the sphere radius ($d = 2r$).

Sutherland [10] proposed an empirical correction to the Stokes-Einstein model, which attempts to account for the size difference of diffusing impurity particles (solute) and the bulk liquid (solvent). The empirical correction was applied to Stokes' law,

$$F_D = 3\pi d\eta v\left(\frac{\beta d + 2\eta}{\beta d + 3\eta}\right) \tag{45}$$

where β is the coefficient of sliding friction between the diffusing particle and the solution. Sutherland reasoned that no slipping should occur at the surface of a relatively large diffusing particle within the liquid, implying as $\beta \to \infty$ the corrective term approaches unity, resulting in Einstein's original equation. However, if all particles in the fluid are assumed to be of similar size, the diffusing sphere would move through the liquid via voids (holes). In this event, the sliding friction of the diffusing particle is essentially zero, and Equation (42) becomes

$$F_D = 2\pi d\eta v. \tag{46}$$

The resulting equation for diffusion in the event of equal sized particles, which is applicable to instances of both self-diffusion and impurity diffusion, becomes

$$D = \frac{k_B T}{4r\pi\eta}. \tag{47}$$

It should be noted that in both the Stokes-Einstein and Sutherland models, the interactions of the atoms (spheres) are not equated with any form of interatomic potential. In addition, the atomic radius of the diffusing particle used in the equations must be chosen carefully to accurately reflect the characteristics of the liquid state.

2.5.1.4. ENSKOG'S THEORY

Enskog`s theory [43, 42] provides a solute impurity diffusion D_i^E in a hard sphere (dense) fluid given as

$$D_i^E = \frac{3}{8n_S \mathrm{g}_{is}(\sigma_{is})\sigma_{is}^2}\left(\frac{k_B T}{2\pi\mu}\right)^{1/2}, \qquad \mu = \frac{m_i m_s}{m_i + m_s}, \qquad \sigma_{is} = \frac{\sigma_i + \sigma_s}{2}, \tag{48}$$

where n_S is the atom density of solvent particles, $\mathrm{g}_{is}(\sigma_{is})$ is the radial distribution function of the binary alloy evaluated at σ_{is}, k_B is Boltzmann`s constant, T is the temperature, σ_i and σ_s are the atomic diameters of the solute and solvent atoms, μ is the reduced mass of the solute and solvent

atoms of mass m_i and m_s respectively, and σ_{is} is in average of the solute and solvent atomic diameters.

The determination of σ_i, σ_s, and $g_{is}(\sigma_{is})$ for a binary mixture allows for comparison with experimental data, and the hard sphere diameter σ is determined following the theory of Protopapas et al.

$$\sigma = \sigma_0 \left[1 - 0.112\left(\frac{T}{T_m}\right)^{1/2}\right], \qquad \sigma_0 \approx 1.0878 {n_m}^{-1/3}. \tag{49}$$

where σ_0 is the distance at which the interatomic potential assumes its minimum value (typically taken as twice the distance of first peak maximum of the radial distribution function), T_m is the melting point of the pure metal, and n_m is the number density of the liquid at the melting temperature. It is assumed in this model that the hard sphere diameters of the solute and solvent remain unchanged upon mixing in the alloy.

A corrective factor C is applied to the solute impurity diffusion coefficient D_i^E determined using Enskog's theory, which is necessary to compensate for the many-body correlations in the liquid. The correlations have been shown to depend primarily on the density of the fluid (v/v_0), and the relative mass Δm and size $\Delta\sigma$ of the solute atom in comparison with the solute. The solute impurity diffusion coefficient D_i then becomes

$$D_i = D_i^E C\left(\frac{v}{v_0}, \Delta m, \Delta\sigma\right), \qquad \frac{v}{v_0} = \frac{\pi\sqrt{2}}{6y_s}, \qquad \Delta m = m_i - m_s, \qquad \Delta\sigma = \sigma_i - \sigma_s. \tag{50}$$

where y_s is the packing fraction of the pure solvent. Based on molecular dynamics simulations, Alder et al. [49] have published a table in which values of C are provided for a range of atomic mass and diameters.

2.5.2. CONCENTRATION DEPEDENT DIFFUSION IN BINARY MIXTURES

In 1948 Darken [50] developed a phenomenological equation that related the two self-diffusion coefficients to the interdiffusion coefficient in a binary solid mixture. In a liquid a mixture that contains A- and B-type atoms, a similar equation for interdiffusion is derived by using a specific Green-Kubo formula that combines Fick's equation with mass conservation (Section 2.1) and solves the equations in the frequency domain and reciprocal space [51]. For a binary mixture the (Fickian) interdiffusion coefficient is described by

$$D_{AB} = \frac{\Phi}{3NX_AX_B}\int_0^\infty dt\langle\, \mathbf{j}(t)\cdot\mathbf{j}(0)\rangle \tag{51}$$

where **j** is the interdiffusion current calculated in a center-of-mass reference frame, defined by

$$\mathbf{j}(t) = X_B\sum_{i=1}^{N_A}\mathbf{v}_i - X_A\sum_{j=1}^{N_B}\mathbf{v}_j = NX_AX_B(\mathbf{v}_A - \mathbf{v}_B),\ \ i = 1,2,\dots,N_A,\quad j = 1,2,\dots,N_B. \tag{52}$$

The correlation between the interdiffusion current is then given by

$$\langle\, \mathbf{j}(t)\cdot\mathbf{j}(0)\rangle = NX_AX_B\langle[(\mathbf{v}_A(t) - \mathbf{v}_B(t))\cdot(\mathbf{v}_A(0) - \mathbf{v}_B(0)]\rangle. \tag{53}$$

The velocity vectors $\mathbf{v}_A$ and $\mathbf{v}_B$ of species A and B, respectively, are related by the center-of-mass velocity field **v** by

$$\mathbf{v}(\boldsymbol{r},t) = \frac{C_A\mathbf{v}_A(\boldsymbol{r},t) - C_B\mathbf{v}_B(\boldsymbol{r},t)}{C}. \tag{54}$$

The Maxwell-Stefan (MS) equation [23] provides a different description of diffusion based on the kinetic process of ideal gas, where a flux is produced by the balance between the driving force, gradient in the chemical potential μ, and the frictional drag, with

$$-\frac{1}{RT}\cdot\nabla\cdot\mu_A = \frac{X_B(\mathbf{v}_A - \mathbf{v}_B)}{D_{AB}^0}. \tag{55}$$

where D_{AB}^0 is termed the MS diffusion coefficient. The left-hand side of Equation (55) is equal to

$$-\frac{1}{RT}\nabla\mu_A = \left(\frac{\partial ln\gamma_A}{\partial X_A}\right)\cdot\nabla\cdot X_A = \Phi\cdot\nabla\cdot X_A \tag{56}$$

where the gradient in chemical potential is proportional to the partial derivative of the activity γ_A. Rearranging Equation (55) and combining with (51) shows the relationship between the MS diffusion coefficient and the Fickian interdiffusion coefficient

$$D_{AB} = \Phi\cdot D_{AB}^0. \tag{57}$$

Returning to Equation (51), grouping the velocity autocorrelation and cross correlation functions in the MS diffusion coefficient becomes [52]

$$D_{AB}^0 = \left[X_B D_A + X_A D_B + X_A X_B\left(\frac{\mathcal{F}_{AA}}{X_A^2} + \frac{\mathcal{F}_{BB}}{X_B^2} - 2\frac{\mathcal{F}_{AB}}{X_A X_B}\right)\right], \tag{58}$$

where the velocity autocorrelation functions for the self-diffusion coefficients are given as

$$D_\alpha = \frac{1}{3N}\int_0^\infty \langle \mathbf{v}_\alpha(t)\cdot\mathbf{v}_\alpha(0)\rangle dt\,, \qquad \alpha = A\ or\ B, \tag{59}$$

and the $\mathcal{F}$-factors are given by the velocity cross-correlation functions

$$\mathcal{F}_{\alpha,\beta} = \frac{1}{3N}\sum_{i=1}^{N_\alpha}\sum_{j\neq 1}^{N_\beta}\int_0^\infty \langle \mathbf{v}_i^\alpha(t)\cdot\mathbf{v}_k^\beta(0)\rangle dt, \quad \alpha,\beta = A\ or\ B. \tag{60}$$

If the velocity cross-correlations are assumed to be negligible,

$$\frac{\mathcal{F}_{AA}}{X_A^2} + \frac{\mathcal{F}_{BB}}{X_B^2} - 2\frac{\mathcal{F}_{AB}}{X_A X_B} = 0, \tag{61}$$

and a simple linear relationship between self-diffusion coefficients connects the MS diffusivity by

$$D_{AB}^0 = X_B D_A + X_A D_B. \tag{62}$$

In Equation (52) the scalar Φ is the thermodynamic factor that arises from defining diffusion in terms of concentration, rather than chemical potential, and is defined by

$$\Phi = \lim_{k \to 0} \frac{X_A X_B}{S_{XX}(q=0)} \tag{63}$$

where $S_{XX}(q)$ is the concentration-concentration structure factor, which is defined in terms of the partial structure factors by Bhatia and Thornton [53] as

$$S_{XX}(q) = X_A X_B \Big(1 + X_A X_B \big(S_{AA}(q) + S_{BB}(q) - 2S_{AB}(q)\big)\Big). \tag{64}$$

Under isobaric-isothermal conditions, the concentration-concentration structure factor in the low q limit is equal to the inverse of the second derivative of the Gibbs Free energy of the binary mixture w.r.t. concentration

$$S_{xx}(q=0) = \left(\frac{\partial^2 G_{AB}^{rs}}{\partial X_A^2}\right)_{P,T}^{-1} \tag{65}$$

noting that $\partial^2 G_{AB}^{rs}/\partial X_A \partial X_B = \partial^2 G_{AB}^{m}/\partial X_A^2 = \partial^2 G_{AB}^{m}/\partial X_B^2$. The thermodynamic factor is calculated from either the concentration-concentration structure factor or the Gibbs free energy of the solution using

$$\Phi(X,T) = \frac{S_{xx}(q=0)}{X_A X_B} = \frac{X_A X_B}{RT} \frac{\partial^2 G_{AB}^{rs}}{\partial X_A^2}. \tag{66}$$

The substitution of Equation (6) into Equation (66) shows that ϕ is dependent on the excess Gibbs free energy only for the random solution model (Section 2.2.1) with

$$\Phi(X,T) = 1 + \frac{X_A X_B}{RT} \frac{\partial^2 G_{AB}^{ex}}{\partial X_A^2}, \tag{67}$$

that for an ideal solution reduces to unity and does not enhance the value of the interdiffusion coefficient D_{AB}. Substituting Equations (62) and (66) into (57) and simplifying the nomenclature with $X_A + X_B = 1$, the familiar form of the Darken equation is obtained with

$$D_{AB}(X,T) = [(1-X)\cdot D_A(X,T) + X\cdot D_B(X,T)]\cdot\left[\frac{X\cdot(1-X)}{RT}\frac{\partial^2 G_{AB}^{rs}(X,T)}{\partial X^2}\right]. \qquad (68)$$

2.6. LIQUID METAL DIFFUSION EXPERIMENTAL TECHNIQUES AND SIMULATION METHODS

Numerous methods exist to determine diffusion coefficients in liquid metals. Long capillary methods have been extensively used to obtain diffusion coefficients, where concentration data are extracted ex-situ from diffusion samples that have solidified from the liquid state. In-situ methods such as x-ray diffraction and neutron scattering, are also used to extract diffusion coefficients directly from the metal in the liquid state. With increasing frequency in literature in the past decade, numerical simulation methods such as Monte Carlo, molecular dynamics (MD), or ab-intio MD, have been used to determine diffusion coefficients in liquid metals based on the interaction of atoms via theoretical or semi-empirical force fields. Each method offers different insight into diffusion phenomena, and are subject to error that is dependent on experimental method, and/or underlying theoretical assumptions.

2.6.1. LONG CAPILLARY METHODS

The term *long capillary method* encompasses a broad range of experimental techniques used to obtain liquid diffusion coefficients. Common to all methods is the use of a long cylindrical capillary of a specified diameter that contains a liquid metal diffusion couple. Within the diffusion couple, a solute and solvent material are initially separated at a planar interface, establishing a concentration (or chemical potential) gradient along the length of the capillary. The long capillary methods are often described in terms of a specific solution of the diffusion equation, such as the thin-film, finite-column, Boltzmann-Matano, and solid wire techniques. Using the long capillary method, solvent self-diffusion coefficients are obtained using a radioactive isotope as the solute

material, or alternatively, interdiffusion coefficients are obtained when the solute material differs from that of the solvent (which can be pure metal or mixture).

In the simplest design of the experiment, a single diffusion couple is contained in a continuous long capillary that is lowered into a preheated furnace and diffusion annealed for a fixed period, at which point the sample is removed an allowed to solidify. During the diffusion annealing period, the capillary is orientated in the vertical position and a small vertical temperature gradient (~ 0.1 K/mm) is applied to supress convective transport that may otherwise result from density differences within the liquid. Horizontal/radial temperature gradients across the capillary walls may also contribute to convective transport, and a reduction of the capillary diameter has been shown to suppress additional mass transport due to buoyancy driven convection [17].

Variations of the long capillary technique exist, such as the capillary reservoir and shear cell techniques. In the capillary reservoir technique, a long capillary full of solute is immersed within a liquid bath of solvent contained within a large crucible. In the shear cell technique, the long capillary is comprised of several individual sections which can be physically separated by rotating (shearing) each section in and out of alignment along the major axis of the capillary. This approach allows precise control over the duration of the diffusion experiment. Despite the widespread use of both methods, it is now widely accepted that data obtained using capillary reservoir and shear cell experiments are subject to error. For the capillary reservoir method, lid-driven flow across the mouth (top) of the capillary while immersed in the fluid bath has been found to add a convective component to the experiment and increase the value of the diffusion coefficient [11]. Similarly, diffusion coefficients obtained using the shear cell method have been shown to be influenced by the shearing motion of the rotating disks, where solute is redistributed within each disk section by convective motion.

More recently, time resolved x-ray radiography has been used to determine interdiffusion coefficients where x-ray image intensity is used as the basis for the concentration measurement [22]. This experimental method has the advantage of monitoring diffusion specimens in-situ, however, it still requires the use of a long capillary with a concentration gradient and is subject to the same potential sources of error.

2.6.2. X-RAY DIFRACTION, NEUTRON SCATTERING, AND SIMULATION METHODS

Liquid diffusion coefficients may also be determined from metal in the liquid state using methods such as X-ray diffraction, quasi-elastic neutron scattering, or computer based simulation methods. In X-ray diffraction and quasi-elastic neutron scattering (QNS) experiments, the intrinsic diffusion coefficient of one species of atom is determined for an alloy of constant composition and temperature. This experimental method can be used to determine of the self- and interdiffusion coefficients within pure metals or alloys mixtures, however, an assumption must be made regarding the diffusion mechanism in the liquid during analysis [54].

Computer based simulation methods such as molecular dynamics (MD), Monte Carlo, and ab-initio MD can also be used to obtain liquid diffusion coefficients [55]. The development of standardized supercomputing code such as LAMMPS (Large-scale Atomic/Molecular Massively Parallel Simulator) [37] has opened this field of research to a wider audience, which allows researchers to focus on developing/refining theoretical atomic interaction potentials. Despite the advantages of studying diffusion in liquid metals using molecular dynamics, interatomic potentials do not exist for the clear majority of binary liquid metal systems, and force fields developed for the solid are not readily transferable to the liquid [28].

2.7. OVERVIEW OF PAST RESEARCH ON THE THERMODYNAMICS AND DIFFUSION IN THE LIQUID AL-CU BINARY SYSTEM

2.7.1. THERMODYNAMICS

The structure of liquid Al-Cu is of current interest literature, as several studies have discussed the possibility that chemical order within the melt is not random, exhibiting concentration and temperature dependent behavior [56, 29, 57]. The Al-Cu system is characterized by several intermetallic phases in the Cu rich portion of the phase diagram that persist to high temperature, and their presence suggests that energetically favorable configurations of atoms may exist within liquid state [29]. The chemical structure of liquid Al-Cu alloys has been investigated using x-ray diffraction [29], cold neutron scattering [57], and high-energy synchrotron x-ray diffraction in conjunction with ab-initio molecular dynamics simulation [56]. These studies suggest that as the temperature of the melt is lowered, the coordination number of the liquid increases, indicating a temperature dependent structure. Also, reported was that the peaks in the structure factor and radial distribution function are sharper (increased chemical order) for the intermetallic compositions as compared to Al-rich compositions at the same temperature, indicating a concentration-dependent structure. The experimentally observed temperature T and concentration X (mole fraction) dependent structural properties of the liquid are further supported by thermodynamic assessment data, where excess Gibbs free energy of solution G_{ex} was reported to be negative (associative/non-random), lessening in effect with increasing temperature as shown in Figure 2. The minimum value in the excess Gibbs free energy occurs at a composition that corresponds to the ε_1 intermetallic phase peritectic [30, 31, 32]. From excess Gibbs free energy of solution data, the thermodynamic factor $\Phi(X,T)$ is calculated using Equation (17) as shown in

Figure 3. It is also important to note that the excess enthalpy of mixing H_{ex} in references [30, 31, 32] is experimentally determined to be independent of temperature.

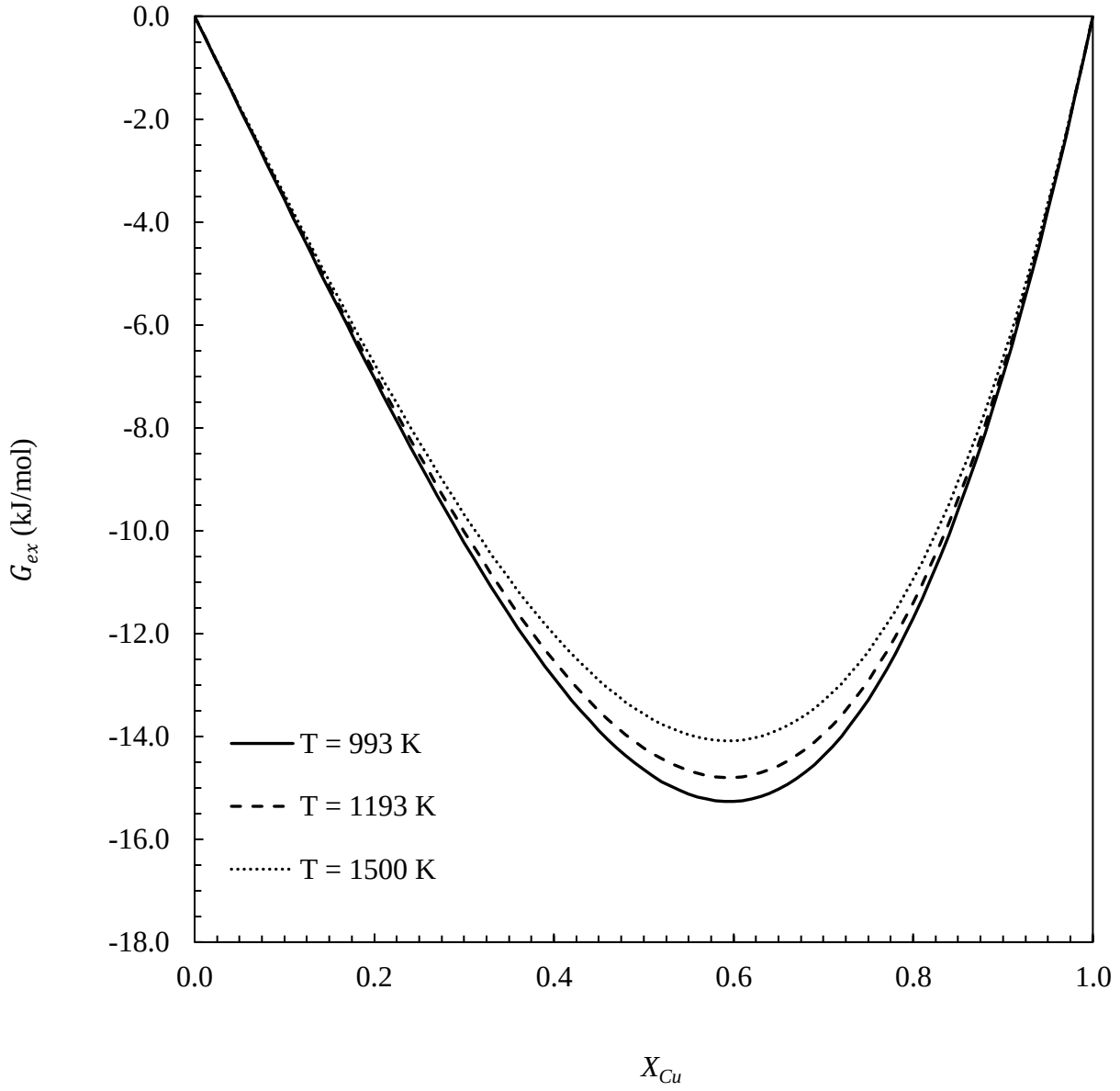

Figure 2 – The excess Gibbs free energy of solution G_{ex} for liquid Al-Cu as a function of the mole fraction concentration X_{Cu} at temperatures of T = 993 K, 1193 K, and 1500 K. The figure was created using data from Witusiewicz et al. [30].

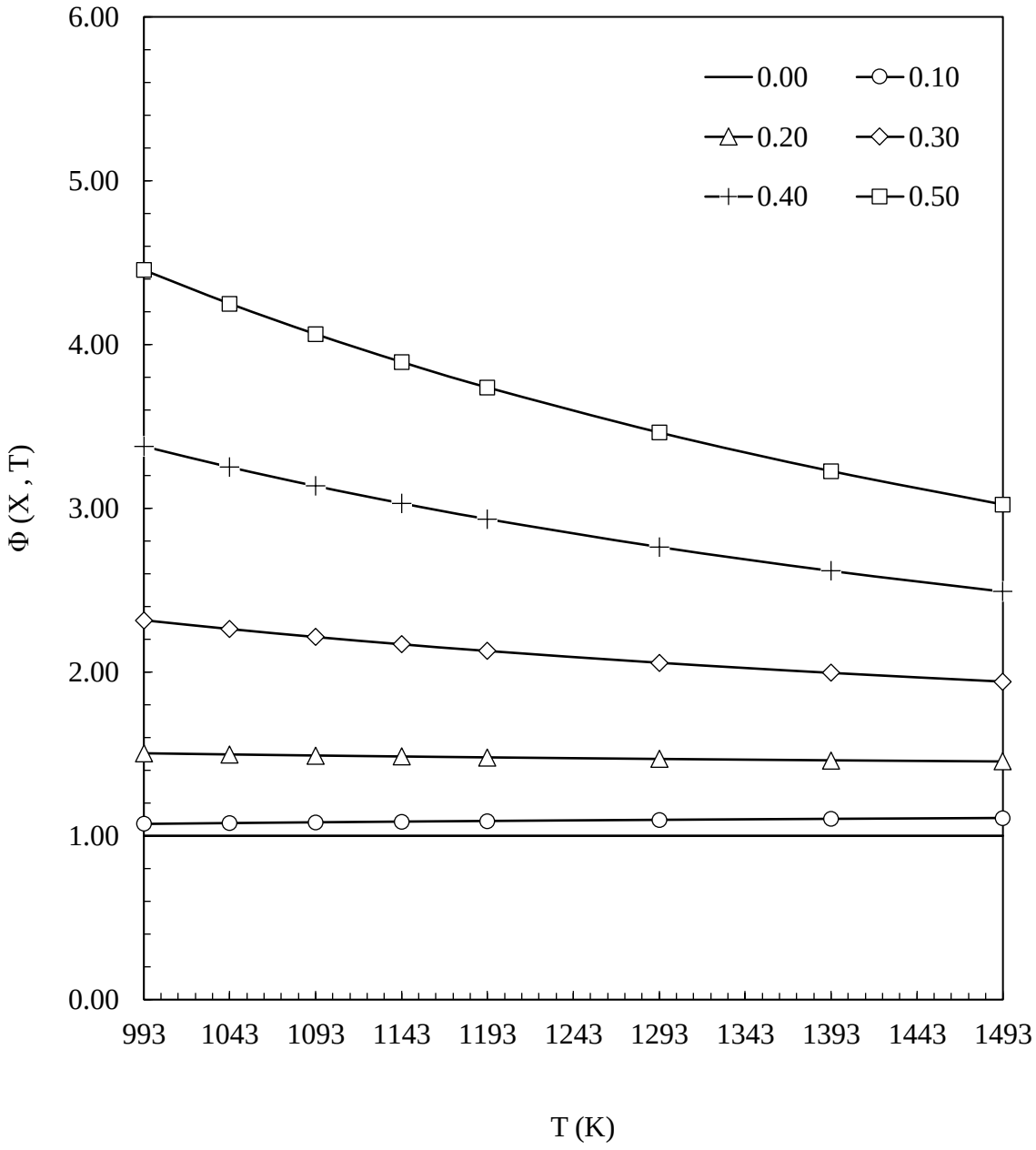

Figure 3 – The thermodynamic factor $\Phi(X, T)$ as a function of temperature T and mole fraction concentration X for the Al-Cu system in the liquid state. In the figure, the value of Φ is calculated at mole fraction concentrations of X_{Cu} = 0.00, 0.10, 0.20, 0.30, 0.40, and 0.50, and the solid line represent the best fit value at constant concentration. The values of the Φ are calculated using Equation (67) with data from Witusiewicz et al. [30].

2.7.2. SELF- AND INTERDIFFUSION IN LIQUID AL-CU

In this section, a review of past studies on self-diffusion and interdiffusion in the binary Al-Cu system is presented. The following figures present data in Arrhenius plot format following Equation (25), as this is the typical convention in diffusion literature. The data presented in this section are used to benchmark the findings of this thesis research. The results from previous studies include values of the self-diffusion coefficients D_{Al} and D_{Cu}, and the interdiffusion coefficient D_{AlCu} for several alloy concentrations and temperatures. If D_{AlCu} is assumed to be constant over a concentration range, it is referred to in the proceeding as the average interdiffusion coefficient (over the stated concentration range).

Figure 4 shows past results from several studies for self-diffusion in pure liquid Al and Cu, interdiffusion of Cu in Al at a concentration of $Al_{\sim 100}Cu_{3.6\text{-}5.7 \times 10^{-5}}$ (tracer quantities of solute), as well as data for the average interdiffusion coefficient obtained in Al alloys within a concentration range of $Al_{100}Cu_0$ to $Al_{60}Cu_{40}$. Self-diffusion in pure liquid Al was studied by Kargl et al. [58] using incoherent quasielastic neutron scattering within a temperature range of 980 K (1/T = 0.00104 1/K) to 1060 K (1/T = 0.00094 1/K), and the Sutherland-Einstein relation was assumed in the calculation of the diffusion coefficients. Meyer [14] determined values of the self-diffusion coefficient for liquid Cu using quasielastic neutron scattering over a temperature range of 1370 K (1/T = 0.00073 1/K) to 1620 K (1/T = 0.00062 1/K). In Ejima et al. [26], values of tracer interdiffusion coefficient D_{AlCu} were obtained using the capillary reservoir technique with the radioactive isotope ^{64}Cu. In their experiment, 1.1 mm graphite capillaries were used to contain the diffusion couple, over a temperature range of 976 K (1/T = 0.00102 1/K) to 1260 K (1/T = 0.00079 1/K) at concentrations of 3.6 to 5.7 x 10^{-5} at% Cu in Al. Tanaka et al. [24, 25] used the solid wire long capillary method to determine interdiffusion coefficients in aluminum alloys with a

concentration range of 0 to ~ 40 at% Cu over a temperature range of 973 K (1/T = 0.00103 1/K) to 1073 K (1/T = 0.00093 1/K). In their study interdiffusion is assumed to be constant, independent of composition, and experiments are performed in 8.5 mm diameter SiO_2 capillaries. Also, shown in the figure are the results of Lee and Cahoon [15], where the solid wire long capillary method was used to determine average interdiffusion coefficients over the same temperature and concentration range as Tanaka et al. [24, 25]. In Lee and Cahoon [15], the interdiffusion coefficient was assumed to be constant (independent of concentration), and 1.6 mm diameter Al_2O_3 capillaries were used to contain the liquid diffusion couples.

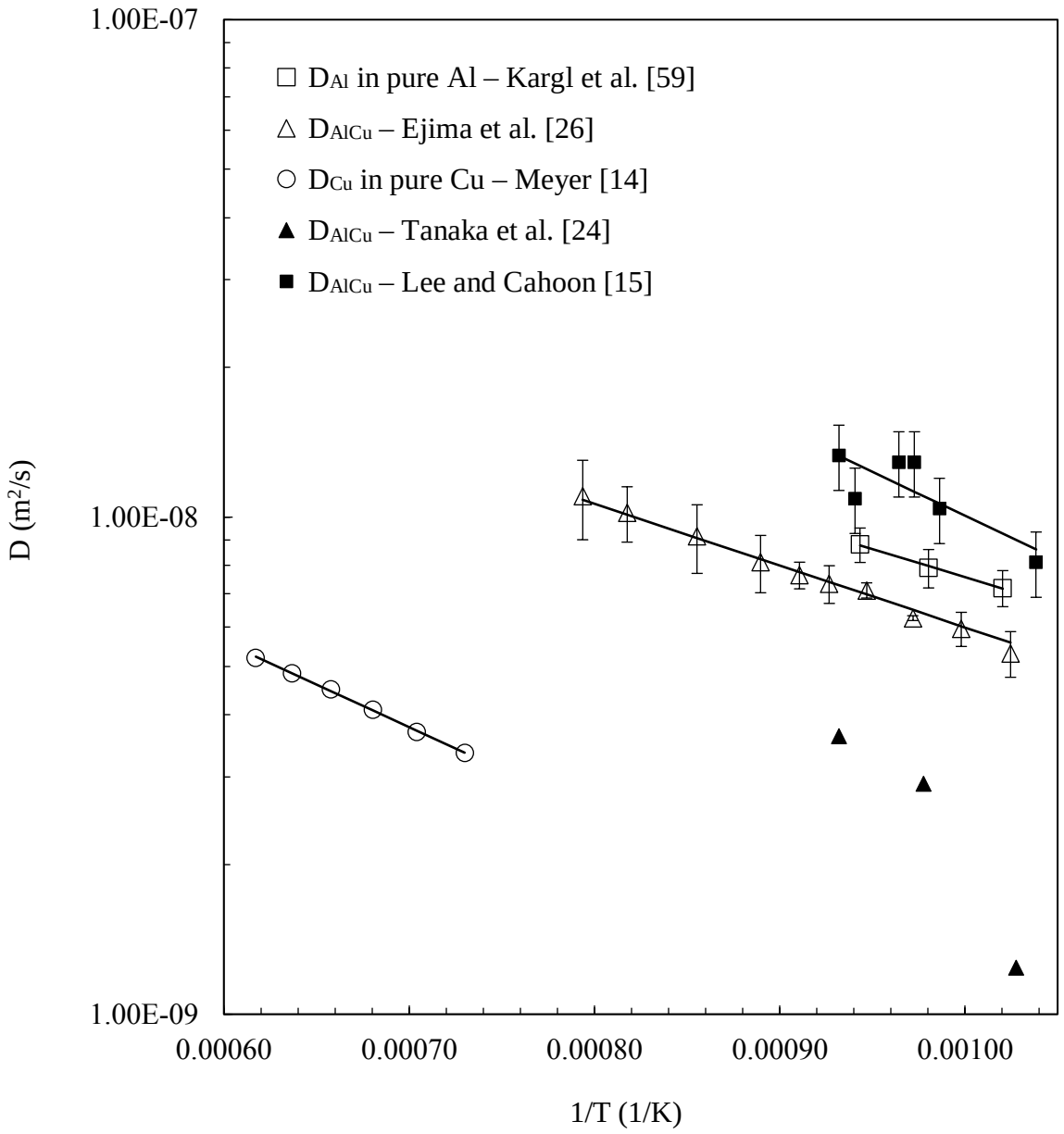

Figure 4 – An Arrhenius plot of self- and interdiffusion in the liquid Al-Cu system. In the figure the □ represents solvent self-diffusion D_{Al} for liquid Al based on data from Kargl et al. [58] and the ○ represents solvent self-diffusion D_{Cu} for liquid Cu measured using quasielastic neutron scattering based on data from Meyer [14]. The △ represents tracer interdiffusion D_{AlCu} of 3.6 to 5.7 x 10^{-5} at% Cu in liquid Al measured using the capillary reservoir technique based on data from Ejima et al. [26]. The ▲ and the ■ are the average interdiffusion coefficients D_{AlCu} obtained over a concentration range of ~ 0 to 40 at% Cu using long capillary reactive diffusion based on data from Tanaka et al. [24] and Lee and Cahoon [15], respectively. The solid black lines represent the best fit Arrhenius equation.

In Figure 5, the results of past studies of self- and interdiffusion in $Al_{20}Cu_{80}$ are shown. Brillo et al. [59] used quasielastic neuron scattering to determine the intrinsic diffusion coefficient for liquid copper D_{Cu} in $Al_{20}Cu_{80}$ over the temperature range of 1000 K (1/T = 0.00100 1/K) to 1795 K (1/T = 0.00056 1/K). Within the limits of error, it was determined that D_{Cu} is accurately described by a linear Arrhenius relationship. Similarly, Dahlborg et al [57] used cold neutron inelastic scattering over a temperature range of 973 K (1/T = 0.00103 1/K) to 1373 K (1/T = 0.00073 1/K) to determine the Cu self-diffusion coefficient in $Al_{83}Cu_{17}$ alloy. Note that the results for the D_{Cu} of Dahlborg et al [57] are considerably higher than those of Brillo et al. [59]. Using time-resolved x-ray radiography, Zhang et al. [22, 21] obtained the liquid interdiffusion coefficient D_{AlCu} for an average composition of $Al_{18.7}Cu_{81.3}$ over the temperature range of 983 K (1/T = 0.00102 1/K) to 1173 K (1/T = 0.00085 1/K). In their experiment the liquid diffusion couple was created by placing two equal length rods of $Al_{77.9}Cu_{22.1}$ and $Al_{84.6}Cu_{15.4}$ within a 1.5 mm graphite capillary, and it was found that results were well described over the temperature interval by the Arrhenius equation. In Lee et al. [18], the interdiffusion coefficient was determined using directional solidification in a 0.8 mm capillary at a temperature of 821.1 K (1/T = 0.00122 1/K) that corresponds to the liquidus concentration at the eutectic $Al_{82.6}Cu_{17.4}$. The last set of results included in the Figure 5 are those of Lee and Cahoon [15], where the finite-column long capillary technique was used to obtain the interdiffusion coefficient in 1.6 mm Al_2O_3 capillaries. The values of the average interdiffusion coefficient that are shown correspond to an average composition of $Al_{22}Cu_{78}$.

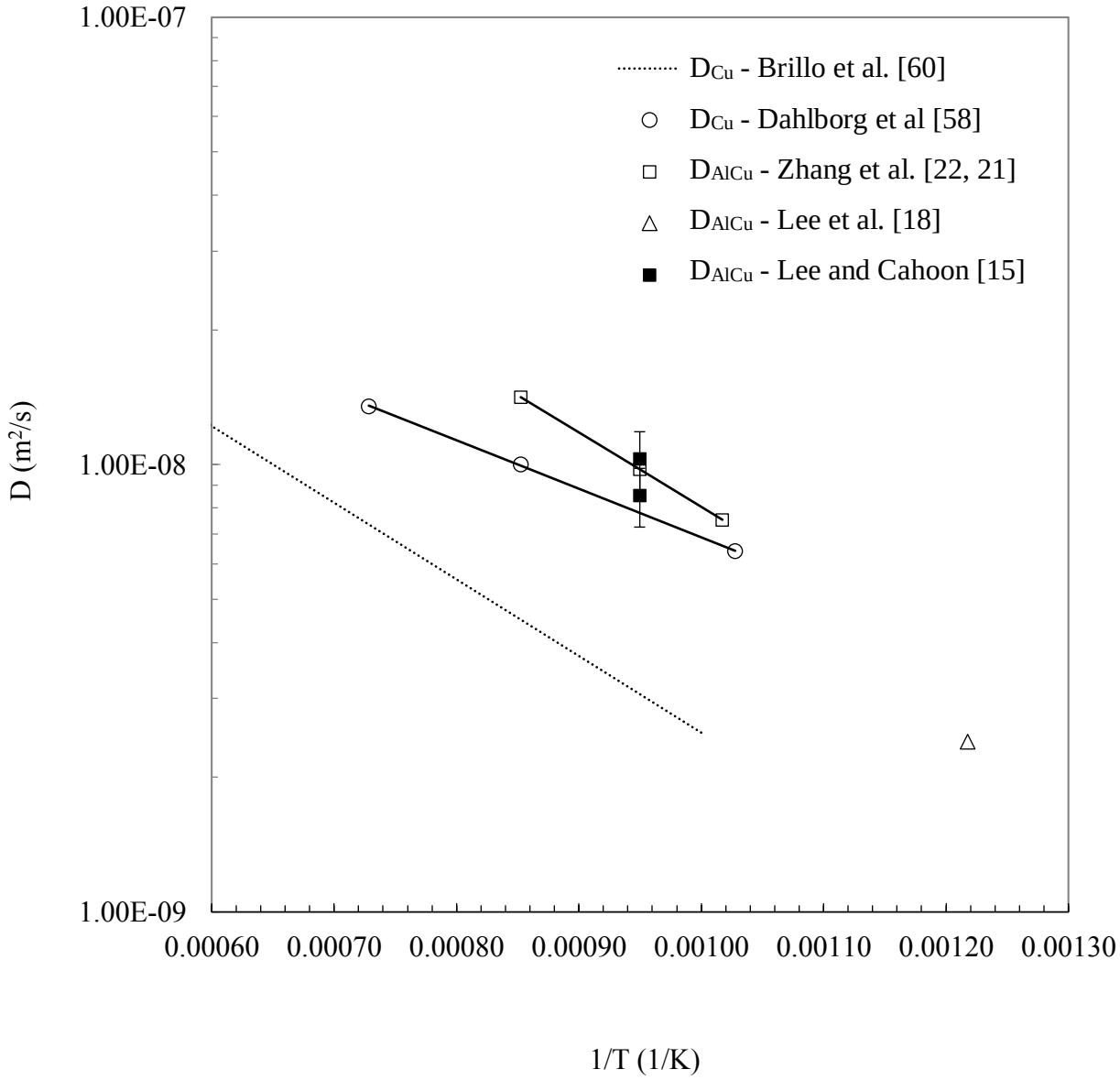

Figure 5 - Arrhenius plot of self- and interdiffusion in liquid $Al_{20}Cu_{80}$. In the figure, the ⋯ line represents the best-fit values of the Cu self-diffusion coefficient D_{Cu} in $Al_{20}Cu_{80}$ determined using quasielastic neuron scattering reported by Brillo et al. [59]. The ○ represents the value of Cu self-diffusion coefficient D_{Cu} in $Al_{83}Cu_{17}$ obtained suing cold neutron inelastic scattering reported by Dahlborg et al [57]. The □, △, and ■ represent the value of the interdiffusion coefficient D_{AlCu} reported by Zhang et al. [22, 21] in $Al_{18.7}Cu_{81.3}$, Lee et al. [18] in $Al_{82.6}Cu_{17.4}$, and Lee and Cahoon [15] in $Al_{22}Cu_{78}$, respectively. The solid black lines represent the best fit Arrhenius equation.

In Figure 6 the diffusion in $Al_{60}Cu_{40}$ alloy is shown. In Cheng et al. [23] the interdiffusion coefficient was calculated using molecular dynamic simulation with an embedded atom method (EAM) potential developed by Cai and Ye [27]. Diffusion was simulated in the NPT ensemble, for a system size of 4000 atoms over a temperature range of 970 K (1/T = 0.00103 1/K) to 1500 K (1/T = 0.00067 1/K). In Wang et al. [56], ab initio molecular dynamic simulation in the NVT ensemble was used to calculate the self-diffusion coefficients for D_{Al} and D_{Cu} over a temperature range of 973 K (1/T = 0.00103 1/K) to 1323 K (1/T = 0.00076 1/K) for a system size of 100 atoms. In addition, the liquid structure factor of $Al_{60}Cu_{40}$ is simulated using ab-intio molecular dynamics, and is found to be in good agreement with structure factor that was determined experimentally using high energy x-ray diffraction. This lends credibility to the reported values of the self-diffusion data, as this key property of the liquid is captured in the simulation model.

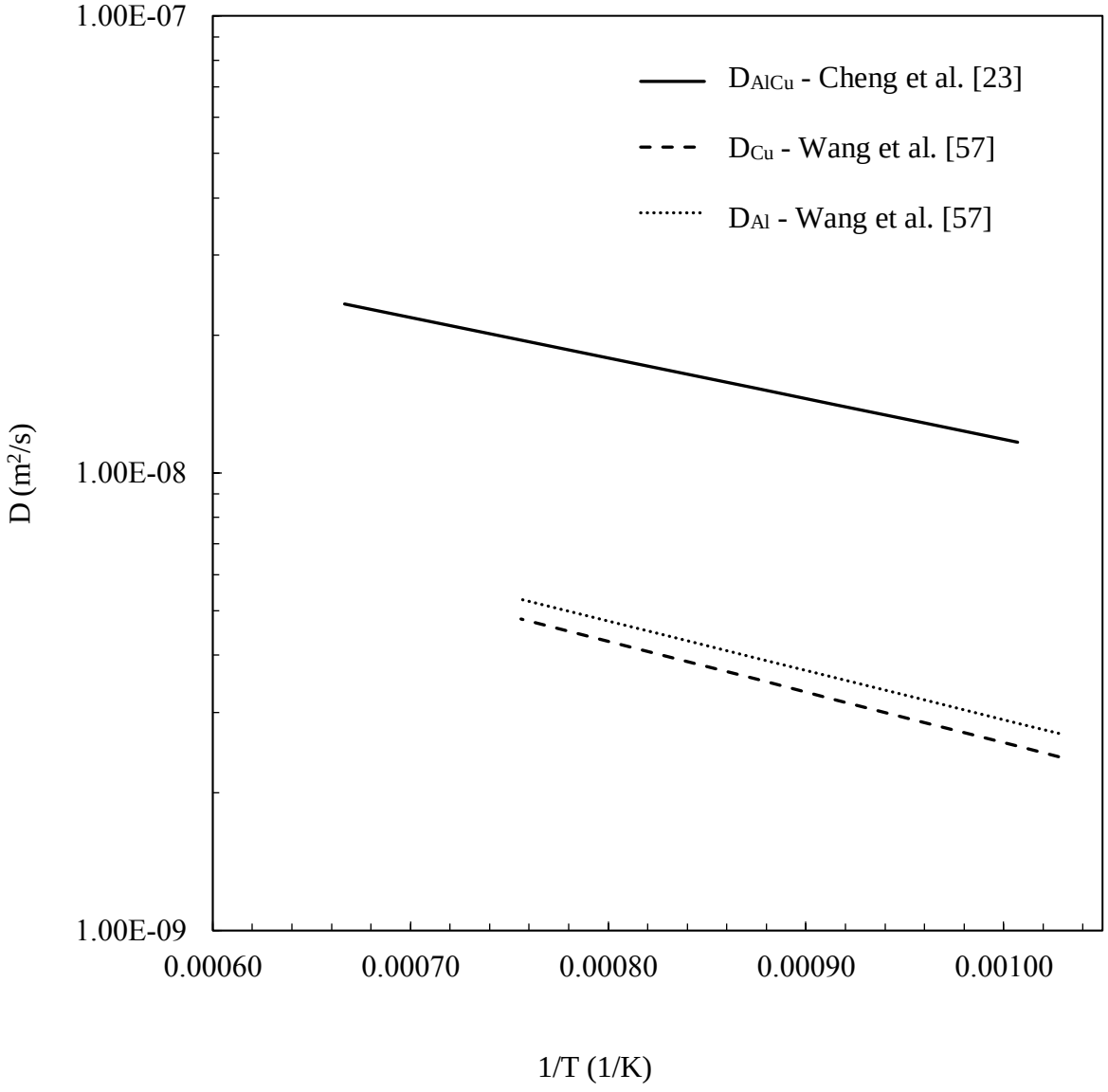

Figure 6 - Arrhenius plot of self- and interdiffusion in liquid $Al_{60}Cu_{40}$. In the figure, the — line represents the best fit values of the interdiffusion coefficient D_{AlCu} obtained using molecular dynamics simulation by Cheng et al. [23]. The --- and ⋯ lines represent the best fit self-diffusion coefficients for D_{Cu} and D_{Al}, respectively, as reported by Wang et al. [56] obtained using ab-intio molecular dynamics.

3. INTERDIFFUSION IN THE AL-CU SYSTEM

3.1. INTRODUCTION

In a binary A-B type liquid metal mixture interdiffusion is described by the Darken equation $D_{AB}(X,T) = D^0_{AB}(X,T) \cdot \Phi(X,T)$, where D^0_{AB} is the purely kinetic MS diffusivity coefficient, and Φ is the thermodynamic factor (see Section 2.5.2). More recently attempts have been made to explore this relationship in the binary metallic Al-Ni [19], Zr-Ni [1], and Al-Cu systems [21, 22, 23] using varied approaches including molecular dynamics simulation, quasi-elastic neutron scattering, and long capillary methods. In this chapter, interdiffusion in the Al-Cu system is further investigated using the solid wire long capillary technique, and compared to the benchmark results of Section 2.7. A main focus of this analysis is on quantifying the concentration and temperature dependence of $D_{AB}(X,T)$.

In the solid wire long capillary (SWLC) method, interdiffusion occurs within a long capillary where the diffusion couple consists of a liquid column of solvent and a solid column of solute metal separated at a planar interface. During isothermal-isobaric diffusion annealing, the solute metal diffuses into solution and the liquid phase grows at the expense of the solid as mass is transferred across the solid/liquid interface. The mathematical framework for this problem is referred to in literature as a moving boundary diffusion or Stefan problem, and it has been used previously to study liquid diffusion in the Cd-Te [60] and Al-Cu systems [15, 24]. Also, it is used in other areas of research in metallurgical science such as transient liquid phase bonding, where the solid phase grows at the expense of the liquid phase via interdiffusion.

Using the SWLC method, Lee and Cahoon [15] and Tanaka and Kajihara [25] obtained interdiffusion data for the liquid Al-Cu system, however, there is a considerable discrepancy in the reported data with results that differ by as much as an order of magnitude for a given temperature

(see Figure 4). In the previous studies, the interdiffusion coefficient is assumed to be independent of concentration within the analysis. In this work, a mathematical model is developed that utilizes the existing framework of the Variable Space Network (VSN) method [33, 34, 35] to solve the Stefan problem. However, the VSN framework is modified to allow for concentration-dependent interdiffusion coefficient function, and the interdiffusion coefficient is shown to exhibit concentration dependence through statistical analysis. The best fit function that describes the concentration dependence of the interdiffusion coefficient is determined through *F*-testing nested candidate models. Overall, the concentration dependence of the interdiffusion coefficient is determined at temperatures of 993 K, 1043 K, 1093 K, 1143 K, and 1193 K, across a range limited by the liquidus of the binary phase diagram of approximately $Al_{100}Cu_0$ to $Al_{50}Cu_{50}$.

3.3. EXPERIMENTAL

The binary diffusion couples are constructed from Al and Cu wire with a diameter of 1 mm and purity of 99.999%. The long capillaries are manufactured from graphite rod, 12 mm in diameter and 110 mm in length, by drilling a 1 mm diameter blind hole into the center of the rod to a depth of 100 mm. Within the capillary, a 10 mm piece of Cu wire is placed at the bottom of the long capillary, followed by a 70 mm length of Al, leaving a 20 mm of void space for volumetric expansion of the Al upon melting. The planar interface of the diffusion couple is prepared to a 9 µm finish, followed by ultrasonic cleaning. A sketch of the diffusion couple can be seen in Figure 7. All materials are purchased and certified from Alfa Aesar, Thermo Fisher Scientific Inc.

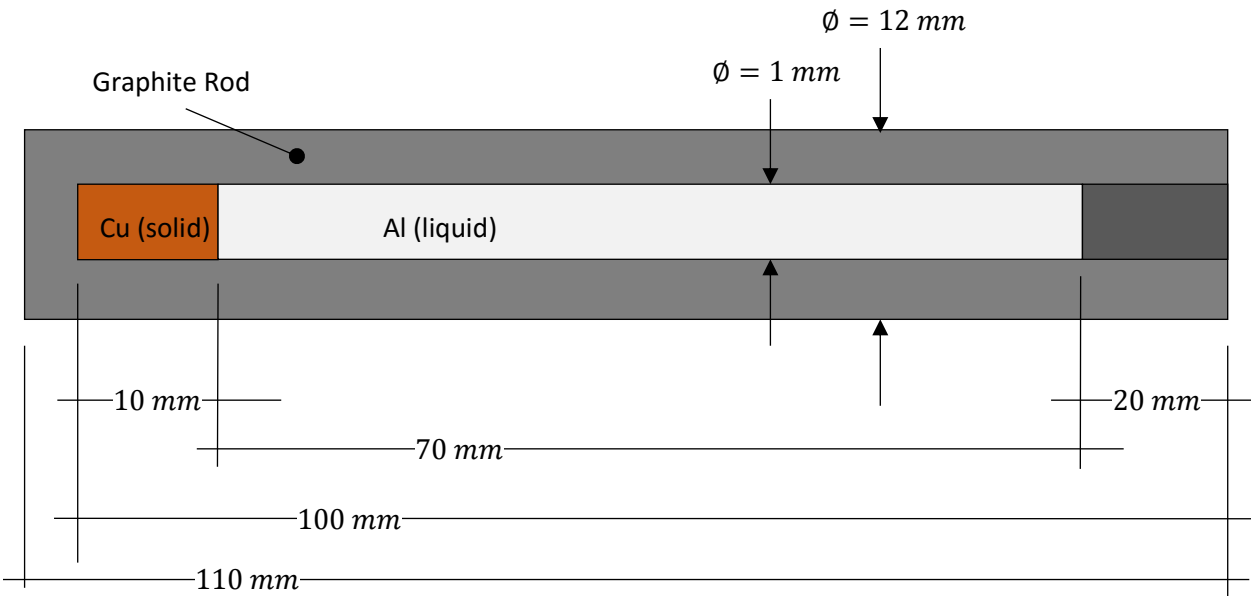

Figure 7 - Diffusion couple sketch.

In the present work, 11 diffusion couples are isothermally diffusion annealed within a vacuum furnace for a time t_f of 7200 s or 10800 s, over a temperature range of 993 K to 1193 K in 50 K increments. All experiments are conducted in a 1 bar atmosphere of ultra-high purity (UHP) Ar to minimize oxidation. The experimental test parameters by sample number are listed in Table 1, and a sketch of the vacuum furnace apparatus is shown in Figure 8.

Table 1 - Experimental test parameters used for each sample.

Sample	Isothermal Temperature, T_A (K)	Total Diffusion Time, t_f (s)
1	993	7200
2	993	7200
3	993	10800
4	1043	7200
5	1043	7200
6	1093	10800
7	1093	7200
8	1093	7200
9	1143	7200
10	1143	7200
11	1193	7200

For the experimental procedure, prior to heating, the vacuum furnace is evacuated and flushed with UHP Ar 3 times. During heating, the diffusion couple remains within the chilled zone of the furnace, and is lowered into the heated zone of the furnace via the stainless-steel rod when the furnace temperature stabilizes at the isothermal temperature T_A. The diffusion specimens are oriented in the vertical position within the furnace, with the Cu solute at the bottom of the

capillary to ensure the density gradient within the melt opposes gravity. In addition, a stabilizing vertical temperature gradient regulated to ~0.05 K per mm is maintained throughout the experiment to prevent density driven transport due to temperature inversion. The temperature gradient within the furnace at the sample location is monitored within using a 3-point thermocouple.

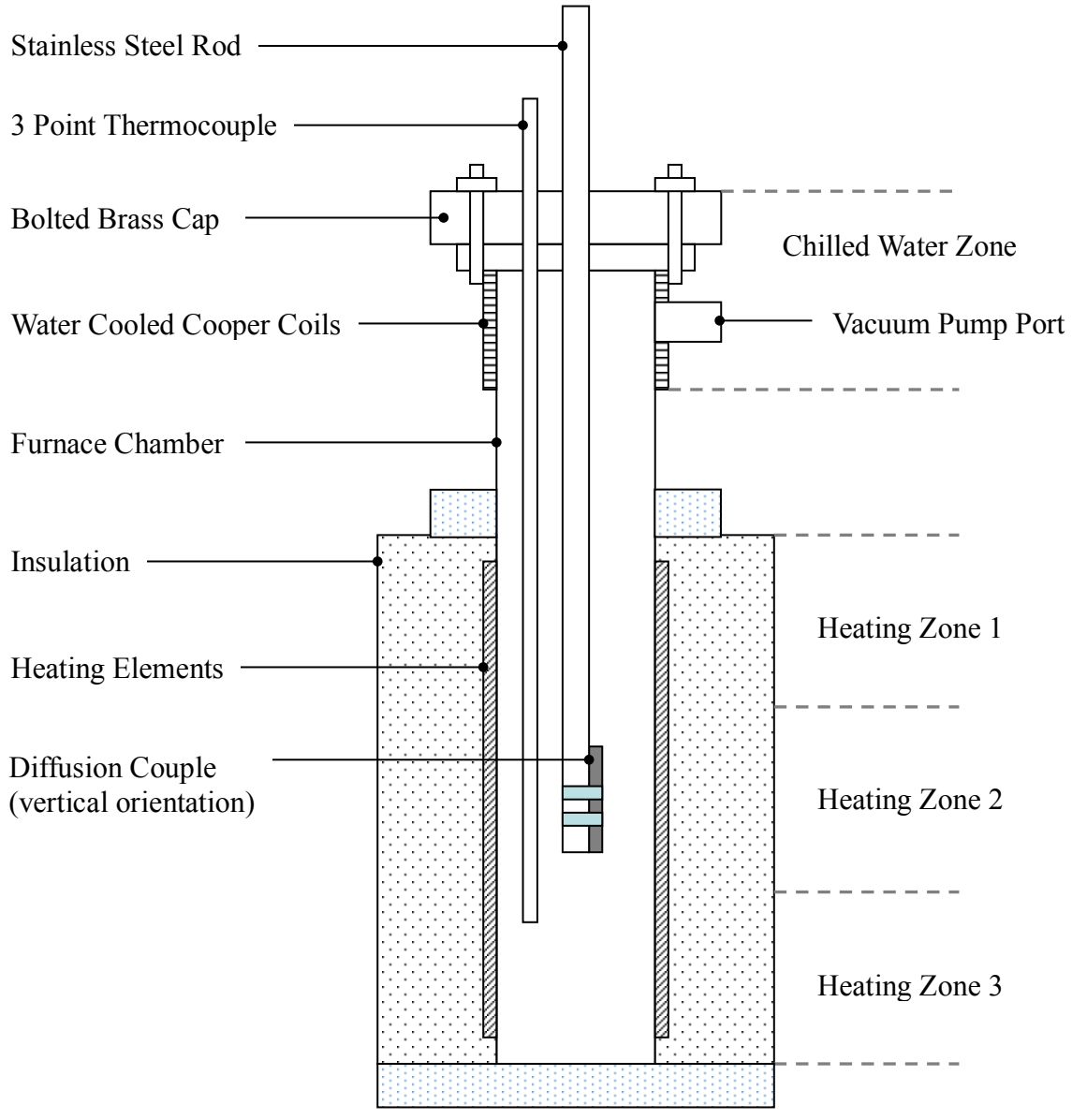

Figure 8 - Vacuum furnace sketch.

The solidified diffusion couples are cross-sectioned, mounted in plastic, and polished to a 1 micron finish. Quantitative compositional analysis is performed using a JEOL JSM-5900LV scanning electron microscope (SEM), equipped with an Oxford Instruments X-Max^N energy dispersive spectrometer (EDS) with a 80 mm^2 silicon drift detector. The concentration C versus distance profile x is determined by analyzing 1 mm distance increments along the length of the capillary, beginning at the location of Cu/Al interface. The average mole fraction concentration of Cu X_{Cu} per unit volume is taken to be the average concentration of a scanned area equal to the distance increment multiplied by the width of the capillary (i.e. 1 mm x 1 mm). The live time for each area scan is 180 s.

3.4. MATHEMATICAL DESCRIPTION OF THE SOLID-WIRE LONG CAPILLARY TECHNIQUE

In the mathematical description of the problem, the diffusion couple is modelled in a single plane only, with the positon vector $\boldsymbol{r}$ in Equation (3) set equal x. An Al-Cu diffusion couple of finite length within the region $0 \leq x \leq l$ initially consists of a domain of pure solid Cu, or α phase of concentration $C_{\alpha 0}$, and a region of pure liquid Al, or β phase of concentration $C_{\beta 0}$, separated at a planar interface s such that

$$C = C_{\alpha 0}, \qquad 0 \leq x \leq s^{-}(t), \qquad t = 0, \tag{69}$$

and

$$C = C_{\beta 0}, \qquad s^{+}(t) < x \leq l, \qquad t = 0. \tag{70}$$

During isothermal-isobaric diffusion annealing, a phase transformation occurs where the liquid β phase grows and becomes a heterogeneous mixture of Al and Cu as the α phase diffuses into solution, resulting in the migration of the solid/liquid interface. With the assumption that the phase

transformation is controlled by volume diffusion, the velocity of the solid/liquid interface ds/dt is given by the Stefan condition,

$$\left(C_{\alpha\beta} - C_{\beta\alpha}\right)\frac{ds}{dt} = D_\beta \left.\frac{\partial C_\beta}{\partial x}\right|_{x=s^+(t)} - D_\alpha \left.\frac{\partial C_\alpha}{\partial x}\right|_{x=s^-(t)}, \qquad x = s(t), \qquad t > 0 \tag{71}$$

where $C_{\alpha\beta}$ and $C_{\beta\alpha}$ are the equilibrium concentrations of the solid and liquid phases at the interface, C_α and C_β are the concentrations in the solid and liquid phases, D_α and D_β are the interdiffusion coefficients in the solid and liquid phases, x is the distance, t is the time, and $s^+(t)$ and $s^-(t)$ denote the solidus and liquidus side of the interface position, respectively.

The Stefan condition can be simplified recognizing that diffusion in the solid is typically several orders of magnitude slower than in the liquid, and the term $-D_\alpha \left.\frac{\partial C_\alpha}{\partial x}\right|_{x=s^-}$ becomes negligible values of $D_\alpha \ll D_\beta$. This simplifies Equation (71) such that

$$\left(C_{\alpha 0} - C_{\beta\alpha}\right)\frac{ds}{dt} = D_\beta \left.\frac{\partial C_\beta}{\partial x}\right|_{x=s^+(t)}, \qquad x = s(t), \qquad t > 0, \tag{72}$$

where the equilibrium concentration of the α phase at the interface $C_{\alpha\beta}$ (solidus) is set equal to the value of the pure Cu region

$$C_{\alpha\beta} = C_{\alpha 0}, \qquad 0 \le x \le s^-(t), \qquad t \ge 0, \tag{73}$$

as no interdiffusion in the solid is assumed to occur. The diffusion in the liquid β phase region is then described by the one-dimensional planar diffusion equation

$$\frac{\partial C}{\partial t} = \frac{\partial}{\partial x}\left(D_\beta \frac{\partial C}{\partial x}\right), \qquad s^+(t) < x \le l, \qquad t > 0 \tag{74}$$

and is subject to the Neumann boundary condition at the end of the finite diffusion couple where

$$\frac{\partial C}{\partial x} = 0, \qquad x = l, \qquad t \ge 0. \tag{75}$$

The evolution of the concentration versus distance profile with time for a typical diffusion couple is shown in Figure 9.

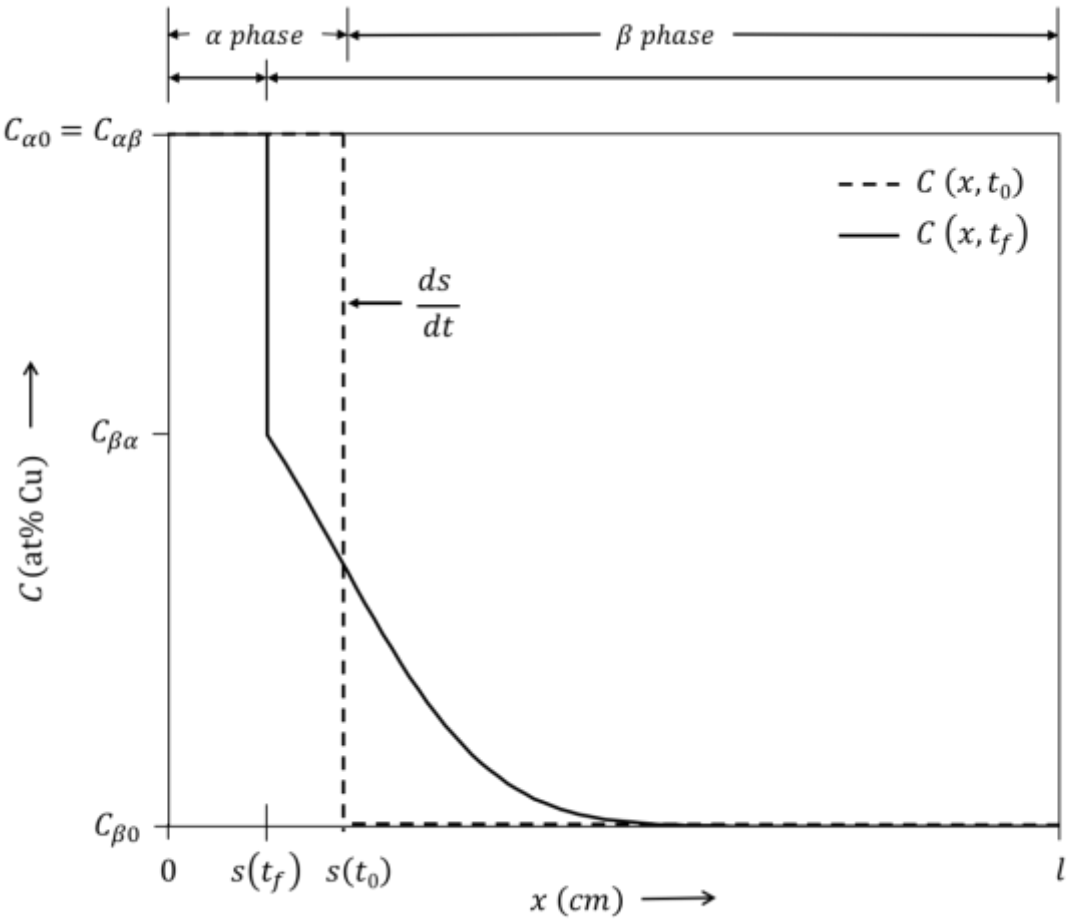

Figure 9 – The concentration *C* versus distance *x* profile for an A-B binary diffusion couple under isothermal and isobaric conditions, showing the initial $(t = 0)$ and final $(t = t_f)$ conditions, and the direction of the interface velocity ds/dt.

3.4.1. ANALYTICAL SOLUTION

An analytical solution exists [61] for the solid-wire long capillary technique provided the interdiffusion diffusion coefficient is constant, is of semi-infinite length $x \to \infty$, and the concentration at infinity remains constant $C(\infty, t) = C_{\beta 0}$. It can be shown that the location of the interface is given by

$$s(t) = s_0 + 2\omega\sqrt{t}, \tag{76}$$

where $s_0 = s(0)$ is the initial position of the interface, and the parameter α is defined as

$$\omega = \left(\frac{C_{\beta 0} - C_{\alpha\beta}}{C_{\beta\alpha} - C_{\alpha\beta}}\right)\sqrt{\frac{D_\beta}{\pi}}\frac{exp\left(-\frac{\alpha^2}{D_\beta}\right)}{erf\left(\frac{\alpha}{\sqrt{D_\beta}}\right)}. \tag{77}$$

The concentration distribution within the diffusion couple for $t > 0$ is then equal to

$$C(x,t) = \begin{cases} C_{\beta\alpha}, & 0 \le x < s^-(t), \\ C_{\beta 0} + \dfrac{(C_{\alpha\beta} - C_{\beta 0})erfc\left(\frac{(x - s_0)}{2\sqrt{D_\beta t}}\right)}{erfc\left(\frac{\omega}{\sqrt{D_\beta}}\right)}, & s^+(t) \le x < \infty. \end{cases} \tag{78}$$

3.4.2. NUMERICAL MODEL

When the liquid interdiffusion coefficient is dependent on concentration, no closed-form expression is known to exist for the problem [25] and a numerical method must be used to approximate the solution. For this purpose, the Variable Space Network (VSN) method [33, 34, 35] is applied, where the partial differential equations governing the model are replaced with finite difference approximations. In the finite difference method, a region is created on the xt-plane defined by the inequalities $s^+(t) \le x \le l$ and $0 \le t \le t_f$, where t_f is the total diffusion annealing time. Within the region is a mesh of vertical and horizontal lines that discretize distance and time, spaced Δx units and Δt units apart, respectively. If n and m are positive integers, the distance and time step are defined

$$\Delta x(t) = \frac{l - s(t)}{n} \quad and \quad \Delta t = \frac{t_f}{m}, \tag{79}$$

and the vertical and horizontal gridlines are defined by

$$x_i = i\Delta x(t), \quad i = 0, 1, \dots n \quad and \quad t_j = j\Delta t, \quad j = 0, 1, \dots, m. \tag{80}$$

The key feature of the VSN method is that the total number of distance steps n remains constant as the liquid β phase grows and the position of the interface changes with time. The distance step is therefore uniformly adjusted at each time step, allowing the interface to remain located at a constant gridline $i = 0$ for all j. The total change in concentration with time at each grid point under isothermal and isobaric conditions is therefore given by

$$\frac{dC_i}{dt} = \frac{\partial C}{\partial x}\Big|_{x=x_i} \frac{dx_i}{dt} + \frac{\partial C}{\partial t}\Big|_{x=x_i}, \tag{81}$$

where the velocity of each grid point is related to the velocity of the interface by

$$\frac{dx_i}{dt} = \frac{(l - x_i)}{(l - s)} \frac{ds}{dt}. \tag{82}$$

Combining Equations (81) and (82), provides a relationship for the diffusion equation at each grid point

$$\frac{dC_i}{dt} = \frac{\partial C}{\partial x}\Big|_{x=x_i} \frac{(l - x_i)}{(l - s)} \frac{ds}{dt} + \frac{\partial}{\partial x}\left(D_\beta \frac{\partial C}{\partial x}\right)\Big|_{x=x_i}, \qquad i = 1, 2, \dots, n. \tag{83}$$

It should also be noted that in this model, only the concentration in the domain of liquid β phase $s^+(t) \le x \le l$ is considered, as it is assumed that the solid α phase $0 \le x \le s^-(t)$ is of sufficient length that Equation (73) remains satisfied for the duration of the experiment.

Next, an explicit numerical solution for the problem with a truncation error of $\mathcal{O}(\Delta x^2) + \mathcal{O}(\Delta t)$ is developed, where the value of the concentration at any representative grid point $(x_i,\ t_j)$ is denoted as $C_{i,j}$, and the value of the time step and the interface position at time t_j are expressed as $\Delta x(t_j) = \Delta x_j$ and $s(t_j) = s_j$. In the algorithm, the initial condition of Equation (70) is written for each grid point where

$$C_{i,j} = C_{\beta 0}, \;\; i = 1, 2, \dots, n, \;\; j = 0, \tag{84}$$

with the boundary condition of Equation (70) at the interface

$$C_{i,j} = C_{\beta\alpha}, \;\; i = 0, \;\; j = 0, 1, \dots, m. \tag{85}$$

For each time step, the distance step is updated via

$$\Delta x_j = \frac{(l - s_j)}{n}, \;\; j = 0, 1, \dots, m, \tag{86}$$

where again $s_0 = s(0)$ is the initial position of the interface. The concentration at each internal grid point per Equation (83) is now written

$$\begin{aligned} C_{i,j+1} = C_{i,j} + \Delta t \Bigg[& \left(1 - \frac{i}{n}\right)\left(\frac{C_{i+1,j} - C_{i-1,j}}{2\Delta x_j}\right)\frac{ds}{dt} + \frac{\partial D_\beta}{\partial \mathrm{c}}\left(\frac{C_{i+1,j} - C_{i-1,j}}{2\Delta x_j}\right)^2 \\ & + D_\beta\left(\frac{C_{i+1,j} - 2C_{i,j} + C_{i-1,j}}{{\Delta x_j}^2}\right)\Bigg], \qquad i = 1, 2, \dots, n-1, \\ & j = 0, 1, \dots, m, \end{aligned} \tag{87}$$

where the interdiffusion coefficient is assumed to follow a continuous function such that $D_\beta = f(C)$. The velocity of the interface is determined using Equation (72)

$$\frac{ds}{dt} = \frac{D_\beta}{(C_{\alpha\beta} - C_{\beta\alpha})}\left(\frac{-3C_{\beta\alpha} + 4C_{1,j} - C_{2,j}}{2\Delta x_j}\right), \qquad j = 0, 1, \dots, m, \tag{88}$$

noting that second order forward difference is used to approximate the spatial derivative at the moving interface. At the last node, the boundary condition is considered resulting in a different form of Equation (83)

$$C_{i,j+1} = C_{i,j} + \frac{2D_\beta \Delta t}{{\Delta x_j}^2}(C_{i-1,j} - C_{i,j}), \qquad i = n, \qquad j = 0, 1, \dots, m. \tag{89}$$

The position of the interface is then updated at each time step using

$$s_{j+1} = s_j + \Delta t \frac{ds}{dt}, \qquad j = 0, 1, \dots, m. \tag{90}$$

A noted limitation of the explicit numerical solution is that it is not unconditionally stable, and is subject to a temporal constraint [35].

3.4.3. VOLUME CORRECTION

In the Al-Cu system the molar volume of the mixture is temperature and concentration-dependent in both the liquid and solid state as shown in Figure 10. In the model, the final concentration profile of the finite difference model with concentrations $C_{i,j=m}$ located at grid points $\left(x_i, t_{j=m}\right)$ for $i = 1, 2, \dots n$, represents the simulated diffusion couple at the isothermal temperature T_A. To compare the final concentration profile simulated *in-situ* with the experimental concentration observations C^{exp} obtained from a sample *ex-situ* (at room temperature), a correction must be made to account for the translation of the concentration profile resulting from the change in volume during solidification. Assuming the change in volume of the sample during solidification is isotropic, an adjustment is made to the location of each grid point such that a new position coordinate x_i' is defined

$$x_i' = x_0 + \Delta x_{j=m} \sum_{1}^{i} \cdot \left(\frac{V_{AB}^{T_{298K}}\big|_{\overline{C_{i,j}}}}{V_{AB}^{T_A}\big|_{\overline{C_{i,j}}}} \right)^{\frac{1}{3}}, \qquad i = 1, 2, \dots n, \qquad j = m, \tag{91}$$

where molar volume V_{AB} is evaluated at the average value of the concentration $\overline{C_{i,j}}$ within the distance step (note: the location of the grid point $x_0' = x_0 = 0$ remains unchanged). In Equation (91), $V_{AB}^{T_{298K}}\big|_{\overline{C_{i,j}}}$ and $V_{AB}^{T_A}\big|_{\overline{C_{i,j}}}$ are determined using the best-fit line for the liquid and solid phases

as shown in Figure 10. The concentration profile consisting of n concentrations $C_{i,j=m}$ located at grid points $(x_i', t_{j=m})$ is then fit to the experimental data by optimizing the value of the interdiffusion coefficient function using nonlinear regression.

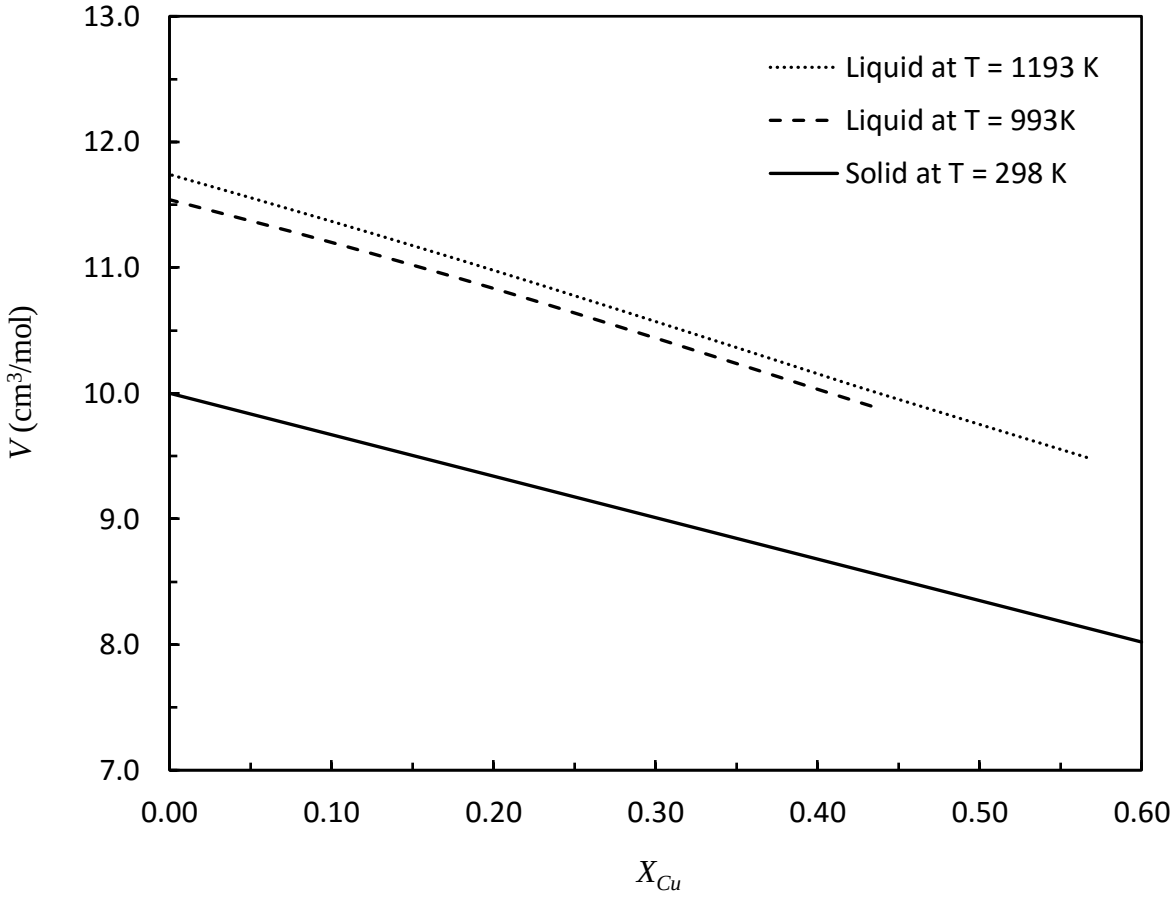

Figure 10 - Molar volume versus mole fraction for the Al-Cu system. Solid phase values calculated from Turnbull [62] and liquid phase values calculated using data from Brillo et al. [63].

3.4.4. INTERDIFFUSION COEFFICIENT FUNCTION, ERROR ANALYSIS, AND MODEL SELECTION

The interdiffusion coefficient is defined in terms of the continuous polynomial function

$$D_\beta(C) = \sum_{k=1}^{P} a_k {C_{i,j}}^{k-1}, \qquad for\ k = 1, 2, \dots, \wp \tag{92}$$

where a_k is the fitting parameter, up to $\wp$ parameters. By substituting Equation (92) into Equations (87) - (89), a candidate model $C(x', t, \boldsymbol{a})$ is created which depends on the volume corrected position variable x', the time t, and the vector-valued parameter $\boldsymbol{a} = (a_1, a_2, \dots, a_k)$. For each experimental data set, the candidate models are fit using nonlinear regression [64] where estimates of the parameter values are obtained by minimizing the residual sum of squares *S*

$$S(\boldsymbol{a}) = \sum_{l=1}^{N} w_l \left[C_l^{exp}\left(x_l^{exp}\right) - C\left(x' = x_l^{exp}, t_{j=m}, \boldsymbol{a}\right) \right]^2, \qquad for\ l = 1, 2, \dots, \mathcal{L}, \tag{93}$$

where C_l^{exp} denotes the experimental concentration measurement at distance x_l^{exp} up to $\mathcal{L}$ observations. Equation (93) assumes that the residual errors are normally distributed $\varepsilon \sim \mathcal{N}(0, \sigma^2)$. However, the measurement error obtained using EDS analysis is proportional to the concentration. This results in heteroskedastic error estimates across the length of the sample, which scale linearly with concentration if the operating parameters remain constant during the analysis (live time, accelerating voltage, etc.) as shown in Figure 11. To account for heteroskedasticity Equation (93) includes a weight factor w_l for each measurement that is proportional to the EDS error $w_l = 1/\sigma_l$. The details of nonlinear regression analysis are provided in Appendix A – Nonlinear Regression Analysis.

The Marquardt algorithm [65] is used to obtain the minimizer $\hat{\boldsymbol{a}}$ of the residual sum of squares, and the uncertainty in the interdiffusion coefficient is evaluated using the error propagation equation (delta method) with values from the error matrix. To select the most probable candidate model as described by Equation (92), an *F*-test is used to determine the optimum number of fitting parameters with a rejection probability of 5% i.e. $F_{(0.05,\wp-(\wp-1),\pounds-\wp)}$.

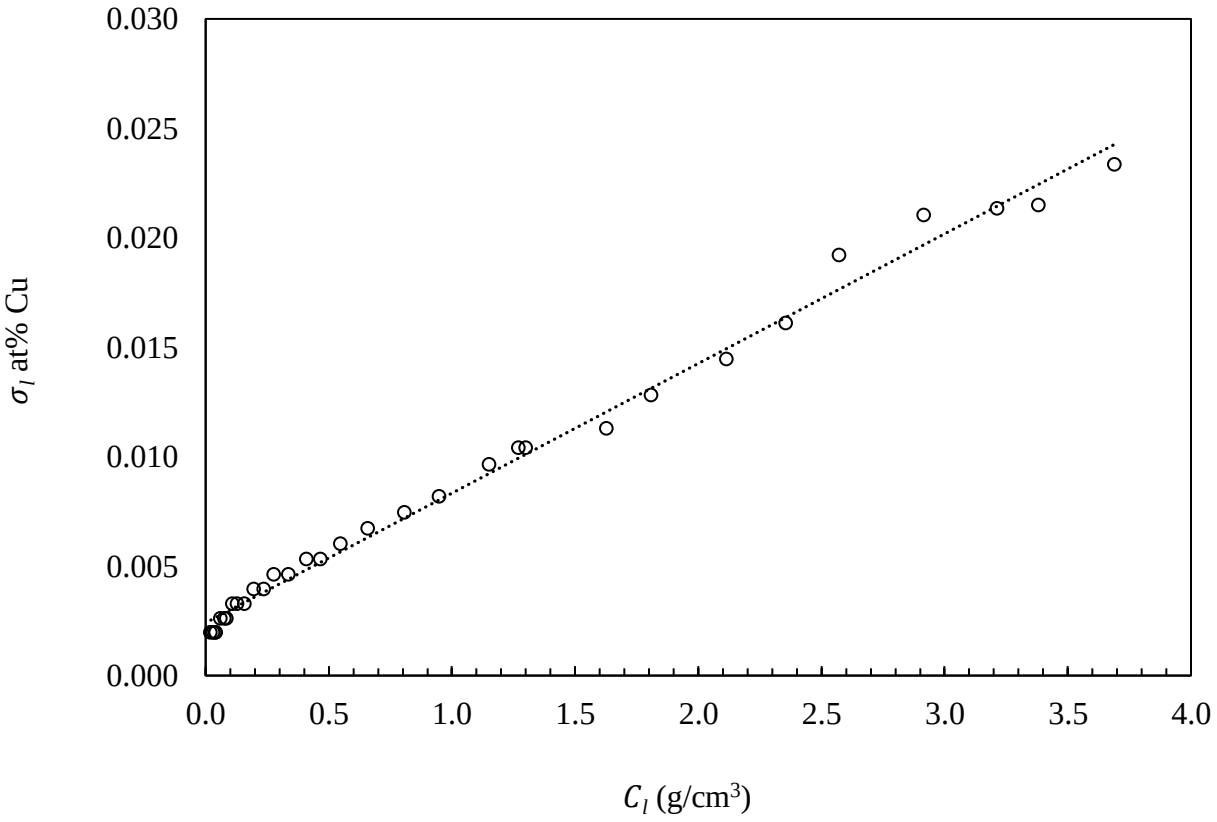

Figure 11 – Experimental EDS error versus concentration at T = 1093 K diffusion annealed for t = 7200 s. The dotted

3.5. RESULTS AND DISCUSSION

Before proceeding with the analysis of the experimental data, the finite difference numerical model is first tested to ensure that it approximates the analytical solution. In Figure 12, the relative error between the value of the concentration profile calculated by the finite difference numerical model C_{FD}, and the similarity solution C_{SS} are shown for a constant value of the interdiffusion coefficient such that $C_{error} = (C_{FD} - C_{SS})/C_{FD}$. The relative error is shown to approach zero as the mesh is refined i.e. increasing n and m subject to the distance and time step constraint. In the analysis of the experimental data, a mesh size of n (280) and m = (3600) is selected. This corresponds to an initial distance increment of $\Delta x(j = 0)$ = 0.025 cm and Δt = 2 s, and although further refinement of the mesh is possible, there is a tradeoff between error reduction and computational efficiency.

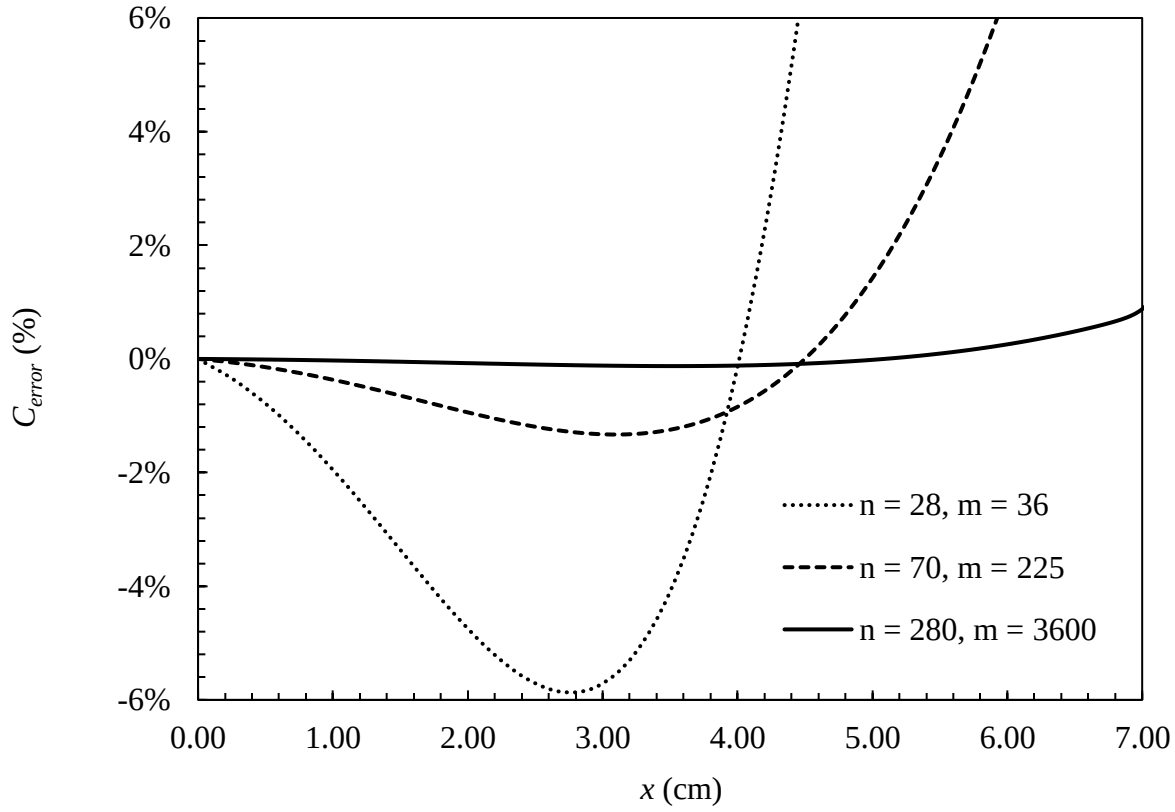

Figure 12 - Relative error in the value of the concentration C_{error} between the finite difference numerical solution and the similarity solution as a function of distance x for various mesh sizes for input parameters D_β = 7.5 x 10^{-5} cm^2/s $C_{\beta 0}$ = 1, $C_{\alpha\beta}$ = 0.5, and t = 7200 s.

When the diffusion equation is of the form given in Equation (74) the concentration C is defined in terms of mass density units. However, the quantitative experimental concentration measurements are obtained using electron microprobe analysis (EDS), where concentration is determined in mole fraction units (as density concentration units would require the additional measurement of lattice parameters). The relationship between mass density and mole fraction in a binary mixture is given by [66]

$$C_i = \frac{X_i M_i}{V_{AB}(X,T)}, \qquad i = A \text{ or } B \tag{94}$$

where C_i is the mass density concentration, X_i is the mole fraction, M_i is molar mass of the pure element, and $V_{AB}(X,T)$ is the molar volume of the mixture that is both concentration and temperature dependent. For small differences in concentration where the change in molar volume between the solvent and solute is assumed negligible the assumption $C_i \approx X_i$ is valid, and the interdiffusion coefficient obtained using either concentration units are approximately equal [66]. However, for large differences in concentration mass density units must be used. Therefore, the experimental mole fraction concentration units X_{Cu} are converted to mass density concentration units C_{Cu} using Equation (94). The molar volume of the mixture at room temperature is calculated from the data presented in Turnbull [62] shown in Figure 10 using $V_{AlCu}(X_{Cu}, 298) = 10.0 \cdot (1 - X_{Cu}) + 6.7 \cdot X_{Cu}$. In Table 2 the input parameter values used in the model are presented. Similarly the initial mass density concentrations $C_{\beta 0}$ and $C_{\beta\alpha}$ are calculated using Equation (94) with $V_{AlCu}(X_{Cu}, T_A) = V_{Cu}$ for pure Cu and $V_{AlCu}(X_{Cu}, T_A) = V_{Al} \cdot (1 - X_{Cu}) + V_{AlCu}^{C_{\beta\alpha}} \cdot X_{Cu}$ for the liquid Al-Cu alloy. The location of the liquidus phase equilibrium mole fraction concentration $X_{\beta\alpha}$ at the isothermal temperature T_A is shown on the Al-Cu binary phase diagram [67] in Figure 13.

Table 2 – Numerical Model Input Parameters

T_A (K)	$X_{\beta\alpha}$ -1-	V_{Al} (cm^3/mol) -2-	$V_{AlCu}^{X_{\beta\alpha}}$ at $X_{\beta\alpha}$ (cm^3/mol) -2-	V_{Cu} (cm^3/mol) -3-
993	0.434	11.540	9.394	7.382
1043	0.469	11.590	9.546	7.412
1093	0.503	11.640	9.703	7.442
1143	0.538	11.690	9.871	7.473
1193	0.567	11.741	10.019	7.504

1. The equilibrium liquidus mole fraction concentration $X_{\beta\alpha}$ is calculated using data from Murray [67].
2. The molar volume of liquid Al and the molar volume of the liquid Al-Cu mixture at the liquidus concentration $X_{\beta\alpha}$ is calculated using the data from Brillo et al. [63].
3. The molar volume of solid Cu is calculated using data from Davis [68].

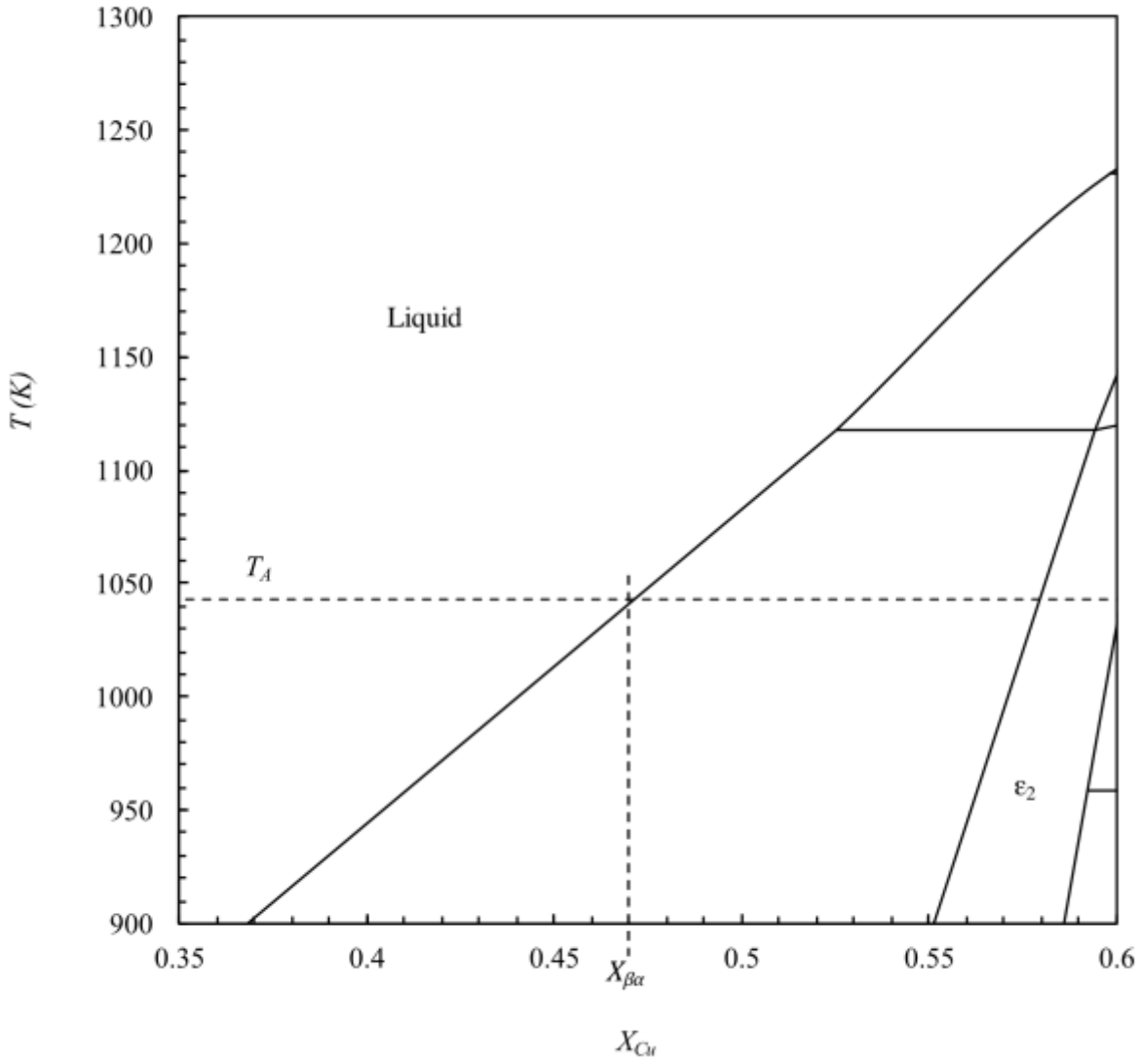

Figure 13 - The liquidus phase equilibrium mole fraction concentration $X_{\beta\alpha}$ at the isothermal temperature T_A is shown on an approximation of the Al-Cu phase diagram, created using data from Murray [67].

A micrograph for an experimental Al-Cu diffusion couple is shown in Figure 14 after diffusion annealing at T = 1043 K for t = 7200 s. The image shows the multi-phase region formed from the single-phase liquid Al-Cu β phase after solidification, and a region of solid Cu α phase, separated at a planar interface. Of note in the figure is the region of intermetallic compound layers that is formed by interdiffusion of the liquid into the solid phase. In the derivation of the model, it is assumed in Equation (72) that the interdiffusion of the liquid into the solid Cu phase is several orders of magnitude slower than the diffusion of the solid Cu phase into the liquid ($D_\alpha \ll D_\beta$), and that the contribution of the D_α term to the Stefan condition is therefore negligible. Experimentally, this assumption is proved reasonable in Figure 14 where the solid interdiffusion distance of 146 μm is significantly less than the liquid phase interdiffusion distance of approximately 3.50 cm, which implies D_α is of the order of 10^{-12} m^2/s (versus D_β that is of the order of 10^{-9} m^2/s).

An experimental concentration versus distance profile is shown in Figure 15 for an Al-Cu diffusion couple isothermally diffusion annealed at T = 1093 K, for t_f = 7200 s. In the figure, the experimental concentration measurements obtained using energy dispersive spectroscopy (EDS) are shown as open circles. Also in the figure, the best fit ex-situ solid phase concentration profile is shown as a solid line, which is calculated iteratively by minimizing Equation (93). In general, the experimental concentration measurements were found to exhibit minimal scatter, indicating that buoyancy driven convective mass transport is suppressed during experimentation [17].

In Table 3, the isothermal temperature, total diffusion annealing time, final interface shift, and the best fit parameter values for the interdiffusion coefficient function $D_\beta\big(C(x,t)\big)$ are presented for an experimental diffusion couple. The nomenclature used for the interdiffusion coefficient D_β is replaced with D_{AlCu} in the following discussion to correspond with the format used in Section 2.7.2. In Table 4, Table 5, and Table 6, the interdiffusion coefficient $D_{AlCu}(X,T)$

results with the corresponding standard deviations σ are presented for alloy concentrations of $Al_{\sim 100}Cu_{\sim 0}$, $Al_{80}Cu_{20}$, and $Al_{60}Cu_{40}$, respectively. The value of the interdiffusion coefficient $D_{AlCu}(C,T)$ can be calculated by substituting the best fit parameter values listed in Table 3 into Equation (92), and $D_{AlCu}(X,T)$ by converting mass density to mole fraction concentration units.

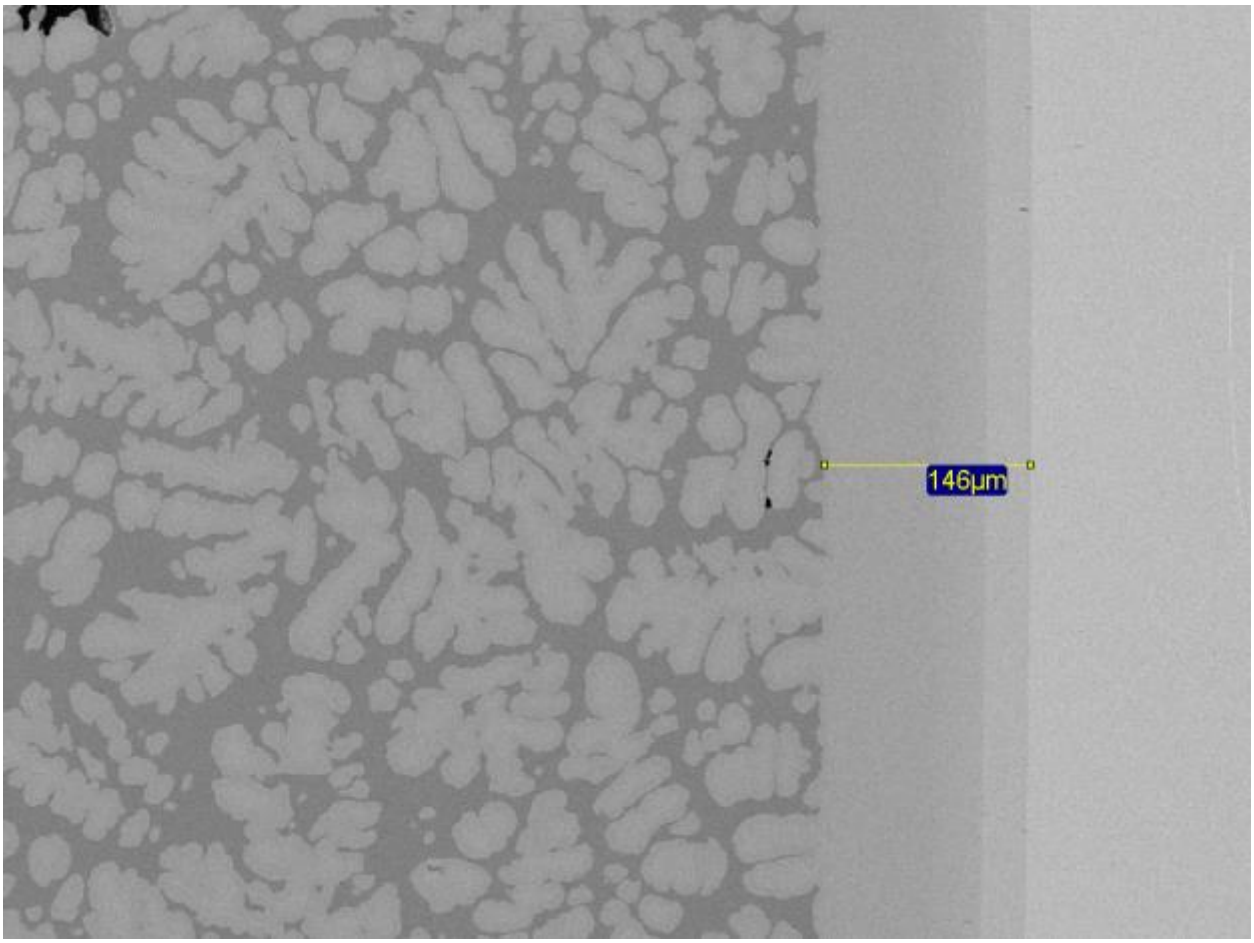

Figure 14 – The interface of the Al-Cu diffusion specimen after isothermal diffusion annealing at T = 1043 K and t_f = 7200 s. Separated by the interface is the Al-Cu β phase region (left), and the Cu α phase region (right). Within the Cu α phase region, intermetallic compound layers are visible, and have formed due to interdiffusion of the liquid into the solid phase during the diffusion anneal. The intermetallic compound layers are shown to extend into the Cu α phase a distance of 146 μm.

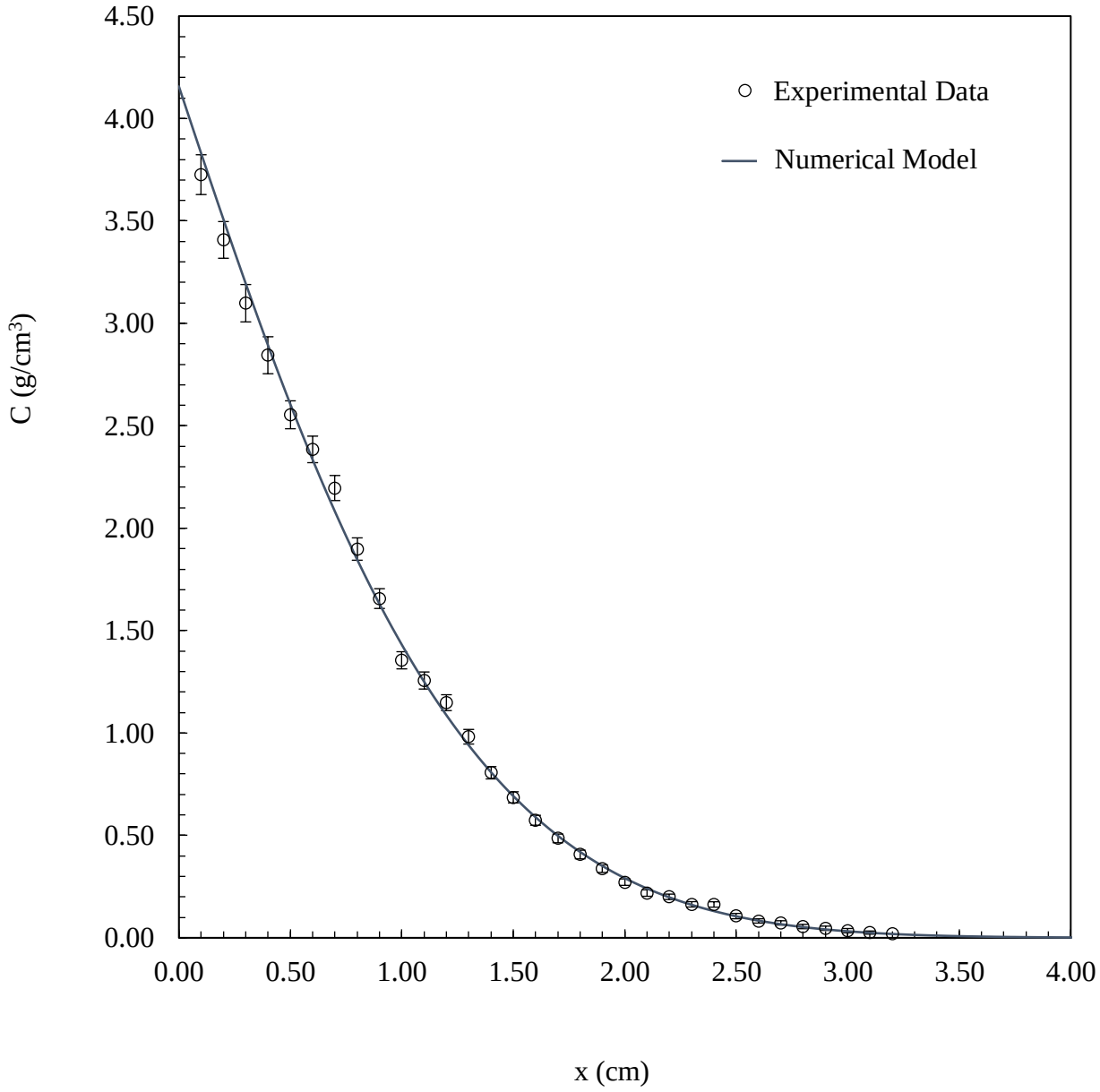

Figure 15 - Concentration C versus distance x profile for sample 8, isothermally diffusion annealed at T = 1093 K for t = 7200 s. In the experiment, the final location of the solid/liquid interface $s(t = 7200)$ has moved -0.293 cm from its original location at $s(\mathrm{t} = 0)$, due to the dissolution of solid Cu α phase into the liquid β phase region. In the figure, the final location of the solid/liquid interface $s(t = 7200)$ is assigned to x = 0 cm.

Table 3 – Best fit parameter values for the interdiffusion coefficient D_{AlCu} *(C, T)* and the final interface position for each experimental sample listed by temperature.

Sample	T_A (K)	t_f (s)	$s(t_f)$ (cm)	a_1*	a_2	a_3
1	993	7200	-0.216	7.095	-3.626	0.979
2	993	7200	-0.207	6.077	-1.154	
3	993	10800	-0.270	6.071	-1.177	
4	1043	7200	-0.256	8.182	-3.495	0.907
5	1043	7200	-0.256	8.045	-3.509	0.893
6	1093	10800	-0.381	8.209	-0.866	
7	1093	7200	-0.300	7.015	-0.488	
8	1093	7200	-0.293	7.096	-0.667	
9	1143	7200	-0.361	9.871	-1.202	
10	1143	7200	-0.360	9.095	-0.864	
11	1193	7200	-0.417	10.791	-2.876	0.717

*The fitting parameter values are in units a_k x 10^{-9} m^2/s.

Table 4 – The experimental interdiffusion coefficients $D_{AlCu}\ (X \sim 0.00,\ T)$ for dilute $Al_{\sim 100}Cu_{\sim 0}$.

Sample	T_A (K)	D_{AlCu} x 10^{-9} (m^2/s)	σ
1	993	7.10	0.42
2	993	6.08	0.17
3	993	6.61	0.23
4	1043	8.18	0.38
5	1043	8.04	0.40
6	1093	8.21	0.18
7	1093	7.02	0.17
8	1093	7.10	0.19
9	1143	9.87	0.17
10	1143	9.10	0.18
11	1193	10.79	0.30

Table 5 – The experimental interdiffusion coefficients $D_{AlCu}\ (X = 0.20,\ T)$ for $Al_{80}Cu_{20}$.

Sample	T_A (K)	D_{AlCu} x 10^{-9} (m^2/s)	σ
1	993	3.97	0.17
2	993	4.51	0.05
3	993	5.02	0.07
4	1043	5.11	0.18
5	1043	4.92	0.16
6	1093	7.03	0.06
7	1093	6.35	0.06
8	1093	6.19	0.07
9	1143	8.24	0.06
10	1143	7.92	0.07
11	1193	8.20	0.14

Table 6 – The experimental interdiffusion coefficients $D_{AlCu}\ (X = 0.40,\ T)$ for $Al_{60}Cu_{40}$.

Sample	T_A (K)	D_{AlCu} x 10^{-9} (m^2/s)	σ
1	993	4.88	0.78
2	993	2.70	0.17
3	993	3.18	0.19
4	1043	5.72	0.65
5	1043	5.42	0.55
6	1093	5.67	0.15
7	1093	5.59	0.15
8	1093	5.14	0.17
9	1143	6.35	0.13
10	1143	6.57	0.15
11	1193	8.51	0.19

In Figure 16 the interdiffusion coefficients listed in Table 4 are extrapolated to the tracer concentration of $Al_{\sim 100}Cu_{\sim 0}$, and are compared with the benchmark data presented in Section 2.7.2. The experimental results for the interdiffusion coefficient at this concentration are well described by the Arrhenius relationship with parameter values for activation energy of Q_0 = 20.85 $\pm$ 4.49 kJ/mol and frequency factor D_0 = 8.21 (+5.4, -3.26) x 10^{-8} m^2/s (noting that D_0 is log-normally distributed). These values agree well with the tracer diffusion values reported by Ejima et al. [26] with Q_0 = 23.8 $\pm$ 1.3 kJ/mol and D_0 = 1.05 $\pm$ 0.15 x 10^{-7} m^2/s, obtained using similar diameter capillaries with the capillary reservoir technique. Despite the limitations of the capillary reservoir technique [11], the values of the interdiffusion coefficient reported by by Ejima et al. [26] appear reasonable and do not appear to exhibit convective behavior at elevated temperatures, possibly due to the use of a 1.1 mm capillary diameter [17]. The results obtained by Lee and Cahoon [15] using the solid-wire technique have a greater slope with Q_0 = 33.8 $\pm$ 11.9 kJ/mol and a considerably higher value for the intercept at D_0 = 5.9 (+23.7, -1.46) x 10^{-7} m^2/s, noting that these results were obtained in 1.6 mm diameter capillaries. For long capillary experiments, Porth and Cahoon [17] and Lee et al. [18] have shown that capillary diameter $\mathcal{D}$ plays a critical role in the determination of liquid diffusion coefficients, and that convective mass transport due to density differences within the diffusion couple are neutralized as the capillary diameter is decreased. This can be explained based on a reduction in the thermal Rayleigh number Ra_T, which indicates the presence and strength of convection within a fluid body, with $Ra_T \propto \mathcal{D}^4$ for a cylinder. In Lee and Cahoon [15], it is possible the results obtained with the 1.6 mm diameter capillaries are inflated due to convective flow within the cylindrical liquid column.

It is also of interest to compare the results of the present study with those obtained by Tanaka et al. [24, 25], where the long capillary solid wire technique is used and a similar numerical analysis

is conducted. Examining Figure 16 it is evident that their reported values are substantially lower than the present findings. The results of Tanaka et al. [24, 25] are likely incorrect for several reasons. The first is the use of mole fraction as the unit of concentration in their analysis, rather than mass density units, violates conservation of mass across the solid/liquid interface. This is readily shown by substituting mole fraction units for mass density units into Equation (72). Second, the use of 8.5 mm capillaries is a large diameter for long capillary experiments, and should manifest as an increase in the value of the calculated interdiffusion coefficient. Third, the use of SiO_2 capillaries will result in additional error as liquid Al reduces $SiO_2 \rightarrow Al_3O_2 + Si$, introducing solid Si into the liquid column [69]. The presence of solid Si crystals within the liquid column would alter interdiffusion to an unknown extent. And fourth, the finite difference model developed and used by Tanaka et al. [24, 25] in their analysis assumed that molar volume was constant, and calculated the interdiffusion coefficient using mole fraction concentration units. As previously discussed and shown in Figure 10, molar volume in the liquid Al-Cu system is not constant and this assumption is not valid over the concentration range considered.

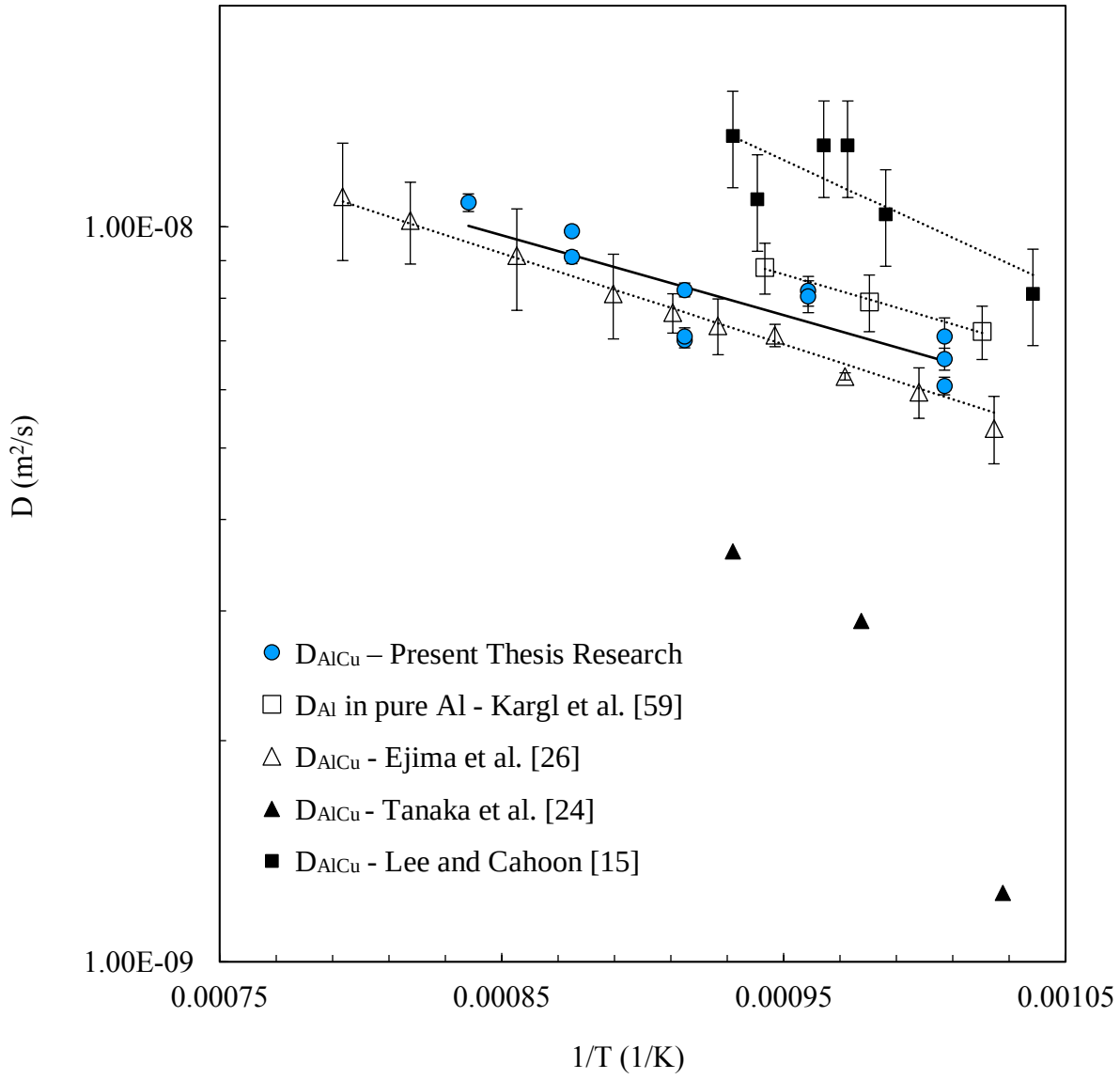

Figure 16 – An Arrhenius plot comparing values of the interdiffusion coefficient D_{AlCu} reported in literature to the present thesis research for the liquid Al-Cu system at the tracer concentration of $Al_{\sim 100}Cu_{\sim 0}$. In the figure, the ● represents the experimental interdiffusion coefficients D_{AlCu} determined in the present thesis research, the □ represents solvent self-diffusion D_{Al} for liquid Al reported in Kargl et al. [58], the △ represents tracer interdiffusion D_{AlCu} data of Ejima et al. [26], the ▲ represents the average value of the interdiffusion coefficient D_{AlCu} from Tanaka et al. [24], and the ■ represents the average interdiffusion coefficients D_{AlCu} determined by Lee and Cahoon [15]. The solid line — represents the best fit Arrhenius relationship for present thesis research, and the dotted line ⋯ represents the best fit Arrhenius relationship for past studies. Further information regarding the past studies is provided in Section 2.7.2.

Quasi-elastic neutron scattering data for self-diffusion in pure Al [58] are also shown for comparison in Figure 16, although it is only provided for a limited temperature range of 980 K (1/T = 0.00102 1/K) to 1060 K (1/T = 0.00094 1/K). The activation energy is determined as Q_0 = 21.63 $\pm$ 1.43 kJ/mol and frequency factor D_0 = 1.02 (+0.18, -0.16) x 10^{-7} m^2/s, in keeping with the phenomenological prediction for the activation energy of $Q_0 = 3.16 \cdot R \cdot T_m$ = 24.52 kJ/mol for pure Al at T_m = 933.44 K [7]. Experimental self-diffusion data are difficult to obtain due to the lack of a stable radioactive isotope for tracer diffusion experiments, and to the best of the author's knowledge reference [58] is the only known study available (excluding molecular simulation models). Overall, the activation energy for self-diffusion in pure Al is similar to that found in the present research for the interdiffusion in dilute Al-Cu alloy, with only a slightly lower value for the frequency factor.

In Figure 17, as well as in Table 5, the interdiffusion coefficients determined in the present research at a concentration of $Al_{80}Cu_{20}$ are shown, and the best fit Arrhenius relationship parameter values are Q_0 = 34.41 $\pm$ 3.71 kJ/mol and D_0 = 2.84 (+1.47, -0.97) x 10^{-7} m^2/s. In the figure, the best fit Arrhenius line (dashed) is extended from the experimental temperature range of 993 K (1/T = 0.00101 1/K) to 1193 K (1/T = 0.00084 1/K), to the liquidus temperature at approximately 821 K (1/T = 0.00122 1/K). The extended trend line is shown to be in range of the interdiffusion coefficient value determined by Lee et al. [18] at the eutectic composition of $Al_{82.6}Cu_{17.4,}$ determined from directional solidification measurements in a 0.8 mm capillary (note: the determination of the trend line does not include the data of Lee et al. [18]) The finite column results of Lee and Cahoon [15] and the time-resolved x-ray radiography of Zhang et al. [22, 21] are also found to be in mutual agreement, but are higher than those determined in the present investigation. In these studies, similar capillary diameters of 1.6 mm and 1.5 mm are used,

respectively. The activation energy in Zhang et al. [22, 21] is quoted at Q_0 = 31.84 kJ/mol, which is within the limits of error of the present work, but differs with a larger value for the frequency factor of D_0 = 3.7 x 10^{-7} m^2/s.

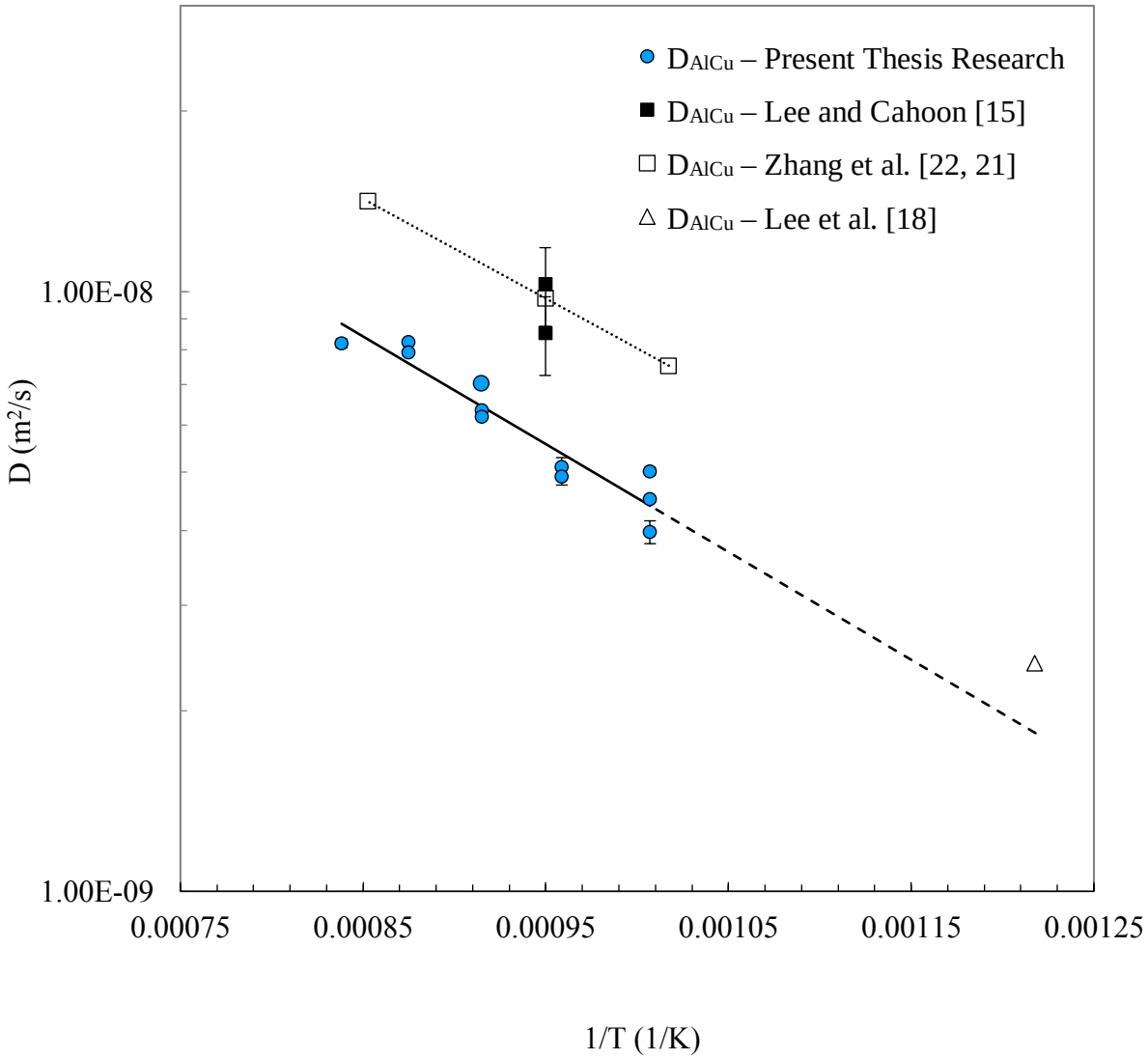

Figure 17 - Arrhenius plot for interdiffusion in $Al_{80}Cu_{20}$. In the figure, the ● represents the experimental interdiffusion coefficients D_{AlCu} of the present thesis research, and the solid black line — represents the best fit Arrhenius line. The dashed line --- is an extrapolation of the best fit Arrhenius line to the liquidus temperature at approximately 821 K (1/T = 0.00122 1/K). The results of past experimental studies are shown for comparison, where the ■ are the values of the interdiffusion coefficients D_{AlCu} obtained by Lee and Cahoon [15], the □ by Zhang et al. [22, 21], and the △ by Lee et al. [18]. Also in the figure, the dotted line ⋯ is the best fit Arrhenius line for the data of Zhang et al. [22, 21].

Zhang et al. [22, 21] discuss their experimental findings for the interdiffusion coefficient in terms of the Darken equation, $D_{AB}(X,T) = D^0_{AB}(X,T) \cdot \Phi(X,T)$. In their analysis, they conclude that dynamic cross-correlations in the MS diffusivity coefficient $D^0_{AB}(X,T)$ in Equation (58) may not be negligible, and may scale the interdiffusion coefficient by a factor of 2. In their analysis, it is assumed that the self-diffusion coefficients of Al and Cu are of similar value $D_{Al} \approx D_{Cu}$, which is supported by QNS data that shows that the coherent correlations decay in a single exponential manner [59]. The assumption of approximately equal self-diffusion coefficients is also supported by MD simulation where studies show that while the self-diffusion coefficients are similar in the Al rich portion of the liquid Al-Cu system [23, 56], while noting the Al self-diffusion coefficient D_{Al} is found to be slightly larger than the Cu self-diffusion coefficient D_{Cu} when taken at the same temperature and concentration (see Figure 19).

In the present thesis research, values for the MS diffusivity coefficient D^0_{AlCu} are calculated using the Darken equation, and are shown in Figure 18. For the calculation of D^0_{AlCu}, it is assumed that the velocity cross-correlations are negligible as in Equation (61), and the value of the thermodynamic factor $\Phi(0.20,T)$ is assumed to be approximately equal to ~1.5 over the temperature range considered [30]. In Figure 18 it is evident that the calculated values for the MS diffusivity coefficient D^0_{AlCu} are close in value to the best fit D_{Cu} trend line determined by Brillo et al. [59]. Noting that the self-diffusion coefficients for Cu D_{Cu} are slightly less than D_{Al} [23, 56], the value of the interdiffusion coefficient $D_{AB}(X,T)$ determined in the present thesis research suggest that the dynamic velocity cross-correlations of atomic motions do not contribute significantly to interdiffusion, and can be considered negligible at this concentration ($Al_{80}Cu_{20}$). A similar conclusion was reached by Horbach et al. [19] for interdiffusion in the liquid Al-Ni system at a composition of $Al_{80}Ni_{20}$. The Al-Ni system is thermodynamically analogous to the Al-

Cu system, with an Al-rich eutectic, strongly ordered intermetallic phases, and negative excess Gibbs free energy in the liquid. In their study, which used a combination or long capillary and molecular dynamics simulation, Horbach et al. [19] determined the effect of the velocity cross-correlations had the opposite effect and decreased the interdiffusion coefficient, however, only by a small scalar factor in the range of 0.8 to 1 [70].

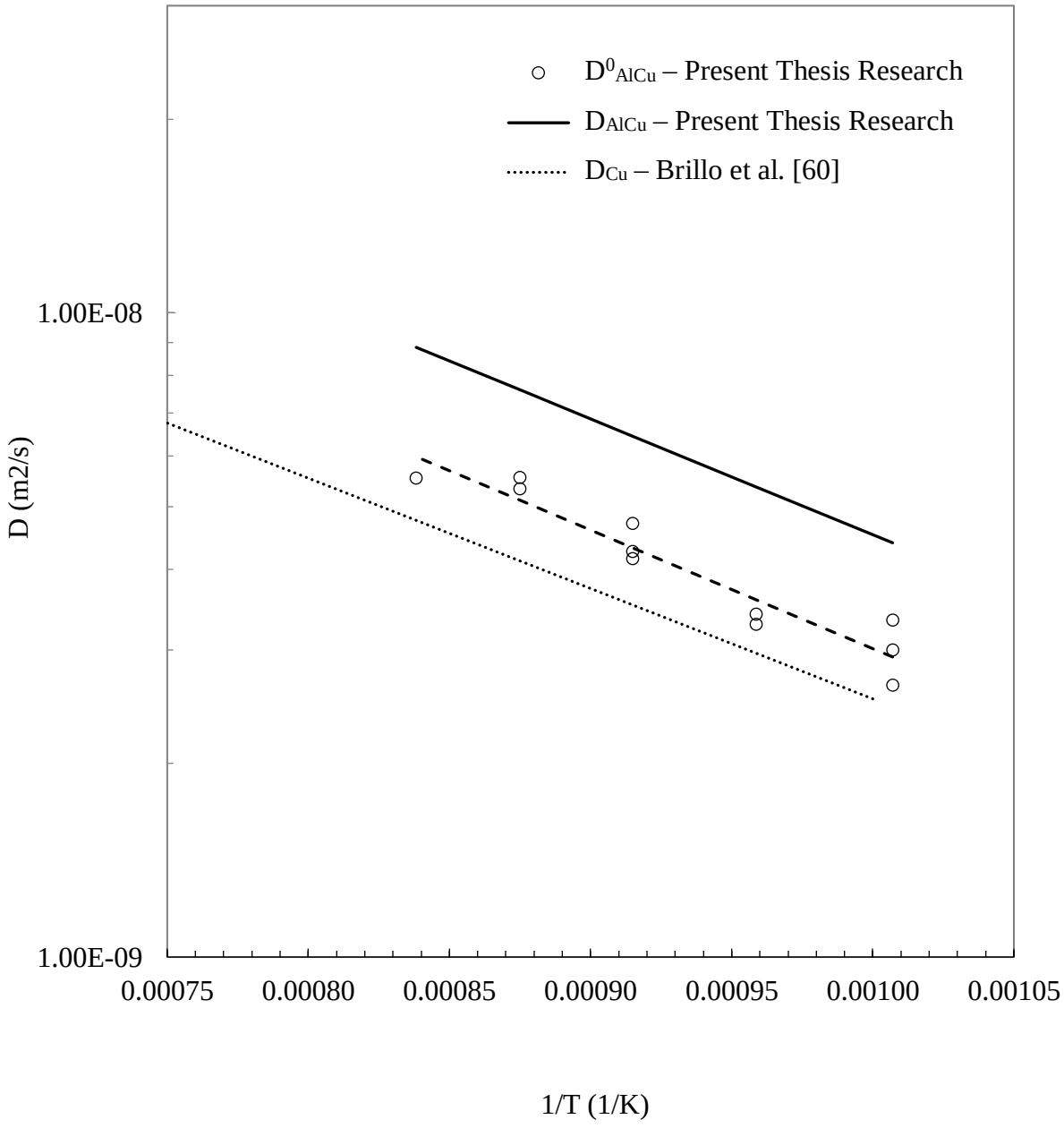

Figure 18 - Arrhenius plot for diffusion in $Al_{80}Cu_{20}$. In the figure, the solid line — is the best fit Arrhenius relationship for D_{AlCu} determined by the present thesis research. The open circles ○ are the MS diffusivity coefficients D^0_{AlCu} calculated from the results of this research, and the dashed line --- is the best fit Arrhenius relationship for D^0_{AlCu}. The dotted line ⋯ is the best fit data for Cu self-diffusion D_{Cu} from Brillo et al. [59].

The last alloy concentration considered in the present thesis research is $Al_{60}Cu_{40}$, and the experimental results are summarized in Table 6 and plotted in Figure 19. Again, the relationship between the interdiffusion coefficient and temperature can be described in terms of Arrhenius equation, noting that the interdiffusion data exhibit increased scatter at low temperature. Consequently, the best fit parameter values present with greater uncertainty relative to those found at lower concentrations, with Q_0 = 38.74 $\pm$ 8.01 kJ/mol and D_0 = 4.03 (+5.89, -2.39) x 10^{-7} m^2/s. Figure 19 also shows the best fit Arrhenius relationship for interdiffusion reported by Cheng et al. [23], which was obtained using a molecular dynamics simulation with an embedded atom method (EAM) interatomic potential developed by Cai and Ye [27]. It is important to note, however, that the EAM potential used in Cheng et al. [23] was developed for Al-Cu alloys in the solid state, and should not be expected to accurately reproduce the thermodynamic properties of the liquid [28]. There is a considerable difference between the values of interdiffusion coefficient D_{AlCu} determined in the present thesis research, and those obtained by Cheng et al. [23] using MD simulation with an approximate error of 119%. A possible explanation for the error could be the use of an EAM interatomic potential that was not developed for the liquid state.

Evaluating the SWLC interdiffusion data for $Al_{60}Cu_{40}$ in terms of the MS diffusivity $D^0_{AlCu}(0.40,T) = D_{AlCu}(0.40,T)/\Phi(0.40,T)$ reveals additional insight, where the value of the thermodynamic factor for $Al_{60}Cu_{40}$ is taken from Figure 3 with values ranging from $\Phi(X = 0.40, T = 993\ K) = 3.38$ to $\Phi(X = 0.40, T = 1193\ K) = 2.93$. From Figure 19, it is evident that the values of the MS diffusion coefficients D^0_{AlCu} determined by the present thesis research are lower than those obtained by Wang et al. [56] when it is assumed that the Maxwell-Stefan diffusion coefficient is the simple linear combination of the self-diffusion coefficients $D^0_{AB} = X_B D_A + X_A D_B$. Another possibility though, is that the velocity cross-correlation functions

are not negligible in $Al_{60}Cu_{40}$, and that they contribute to the value of the interdiffusion coefficient as described by Equation (58). However, given the increased error associated with the calculation of the interdiffusion coefficient at this concentration (specifically at low temperatures), possible uncertainty regarding the value of the thermodynamic factor at this concentration, and the limited data available for both self- or interdiffusion, it is difficult to quantify the contribution the velocity cross-correlation functions, if it exists.

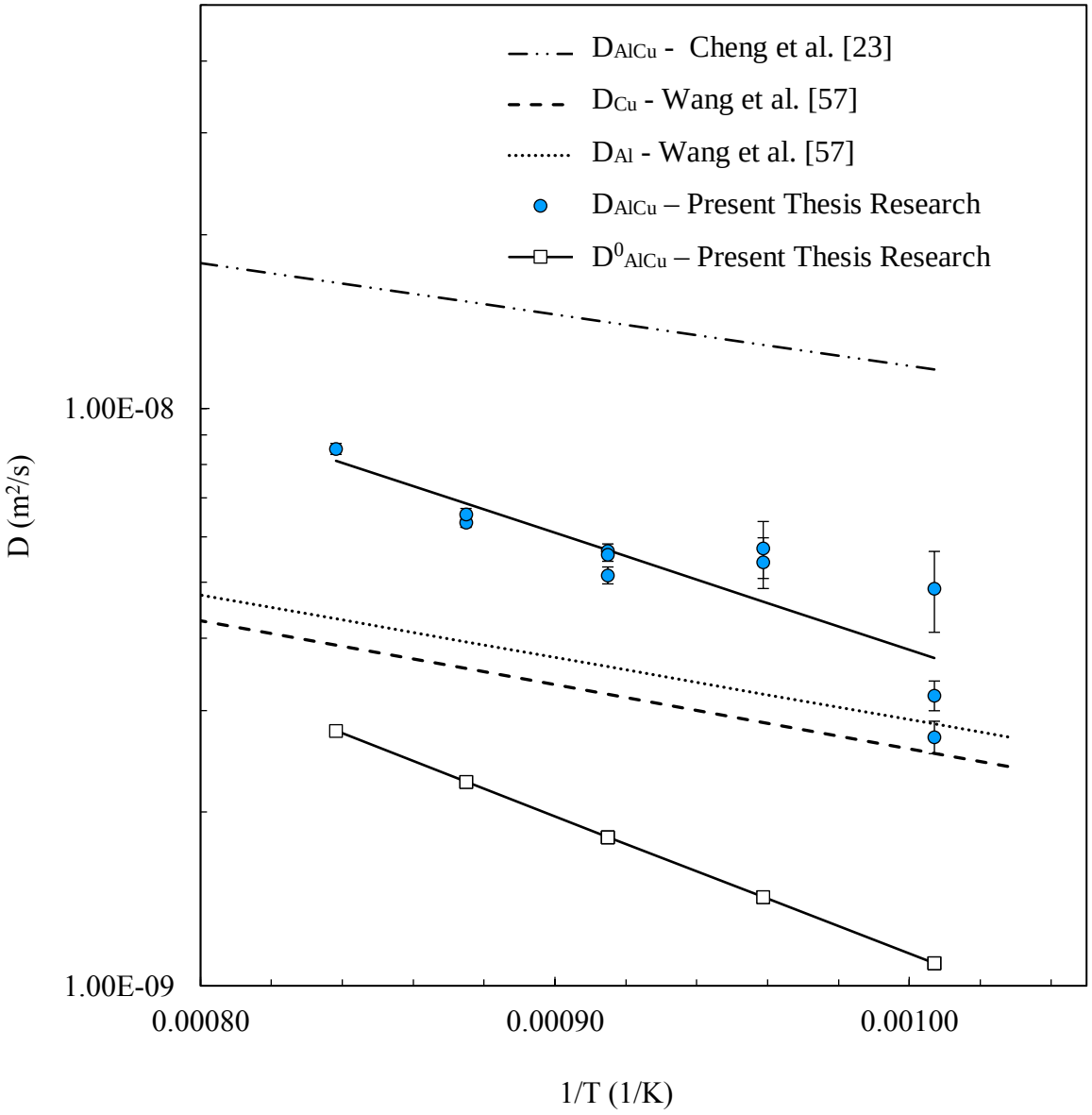

Figure 19 – An Arrhenius plot for self- and interdiffusion in $Al_{60}Cu_{40}$. In the figure, the ● represents the experimental interdiffusion D_{AlCu} coefficients, the □ the MS diffusion D^0_{AlCu} coefficients (for negligible velocity cross-correlations), and the solid black line — represents the best fit Arrhenius relationship determined in the present thesis research using the SWLC method. Also in the figure, the dashed --- and dotted ⋯ lines represent the best fit self-diffusion coefficients D_{Cu} and D_{Al}, respectively, as reported by Wang et al. [56]. The broken line ⋯ – represents the best fit Arrhenius relationship for the interdiffusion coefficient D_{AlCu} as determined by Cheng et al. [23].

A review of the experimental findings determined by the present thesis research using the SWLC method shows that the temperature dependence of the liquid interdiffusion coefficient is well described by the Arrhenius relationship at constant concertation, over the temperature range of 993 K to 1193 K and at the concentrations of $Al_{\sim 100}Cu_{\sim 0}$, $Al_{80}Cu_{20}$, and $Al_{60}Cu_{40}$ for the Al-Cu considered. From the Arrhenius relationship, the best fit parameter values for the activation energy Q_0 and frequency factor D_0 are both found to increase with the concentration of Cu in the liquid, suggesting a complex, nonlinear relationship between concentration, temperature, and the interdiffusion coefficient. When the SWLC interdiffusion data is analyzed in the context of Darken's equation using values for the thermodynamic factor from Figure 3, the dynamic velocity cross-correlations of atomic motions are found to not contribute significantly to interdiffusion at $Al_{80}Cu_{20}$, but may contribute to the value of the interdiffusion coefficient at the composition $Al_{60}Cu_{40}$ (albeit to an unknown extent). The thermodynamic factor, however, is shown to contribute the value of the interdiffusion coefficient for $Al_{80}Cu_{20}$, and is representative of the effect of the associative liquid structure in the Al-Cu system (as inferred from the excess Gibbs free energy of solution [30]). The effect of liquid structure, or chemical ordering, is not unique to the liquid Al-Cu system, and may influence diffusion in other pure or binary liquid metal system.

Some non-simple pure metals, such as Sn, Si, and Ge exhibit chemical ordering within the liquid state [71, 16]. For example, in liquid Sn it has been suggested that the quasi-permanent tetrahedral element randomly forms and dissociates with a frequency on the order of picoseconds [72]. In binary liquid metal mixtures, Turnbull [62] comments on the possibility of chemical order or "clustering" phenomena occurring with dilute additions of Fe or Ti to liquid Al, where a single Fe or Ti atom bounds 7 or 35 Al atoms at 700°C and 800°C respectively. Fe is found to diffuse significantly slower than Cu, Ni, or Al within Al [15, 73], and Isono et al. [73] suggest that because

Fe and Cu have similar masses, the difference in diffusivity must be attributed to cluster formation involving solute and solvent atoms in the liquid. Similarly, C is found to diffuse at the same rate in liquid Fe as most other solute atoms [74], however, it diffuses rapidly within the solid via an interstitial mechanism. Cahoon calculated the first coordination number of Fe in the liquid as 7.7 as compared to 8 in the solid [75], which suggests that an interstitial diffusion path is still available in the liquid. This implies that in liquid Fe, C may be bound in atomic clusters which are much slower to diffuse through the melt. Comparable observations are made for Ag and Au in liquid Pb. In the solid, both solutes diffuse rapidly via an interstitial mechanism where the rate of diffusion is ~3 orders of magnitude higher than that of Pb solvent self-diffusion [38]. However, in the liquid both Ag and Au diffuse at the same rate as Pb in liquid Pb [76, 77]. Also, a non-simple temperature dependence of the diffusion coefficient may be evident in the Bi-Sn [17] and Au-Pb [77] binary systems. Diffusion data for the interdiffusion of Bi in Sn and Au in Pb at low concentrations show anomalous findings at temperatures near the melting point, where diffusion is found to decrease with increasing temperature.

3.6. SUMMARY

In this chapter interdiffusion in the liquid Al-Cu binary system was investigated at temperatures of 993 K, 1043 K, 1093 K, 1143 K, and 1193 K, across a concentration range limited by the liquidus of the binary phase diagram. The interdiffusion coefficients were obtained using the solid wire long capillary (SWLC) technique. In the analysis, a coupled set of non-linear differential equations forming a moving boundary diffusion (Stefan) problem was solved numerically using a finite difference scheme, that considered a concentration-dependent interdiffusion coefficient, and corrected for the change in volume of the diffusion couple that occurs upon solidification from the liquid state. The concentration dependence of the interdiffusion coefficient was quantified using a polynomial fitting function, where the optimum number of parameters were selected using an F-test. Concentration profiles exhibited minimal scatter, indicating that interdiffusion coefficients are accurate and are not inflated due to buoyancy driven convective mixing within the capillary.

In general, interdiffusion is well described by the Arrhenius relationship over the temperature interval considered at a given concentration. At the tracer concentration of $Al_{\sim 100}Cu_{\sim 0}$, interdiffusion is well described by the Arrhenius relationship with best fit parameters for the activation energy of Q_0 = 20.85 $\pm$ 4.49 kJ/mol, and for the frequency factor D_0 = 8.21 (+5.4, -3.26) x 10^{-8} m^2/s. At the concentration $Al_{80}Cu_{20}$, interdiffusion is again well described the Arrhenius relationship with best fit parameter values of Q_0 = 34.41 $\pm$ 3.71 kJ/mol and D_0 = 2.84 (+1.47, -0.97) x 10^{-7} m^2/s. At an increased concentration of $Al_{60}Cu_{40}$, however, experimental data are subject to increased scatter resulting in greater error in the value Arrhenius relationship best fit parameters used to describe interdiffusion, with Q_0 = 38.74 $\pm$ 8.01 kJ/mol and D_0 = 4.03 (+5.89, -2.39) x 10^{-7} m^2/s. The Arrhenius relationship best fit parameter values for activation energy Q_0

and frequency factor D_0 are both found to increase with increasing Cu concentration, suggesting a complex, nonlinear relationship between concentration, temperature, and the interdiffusion coefficient.

4. MOLECULAR DYNAMICS SIMULATION OF DIFFUSION IN THE AL-CU SYSTEM USING A CONCENTRATION-DEPENDENT EMBEDDED ATOM METHOD INTERATOMIC POTENTIAL

Molecular dynamics (MD) is a computer simulation method based in statistical mechanics that can be used to model the dynamic evolution of a *N*-body atomic system by solving the classical Newtonian equations of motion. In a MD simulation, the force interactions between particles are controlled by classical approximations of the electronic structure, using theoretical or semi-empirical interatomic potential models that consider the spatial derivative of the potential energy function. The time evolution of the simulation can be used to determine macroscopic thermodynamic properties of the system, and dynamical properties, including transport coefficients. In this chapter, Darken's equation for interdiffusion in a binary mixture is further examined using MD simulation with an embedded atom method (EAM) interatomic potential. Using a molecular dynamics simulation approach, the self-diffusion coefficients and thermodynamic factor are calculated separately, and from this the interdiffusion coefficient is determined. The MD results for the self- and interdiffusion coefficients are then compared to the experimental results obtained using the solid wire long capillary (SWLC) method in Chapter 3, as well as the benchmark data presented in Section 2.7.2.

Relatively sparse literature exists regarding the simulation of interdiffusion in liquid Al-Cu alloys using MD simulations, Monte Carlo methods, or first principles ab-initio simulations. An exception is the study by Cheng et al. [23], which is introduced in Chapter Section 2.7.2 where the interdiffusion coefficient for the Al-Cu system is determined using MD simulation with an EAM potential. There are several limitations of the work of Cheng et al. [23], and they are briefly outlined next. First, the analysis is limited to the liquid $Al_{60}Cu_{40}$ over an extended temperature

range. Second, to calculate the interdiffusion coefficient, Cheng et al. [23] use self-diffusion data obtained from MD simulation, and calculate the thermodynamic factor with data that is external to the simulation (from a thermodynamic database). If the thermodynamic factor determined by the simulation does not coincide with the MD simulation data, this will result in a failure to accurately model the actual thermodynamics of the mixture within the simulation, possibly leading errors in the determination of self-diffusion coefficients. Third, in Cheng et al. [23] the interatomic potential used in the simulation was originally developed by Cai and Ye [27] for the solid-state. However, recently Becker et al. [28] has commented on the importance of using interatomic potentials developed specifically for the physical state of the system under consideration (i.e. the liquid-state in Cheng et al. [23]).

Therefore, the focus of Chapter 4 is to extend the research by Cheng et al. [23] and address the possible limitations of their work. In the current research, the concentration and temperature range is expanded, including self- and interdiffusion in dilute $Al_{\sim 100}Cu_{\sim 0}$, the $Al_{80}Cu_{20}$, and the $Al_{60}Cu_{40}$ over the temperature range 993 K – 1493 K. In addition, the thermodynamic factor used in this work is reproduced by the simulation data. Further, in this study a new EAM interatomic potential for simulation of the Al-Cu system in the liquid-state is developed by combining the individual Al and Cu EAM potentials of Mendelev et al. [70], and the thermodynamic properties of the liquid mixture are replicated by fitting the excess enthalpy of mixing using concentration-dependent EAM (CD-EAM) developed by Caro et al. [36]. The self- and interdiffusion coefficients calculated in this Chapter are then compared to the benchmark data of Chapter 2 and the SWLC experimental results of Chapter 3.

4.1. BACKGROUND

4.1.1. THE EMBEDDED ATOM METHOD (EAM)

The embedded atom method (EAM) is a semi-empirical interatomic potential developed by Daw and Baskes [78] that has been successfully applied to simulate numerous pure metal and alloy systems [79, 80], and it has been used to determine transport properties in the liquid state [19, 23, 1, 20]. In the EAM model, the total potential energy U_{tot} of a system of N atoms is described by

$$U_{tot} = \sum_{i} F_i(\rho_i) + \sum_{i>j} \phi_i(r_{ij}) \tag{95}$$

where $F_i(\rho_i)$ is the embedding energy required to place an atom i in the host metal's electron density ρ_i at atom i due to all other atoms in the system, $\phi_i(r_{ij})$ is the two-body potential energy between the atom pair i and j, and r_{ij} is the separation distance between the atom pair. The host electron density is written as the sum of the electron densities $f(r_{ij})$ of the individual j atoms to atom i using the linear superposition approximation, such that

$$\rho_i = \sum_{j \neq i} f(r_{ij}) \,. \tag{96}$$

For a monatomic pure element consisting of A-type atoms, three functions must be defined for the EAM model: the embedding energy F_A, the two-body interaction pair potential ϕ_A, and the host electron density f_A. The expression for these functions take different forms depending on the underlying theoretical model of the physical system, and are obtained from first principles calculations or by fitting the EAM model's parameters to produce simulated values that replicate a predefined set of experimentally determined properties of the physical system. The choice of physical properties used to calibrate the potential may have a significant effect on the applicability

of the potential for simulation, and care should be given in selecting a potential for simulation and interpreting results [28]. For a binary alloy with A- and B-type atoms seven separate functions are required for an EAM model, with three functions from each of the monatomic element, plus an additional function describing the cross-interaction energy between elements in the alloy ϕ_{AB}.

4.1.2. THE EAM POTENTIALS FOR THE AL-CU SYSTEM

Cai and Ye [27] developed an EAM model (CY-EAM) for several pure fcc metals and their binary alloy combinations in the solid state, including Al and Cu. In the model the embedding energy function is taken in the form

$$F(\rho) = -F_0\left[1 - ln\left(\frac{\rho}{\rho_e}\right)^n\right] + \left(\frac{\rho}{\rho_e}\right)^n + F_1\left(\frac{\rho}{\rho_e}\right), \tag{97}$$

where the parameter values $F_0 = E_c - E_v^f$ and $n = 0.5$ are taken as constants with E_c as the cohesive energy and E_v^f as the vacancy formation energy, and the parameter value ρ_e represents the host electron density at equilibrium. The two-body potential is defined

$$\phi(r) = -\alpha\left[1 + \beta\left(\frac{r}{r_a} - 1\right)\right] exp\left[-\beta\left(\frac{r}{r_a} - 1\right)\right], \tag{98}$$

and the host electron density as

$$f(r) = f_e exp[-\chi(r - r_e)], \tag{99}$$

where f_e is the electron-density scaling factor that cancels out upon substitution of Equation (99) into Equation (97) for the monatomic potential, and r_e is the equilibrium spacing between nearest neighbors. In the above equations, the remaining 5 parameter values F_1, α, β, r_a, and χ are optimized for each pure fcc metal by fitting the functional forms to during simulation to empirical data. Data considered during fitting included the elastic constants, vacancy formation energy,

equilibrium lattice constant, and the cohesive energy. The cutoff distance for the potential is set to a scalar value of the equilibrium lattice constant $r_{cut} = 1.65a_0$.

The Al-Cu alloy EAM potential is created using Johnson's model [81] by fitting the cross-pair potential function using a density weighted combination of the monatomic pair potentials

$$\phi_{AB}(r) = \frac{1}{2}\left[\frac{f_B(r)}{f_A(r)}\phi_{BB}(r) + \frac{f_A(r)}{f_B(r)}\phi_{BB}(r)\right]. \quad (100)$$

The electron-density scaling factor f_e is no longer arbitrary when Equation (99) is substituted into Equation (100), and is determined for each specific element using $f_e = (E_c/\Omega)^\gamma$ where the symbol Ω is the atomic volume. The exponent γ is included as an adjustable parameter that is used to fit the EAM alloy potential to the dilute-limit heat of solution for several A-B type compounds. For Al and Cu, γ is determined to have a value of 0.6 and 0.8, respectively. The parameter values for the Al-Cu CY-EAM potential are summarized in Table 7

Table 7 – Parameter values used to create the CY-EAM potential for Al-Cu [27].

	Al	Cu
$\chi\ (\text{Å}^{-1})$	2.50	3.00
α (eV)	0.0834	0.3902
β	7.5995	6.0641
F_0 (eV)	2.59	2.21
F_1 (eV)	-0.1392	1.0241
$r_a\ (\text{Å})$	3.0169	2.3051
$r_e\ (\text{Å})$	2.8638	2.5562
f_e	0.3806	0.3797
$a_0\ (\text{Å})$	4.05	3.615
E_c (eV)	3.32	3.52
E_v^f (eV)	0.73	1.31

Mendelev et al. [70] more recently developed pure element EAM potentials appropriate for the simulation of Al and Cu, that accurately reproduce both the properties of the crystalline solid and the properties of the liquid. The fitting procedure used to create EAM potentials for the pure metals included both the properties of the crystalline solid, and the those of the liquid state. For the solid the target properties used in fitting included the cohesive energy, vacancy formation energy, free surface energy, lattice parameters, and elastic moduli of the fcc phase. For the liquid state, the melting temperature, liquid density, latent heat and the change in volume on melting are used. In addition, the radial distribution function is fit to experimental X-ray diffraction data. Overall, the Al1 and Cu1 potentials are determined to be most accurate, and are therefore used in this work. The analytical expressions and parameter values used to fit the potentials are not provided in their paper, however, the values for the functions $F(\rho)$, $f(r)$, and $\phi(r)$ are presented in table format as high order polynomial functions. The EAM potentials are also available in tabulated format at http://www.ctcms.nist.gov/potentials [82], from which the continuous functions can be reconstructed. Unfortunately, the cross-pair potential $\phi_{AlCu}(r)$ required to model Al-Cu alloy is not considered in Mendelev et al. [70].

4.1.2.1. DEVELOPMENT OF THE CONCENTRATION-DEPEDENT EAM POTENTIAL FOR LIQUID AL-CU

To create the cross-pair potential $\phi_{AlCu}(r)$ the concentration-dependent embedded atom method (CD-EAM) [36, 83] is used. CD-EAM provides a theoretical and computational framework to combine pure element EAM interatomic potentials from different sources in literature into binary A-B type EAM alloy models. An important aspect of the CD-EAM framework is that it allows the functional form of cross-pair potential to incorporate complex

concertation dependent functions for excess enthalpy of mixing $H_{AB}^{ex}(X)$. In the liquid Al-Cu system, this is an important consideration for correctly modelling the thermodynamics of the liquid mixture.

The CD-EAM methodology requires that the pure element EAM files are transformed into the effective representation format [36], which reduces the contribution of the embedding functions. This allows the nonlinear behavior of the energy versus concentration profile to be mainly controlled by cross-pair potential function. In the effective representation, the original host electron density ρ_α^0 of the EAM potential is normalized with respect to the equilibrium density ρ_α^e for each pure element $\alpha = A$ or B with

$$\rho_\alpha{}^{eff} = \rho_\alpha^0/\rho_\alpha^e. \tag{101}$$

The embedding energy is then transformed by the function

$$F_\alpha{}^{eff}(\rho_\alpha{}^{eff}) = F_\alpha^0(\rho_\alpha^0) - F_\alpha^{0\prime}(\rho_\alpha^e)\rho_\alpha^0, \tag{102}$$

where $F_\alpha^{0\prime}(\rho_\alpha^e)$ is the first derivative of the embedding function at the host equilibrium electron density. The pair potential is similarly transformed by

$$\phi_\alpha{}^{eff}(r) = \phi_\alpha^0(r) + 2F_\alpha^{0\prime}(\rho_\alpha^e)f_\alpha^0(r), \tag{103}$$

where $f_\alpha^0(r)$ is the original value of the electron density function for a single atom.

The equilibrium electron density ρ_α^e is defined by taking the sum of the electron density around a central atom at site i relative to the individual j atoms in their equilibrium positons at a radial distance r_{ij}^e using $\rho_\alpha^e = \sum_{j\neq i} f(r_{ij}^e)$. For elements with face-centered cubic (fcc) crystal structures, the equilibrium positions in the crystal r_{ij}^e correspond to the nearest neighbor distance $d_1 = a_0/\sqrt{2}$ with a coordination number of 12, and to the next-nearest neighbor distances $d_n = d_1\sqrt{n}$ for $n = 2, 3, 4, 5, 6, \ldots$ with coordination numbers of 6, 24, 12, 24, 8, … respectively. The

electron density function $f(r_{ij})$ is typically chosen to decay exponentially with increasing distance, and the contribution of $f(r_{ij})$ to the equilibrium host electron density can be considered negligible beyond the 5th coordination number.

In the concentration-dependent embedded atom method, an analytical model for the random solution alloy is defined where an atom an atom that sits at site i can be of either species type A or B, but both are embedded in the same average environment. The total potential energy of the system as a random solution U_{tot}^{rs} is described by [84]

$$U_{tot}^{rs} = X_A^2 \sum \phi_A(r_{ij}) + X_B^2 \sum \phi_B(r_{ij}) + 2X_A X_B \sum \phi_{AB}(r_{ij}) + X_B F_B(\tilde{\rho}) + X_A F_A(\tilde{\rho}) \quad (104)$$

where an average electron density $\tilde{\rho} = X_A \sum \rho_A(r_{ij)} + X_B \sum \rho_B(r_{ij})$ is used to determine the embedding energy. The contribution of the embedding energy terms to mixing is therefore defined by

$$\Delta U_{emb} = X_A(F_A(\tilde{\rho}) - F_A(\tilde{\rho} = 1)) + X_B(F_B(\tilde{\rho}) - F_B(\tilde{\rho} = 1)), \quad (105)$$

and it can be shown using a Taylor series expansion about $\tilde{\rho} = 1$ that contribution of the embedding term is typically quite small. To create the functional form of the cross-pair potential ϕ_{AB}, it is assumed that the cross-pair potential is a function of both concentration and position such that $\phi_{AB} = f(X, r)$ that can be separated into the product of separate functions for concentration and position with

$$\phi_{AB}(X, r) = h(X) \cdot \frac{(\phi_A(r) + \phi_B(r))}{2}. \quad (106)$$

The function $h(X)$ is defined to be a fourth order polynomial with $h(X) = \sum_{i=0}^{4} h_i \cdot X^i$, and the substitution of Equation (106) into Equation (104) shows that the cross-pair potential function ϕ_{AB} becomes the main contributor to the concentration-dependent excess enthalpy of mixing $H_{AB}^{ex}(X)$.

In a molecular dynamics simulation, the excess enthalpy of mixing H_{AB}^{ex} for the liquid alloy is determined from the excess internal energy of the system at constant temperature and pressure [85] by

$$U_{AB}^{ex}(X) = U_{AB} - [U_A(1 - X_B) + U_B X_B] \tag{107}$$

where U_{AB} is the total internal energy of the mixture, and U_A and U_B are the internal energies of atomic species A and B, respectively. At zero pressure, the time averaged value of the excess internal energy is equal to the excess enthalpy of the ensemble $U_{AB}^{ex} \approx H_{AB}^{ex}$ noting that $U = H - PV$, and as $U \to H$ as $t \to \infty$.

In this research a new binary alloy interatomic potential is created and optimized for the liquid Al-Cu system using the Al1 and Cu1 EAM potentials developed by Mendelev et al. [70], and applying the concentration-dependent embedded atom method. The Al-Cu CD-EAM interatomic potential is created by first transforming the pure element potentials into their effective representations, followed by fitting the cross-pair potential $\phi_{\mathrm{AlCu}}{}^{\mathrm{eff}}$ to published reference values for the excess enthalpy of mixing $H_{AlCu,ref}^{ex}(X)$ of the liquid [30] via Equation (107). Fitting is performed by optimizing the values of parameters h_i in the 4th order polynomial function $h(X)$ using nonlinear regression (Appendix A – Nonlinear Regression Analysis). It is also important to note that thermodynamic assessment data for liquid Al-Cu [30, 31, 32] show that $H_{AlCu,ref}^{ex}(X)$ is independent of temperature. The newly created Al-Cu CD-EAM interatomic potential is then used in molecular dynamics simulations to determine the self- and interdiffusion coefficients at the tracer concentration of $Al_{0.001}Cu_{99.999}$, and alloy concentrations of $Al_{80}Cu_{20}$ and $Al_{60}Cu_{40}$.

4.2. DETERMINATION OF TRANSPORT COEFFICIENTS IN MD SIMULATION

Recall that the interdiffusion coefficient D_{AB} in a binary A-B type liquid mixture can be described by the Darken equation $D_{AB}(X,T) = D_{AB}^{0}(X,T) \cdot \Phi(X,T)$, where D_{AB}^{0} is the purely

kinetic Maxwell-Stefan (MS) diffusivity coefficient, and Φ is the thermodynamic factor (see Section 2.5.2). The MS diffusivity coefficient is described by a linear combination of the velocity correlation functions of the constituent species, and is reduced to linear combination of the self-diffusion coefficients $D_{AB}^{0} = X_B D_A + X_A D_B$ if the velocity cross-correlation functions are assumed negligible. It follows from Equation (66) that the value of the thermodynamic factor $\Phi(X,T)$ can be determined from the simulation using the concentration-concentration structure factor S_{XX}, or from the excess Gibbs free energy of solution.

The self-diffusion coefficient D_α of atomic species $\alpha = A$ or B can be calculated using the velocity auto correlation function defined in Equation (59). Alternatively, in MD simulations D_α is typically calculated using the Einstein or random walk equation for diffusion that calculates the long-time limit of the mean squared displacement

$$D_\alpha = \lim_{t\to\infty} \frac{1}{N_\alpha} \sum_{i=1}^{N_\alpha} \frac{\langle [{}^{\alpha}r_i(t) - {}^{\alpha}r_i(0)]^2 \rangle}{6t}. \tag{108}$$

It can be shown that Equation (108) is equal to Equation (59) provided that $[{}^{\alpha}r_i(t) - {}^{\alpha}r_i(0))]^2$ is calculated in an origin independent representation within the MD simulation [19].

4.3. DESCRIPTION OF THE MD SIMULATION

The parallel molecular dynamics code LAMMPS (Large-scale Atomic/Molecular Massively Parallel Simulator) [37] is used for the atomistic simulations, and it includes both the EAM and CD-EAM alloy algorithms required to compute the forces from interatomic potential models. The EAM and CD-EAM alloy potentials are provided to LAMMPS in the form of an input file, and the file is structured using a predefined format. For the CY-EAM Al-Cu potential the *setfl* format is used, and for the CD-EAM Al-Cu potential the *cdeam* file format is used. Information regarding the structure of both file formats is available at

http://lammps.sandia.gov/doc/pair_eam.html [86]. The molecular dynamics simulations are performed in parallel using a virtual server cluster consisting of 36 Intel Xeon CPUs at 2.8 GHz located on Amazon's Elastic Compute Cloud (EC2).

Each molecular dynamics simulation is performed in cubic simulation box with periodic boundary conditions for a system size of N = 62,500 atoms with a time step of 1 ps. Initially the concentration of the system is set to the mole fraction of Cu, such that $X_{Cu} = N_{Cu}/N$ with $N_{Al} + N_{Cu} = N$ atoms, and the Al and Cu atoms are randomly distributed on a fcc lattice at equilibrium positons. The neighbor lists for each atom are extended 2 Å past the cutoff distance defined by the interatomic potential. The system temperature is ramped up from 300 K to the 2000K and equilibrated under the isothermal-isobaric ensemble (NPT) at zero pressure, and allowed to cool to the simulation diffusion annealing temperature T_A. At the diffusion annealing temperature the system is again equilibrated under the NPT ensemble at zero pressure, and the average system volume at zero pressure is determined. The cubic simulation box is then rescaled to the average system volume at equilibrium and the simulation is equilibrated in the canonical ensemble (NVT) now at the zero-pressure particle density. Finally, the microcanonical ensemble (NVE) is used for the production run and the self-diffusion coefficients are calculated from ensemble averages over 2 ns (2 x10^6 time steps) using Equation (108). An example of a cubic simulation box with periodic boundary conditions for $Al_{80}Cu_{20}$ in the liquid state is shown in Figure 20.

The radial and partial radial distribution functions are calculated by post processing a data file produced during the NVE production run that contains information including species type, position, and velocity data for each atom by time step. Post processing of the data file allows the radial cutoff distance from an individual atom to be extended to an arbitrarily large distance, here taken as 15 Å. For the post processing, the positon coordinates have already been accurately

determined during the simulation run, and time integration is not performed. This significantly reduces the computation time associated with the large increase in the number of atoms in the neighbor list.

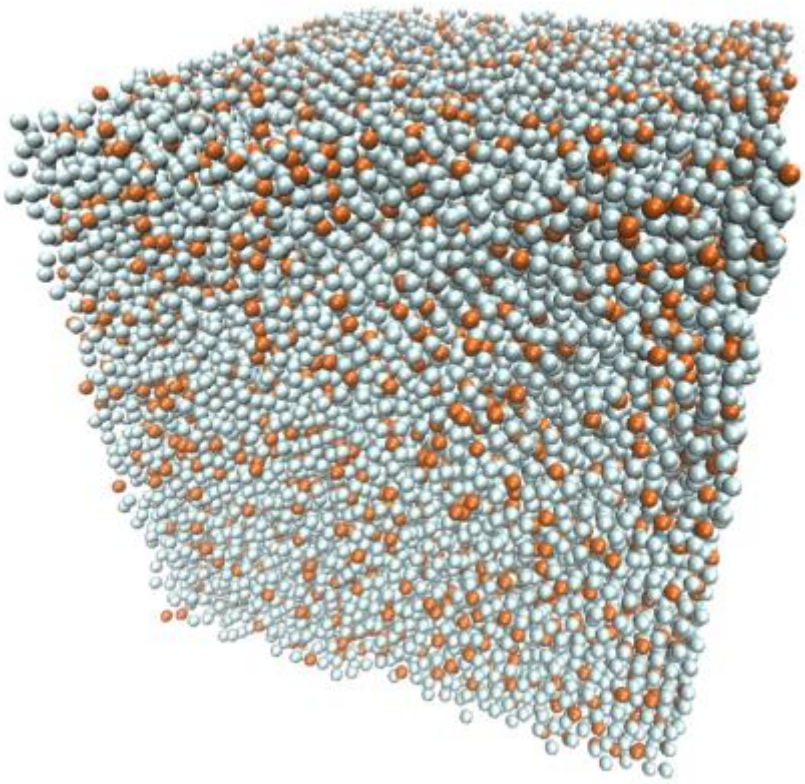

Figure 20 - An example of a cubic simulation box with periodic boundaries for $Al_{80}Cu_{20}$ in the liquid state, created using the VMD (Visual Molecular Dynamics) program [87]. In the figure, Cu atoms shown in orange and Al atoms in grey.

4.4. RESULTS AND DISCUSSION

The pair potentials developed by Mendelev et al. [70] and the cross-pair potential developed in the present work are shown in Figure 21 in effective representation format. From the figure, the minimum values of the pure element pair potentials correspond to the equilibrium nearest neighbor distance in the solid, and all values of the pair potential go to zero at the radial cutoff distance of 6.50 Å. In Figure 22, the transformed value of the embedding energy is shown.

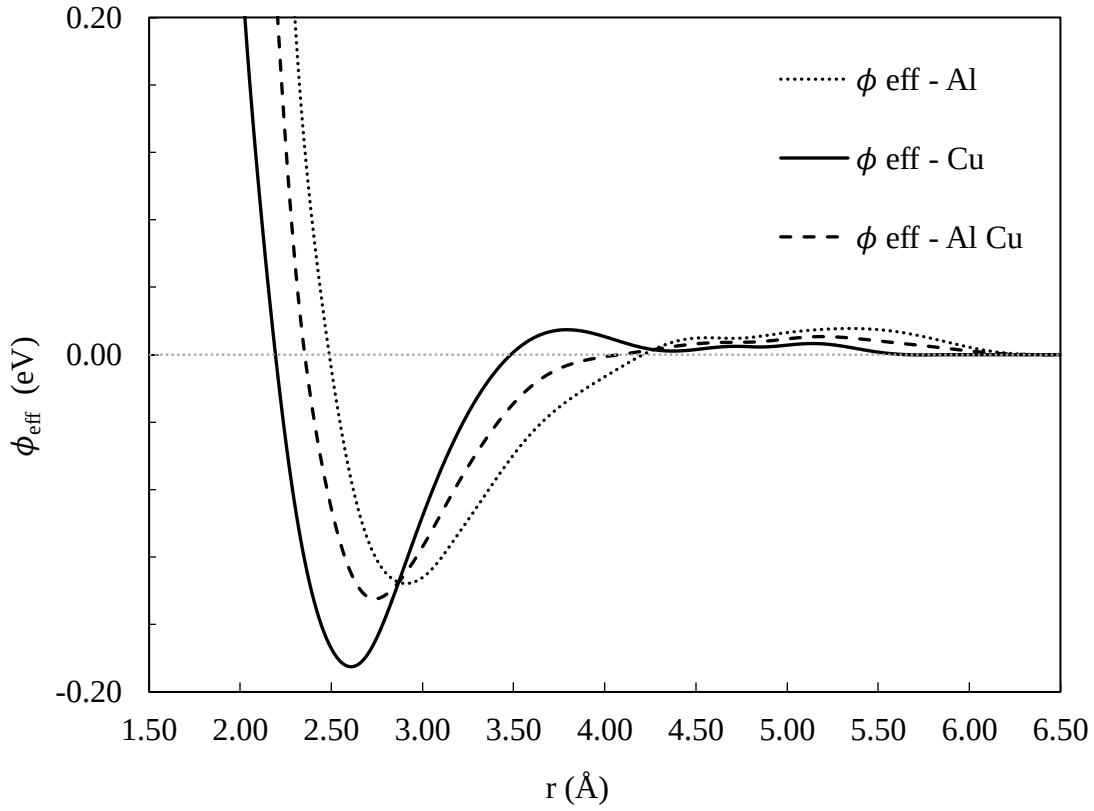

Figure 21 – The effective pair potentials ϕ^{eff} (eV) versus distance r (Å) for the Al-Cu CD-EAM model. The ϕ_{Al}^{eff} and ϕ_{Cu}^{eff} pair potentials are adapted from Mendelev et al. [70], and the cross-pair potential ϕ_{AlCu}^{eff} is fit using using the CD-EAM method [36].

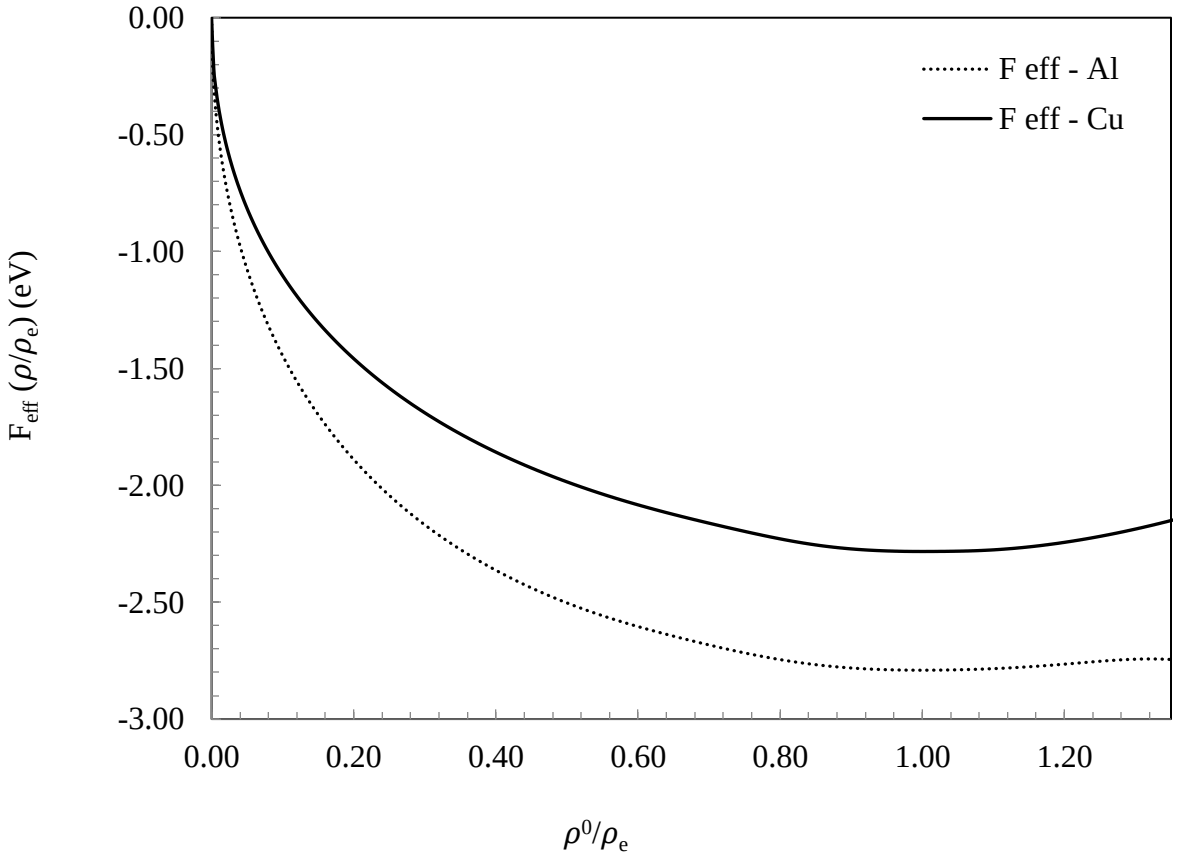

Figure 22 - The effective embedding energy F_{eff} (eV) versus the normalized electron density ρ^0/ρ_e for the Al-Cu CD-EAM model. The pure Al and Cu functions are adapted from Mendelev et al. [70].

The best-fit parameter values used to fit the concentration dependence of the cross-pair potential to the experimental values of excess enthalpy are listed in Table 8 for the fourth-order polynomial $h(X)$. The reference values for the excess enthalpy of mixing $H_{AlCu,ref}^{ex}(X)$ [30] are shown in Figure 23, and the values of the excess enthalpy of mixing H_{AlCu}^{ex} produced from molecular dynamics simulation from the Al-Cu CD-EAM potential developed in the present thesis research are shown as triangles. The molecular dynamics simulation model was fit to the target function using nonlinear regression. In addition, the excess enthalpy of the CY-EAM potential is shown for comparison and has approximately twice the experimental value at the minimum.

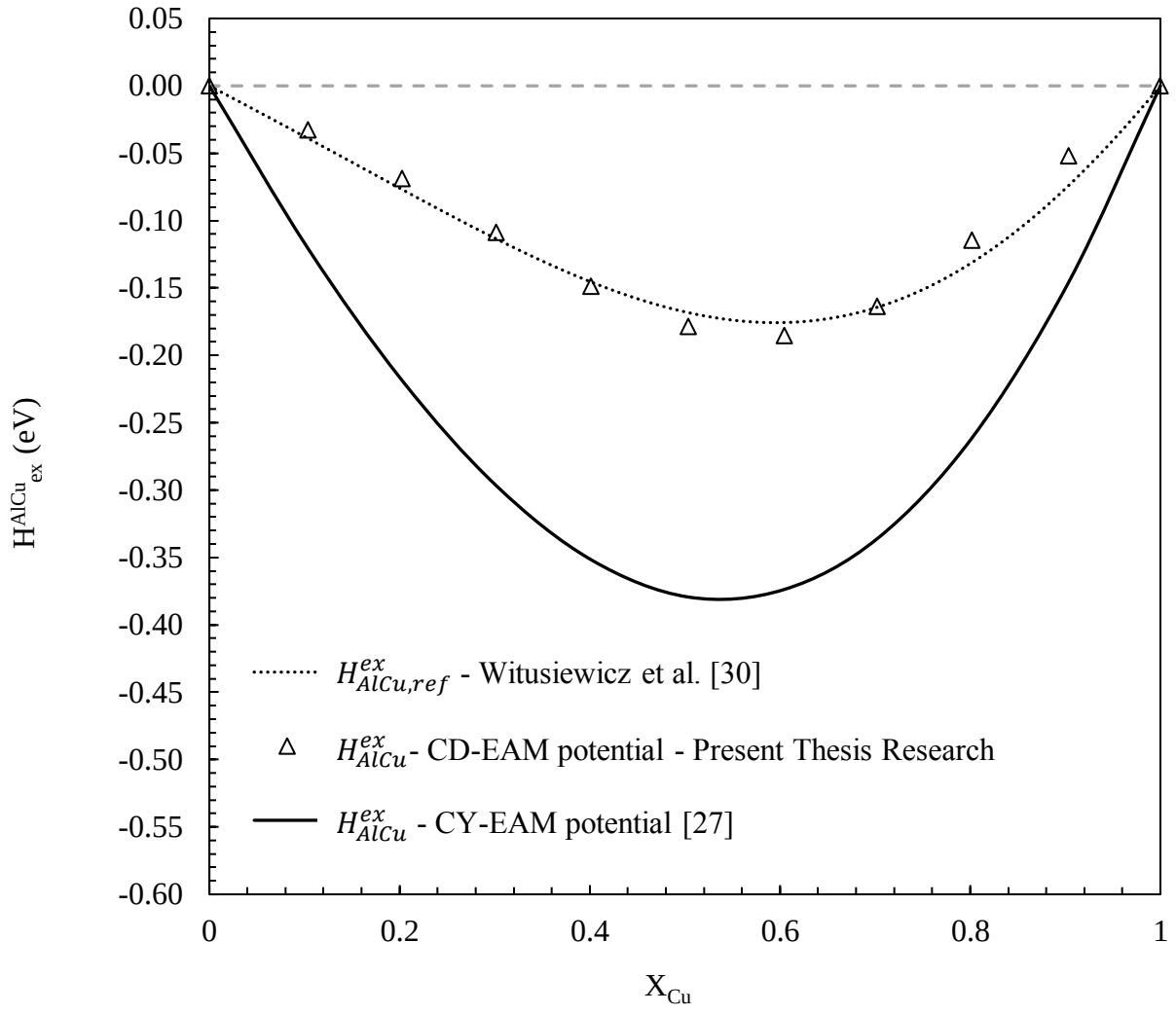

Figure 23 - Excess enthalpy of mixing $H^{ex}_{AlCu}(X)$ versus concentration X for the Al-Cu binary liquid system at T = 1493 K. The experimental reference data for $H^{ex}_{AlCu,ref}(X)$ from Witusiewicz et al. [30] are compared to the CY-EAM [27] potential and the CD-EAM potential.

Table 8 - Best fit parameters for the 4th order polynomial function $h(X)$.

h_0	h_1	h_2	h_3	h_4
1.385	0.9	-0.45	-0.4	-0.05

In Table 9, a summary of the self-diffusion D_{Al} and D_{Cu}, the Maxwell-Stefan (MS) diffusion coefficient D^0_{AlCu}, and the interdiffusion coefficient D_{AlCu} is presented for each temperature *T* and the mole fraction concentration *X* simulated in this thesis research using the Al-Cu CD-EAM potential. In the table, the values of the self-diffusion coefficients are determined in the molecular dynamics simulation using the Einstein equation, Equation (107). The value of the interdiffusion coefficient is determined using Darken's equation $D_{AlCu}(X,T) = D^0_{AlCu}(X,T) \cdot \Phi(X,T)$, where the MS diffusion coefficient is taken as the linear combination of the self-diffusion coefficients $D^0_{AlCu} = X_{Cu}D_{Al} + X_{Al}D_{Cu}$, and the values of the thermodynamic factor $\Phi(X,T)$ are taken from Figure 3.

In Figure 24, the results for the interdiffusion coefficient in $Al_{99.999}Cu_{0.001}$ obtained using the Al-Cu CD-EAM potential are shown, and the temperature dependence of the interdiffusion coefficient is well described by the Arrhenius relationship with best fit parameter values of Q_0 = 22.81 $\pm$ 0.27 kJ/mol and D_0 = 1.04 (+0.03, -0.03) x 10^{-7} m^2/s. These results are in good agreement with the results obtained using the solid wire long capillary method (SWLC) in Chapter 3, where the activation energy was determined to be Q_0 = 20.85 $\pm$ 4.49 kJ/mol with a frequency factor D_0 = 8.21 (+5.4, -3.26) x 10^{-8} m^2/s. In addition, the activation energy agrees with the tracer results of Ejima et al. [26] and the Al solvent self-diffusion results of Kargl et al. [58]. However, Cu is found to diffusion slower in Al than Al solvent self-diffusion [58], albeit by a small amount. In the same figure, the values interdiffusion coefficient D_{AlCu} determined using the CY-EAM potential are shown. The CY-EAM results are approximately 35% higher than those obtained using CD-EAM potential over the temperature range considered, and overestimate the value of the interdiffusion coefficient when compared to the work of Ejima et al. [26] and the present thesis research.

Table 9 – Self-diffusion, MS diffusivity, and interdiffusion coefficients determined using the Al-Cu CD-EAM potential listed by mole fraction concentration and temperature.

X_{Cu}	T (K)	D_{Al} [-1-]	D_{Cu} [-1-]	D^{0}_{AlCu} [-1-]	D_{AlCu} [-1, 2-]
0.001	993	6.54	4.27	6.54	6.54
0.001	1093	8.60	7.73	8.60	8.60
0.001	1193	10.36	7.76	10.36	10.36
0.001	1293	12.34	9.91	12.34	12.34
0.001	1393	14.34	11.80	14.34	14.34
0.001	1493	16.62	13.02	16.62	16.62
0.20	993	3.25	2.37	2.55	3.70
0.20	1093	4.74	3.59	3.83	5.56
0.20	1193	6.25	4.88	5.16	7.50
0.20	1293	7.75	6.09	6.43	9.34
0.20	1393	9.31	7.42	7.80	11.34
0.20	1493	11.25	9.35	9.73	14.15
0.40	993	1.10	0.93	1.03	3.70
0.40	1093	1.99	1.75	1.90	5.68
0.40	1193	3.04	2.66	2.89	8.09
0.40	1293	4.06	3.61	3.88	10.48
0.40	1393	5.16	4.65	4.96	13.26
0.40	1493	6.65	5.90	6.35	16.37

[-1-] Diffusion coefficients have units of D x 10^{-9} m^2/s.

[-2-] The thermodynamic factor $\Phi(X,T)$ is calculated using Equation (67).

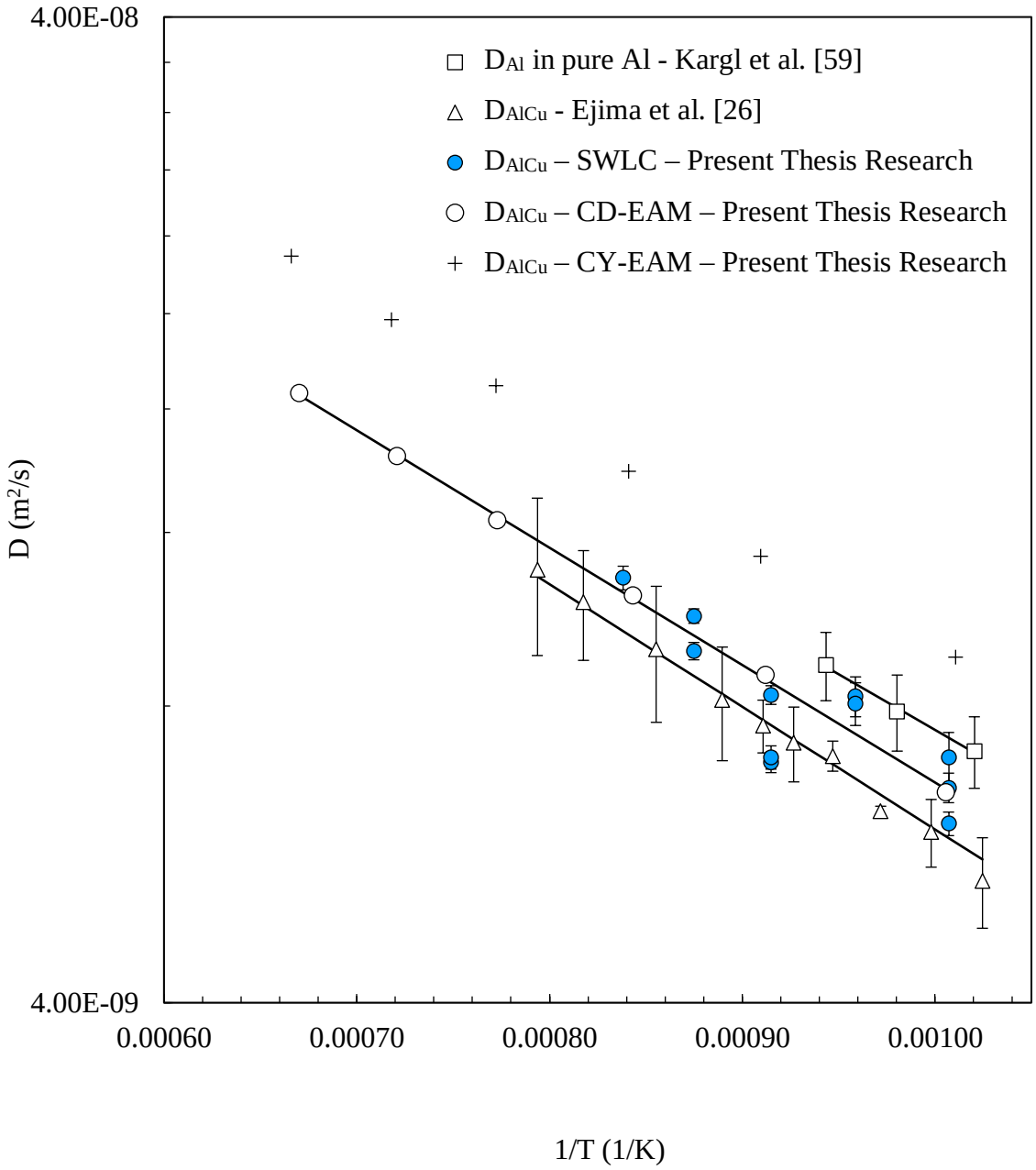

Figure 24 – Self-diffusion in pure Al and interdiffusion in $Al_{99.999}Cu_{0.001}$. In the figure, the ○ represents the interdiffusion coefficients D_{AlCu} determined in the present thesis research using MD simulation with the CD-EAM interatomic potential, and the ● represents the experimental interdiffusion coefficients D_{AlCu} determined using the SWLC method in Chapter 3. the □ represents solvent self-diffusion D_{Al} for liquid Al reported in Kargl et al. [58], the △ represents tracer interdiffusion D_{AlCu} data of Ejima et al. [26]. The solid black lines represent the best fit Arrhenius equation. Further information regarding past studies is provided in Section 2.7.2.

Interdiffusion results for $Al_{80}Cu_{20}$ obtained using molecular dynamics simulation with the Al-Cu CD-EAM potential in the present thesis research are shown in Figure 25 and are listed numerically in Table 9. The temperature dependence of the interdiffusion coefficient is well described over the simulation temperature range of 993 K (1/T = 0.001011/K) to 1493 K (1/T = 0.00067 1/K) by the Arrhenius relationship, with best fit parameter values of Q_0 = 30.15 $\pm$ 0.49 kJ/mol and D_0 = 1.78 (+0.08, -0.08) x 10^{-7} m^2/s. A visual comparison of results in Figure 25 shows that the values of MD simulation interdiffusion coefficients are in good agreement with the experimental data of Chapter 3, with similar values for the activation energy and frequency factor of Q_0 = 34.41 $\pm$ 3.71 kJ/mol and D_0 = 2.84 (+1.47, -0.97) x 10^{-7} m^2/s, respectively.

In Figure 25, the best fit Arrhenius relationship for the present MD Al-Cu CD-EAM simulation results is extended from the simulation temperature range of 993 K (1/T = 0.001011/K) to 1493 K (1/T = 0.00067 1/K) to the liquidus temperature at approximately 821 K (1/T = 0.00122 1/K). It is interesting to note that the trend line for the interdiffusion coefficient agrees with the experimental findings of Lee at al. [18]. Lee at al. [18] obtained their result using directional solidification in 0.8 mm capillaries, yet another independent method, and the result is in keeping with both the SWLC and MD Al-Cu CD-EAM data further supporting the validity of findings in the current work. Also in the figure, the results of the MD simulation for Cu self-diffusion D_{Cu} are shown to be in exact agreement with the quasielastic neutron scattering results of Brillo et al. [59] for $Al_{80}Cu_{20}$. This finding is significant, and further validates the ability of the Al-Cu CD-EAM potential developed in the current thesis research to accurately model diffusion in the liquid at this alloy composition.

Also from Figure 25, it evident that the values of the interdiffusion coefficient are lower than those obtained using x-ray radiography of Zhang et al. [21, 22], and those obtained using the

solid wire technique in Lee and Cahoon [15]. Taking into consideration the previously discussed agreement of data obtained in present thesis research using MD simulation and the SWLC method with the work of Lee at al. [18], and the self-diffusion findings of Brillo et al. [59], creates a strong argument to support the assertion that interdiffusion coefficients obtained in Zhang et al. [21, 22] and Lee and Cahoon [15] in ~1.5 mm diameter capillaries are influenced by convective mixing, and are overstated by approximately 63%. In addition, in Zhang et al. [21, 22] it was discussed that the value of the interdiffusion coefficient was the enhanced by a factor of ~2 due to the contribution of dynamic velocity cross-correlations to the MS diffusivity D^0_{AlCu} (see Equation (58)), based on the Cu self-diffusion data of Brillo et al. [59]. The findings of the present thesis research suggest that contribution of the dynamic velocity cross-correlations are in fact negligible, as assumed in Equation (61).

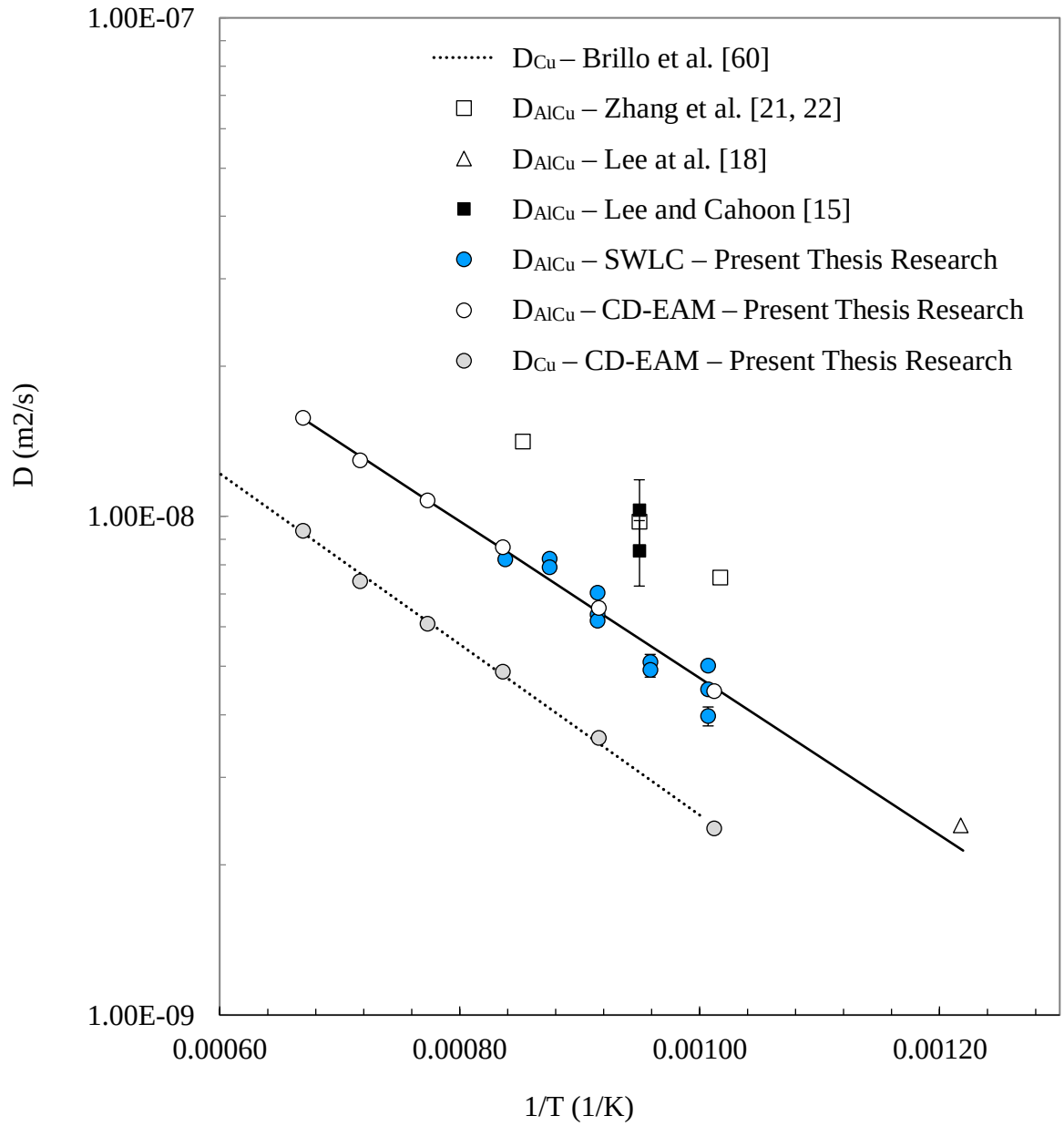

Figure 25 – Comparison of diffusion studies in $Al_{80}Cu_{20}$. In the figure, the ○ represents the interdiffusion coefficients D_{AlCu} determined in the present thesis research using MD simulation with the Al-Cu CD-EAM interatomic potential, and the solid black line — represents the best fit Arrhenius relationship. Also in the figure, the ○ represents the Cu self-diffusion coefficients obtained using MD simulation with the Al-Cu CD-EAM interatomic potential, and the ● represents the experimental interdiffusion coefficients D_{AlCu} determined using the SWLC method in Chapter 3. The results of previous studies are shown for comparison where the ■ are the values of the interdiffusion coefficients D_{AlCu} obtained by Lee and Cahoon [15], the □ by Zhang et al. [22, 21], and the △ by Lee et al. [18]. The Cu self-diffusion data of Brillo et al. [59] is shown as the dotted ⋯ line.

Recall that the Maxwell-Stefan (MS) diffusivity coefficient is described by a linear combination of the self-diffusion coefficients $D^0_{AlCu} = X_{Cu}D_{Al} + X_{Al}D_{Cu}$. In Figure 26, the values of MS diffusion coefficients for $Al_{60}Cu_{40}$ determined using molecular dynamics simulation with the Al-Cu CD-EAM interatomic potential and the CY-EAM interatomic potential, are compared to the MS diffusion coefficients based on the ab-initio molecular dynamics simulation data of Wang et al. [56]. From the figure, it is evident that the results obtained using the Al-Cu CD-EAM potential differ significantly from those obtained using the CY-EAM interatomic potential (present research), and the results of Wang et al. [56]. Also of note, is that the value of the MS diffusion coefficient obtained using the CY-EAM interatomic potential obtained at a temperature of 1493 K (1/T = 0.00067 1/K), agrees with the data of Cheng et al. [23].

In Figure 27, the value of interdiffusion coefficients D_{AlCu} for $Al_{60}Cu_{40}$ are shown. The MD simulation values for the Al-Cu CD-EAM potential are well described by the Arrhenius relationship with parameter values of Q_0 = 37.01 $\pm$ 1.48 kJ/mol and D_0 = 3.29 (+0.52, -0.45) x 10^{-7} m^2/s, and are in good agreement with the experimental best fit parameter values obtained in Chapter 3 using the SWLC method of Q_0 = 38.74 $\pm$ 8.01 kJ/mol and D_0 = 4.03 (+5.23, -4.51) x 10^{-7} m^2/s. Also, shown in the figure are the results of Cheng et al. [23] obtained using the CY-EAM potential, that are considerably higher at low temperature and exhibit lower activation energy and frequency factor. This result can be explained on the basis that Cheng et al. [23] use the CY-EAM interatomic potential in their analysis that was developed for the Al-Cu system in the solid state, and is shown in Figure 23 to overestimate the value of the excess enthalpy of mixing Hex

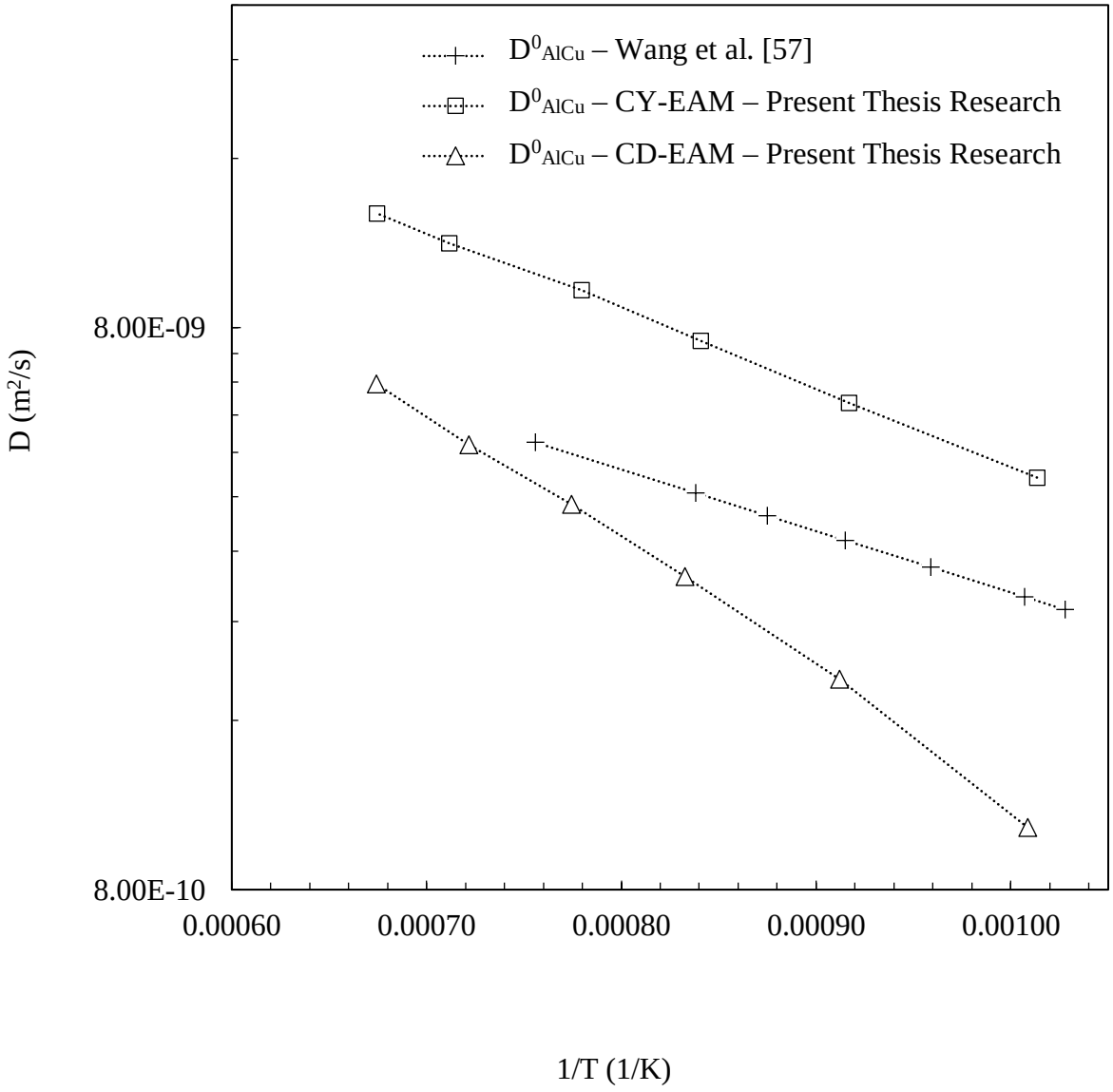

Figure 26 – An Arrhenius plot of Maxwell-Stefan diffusion coefficients D^0_{AlCu} in liquid $Al_{60}Cu_{40}$.

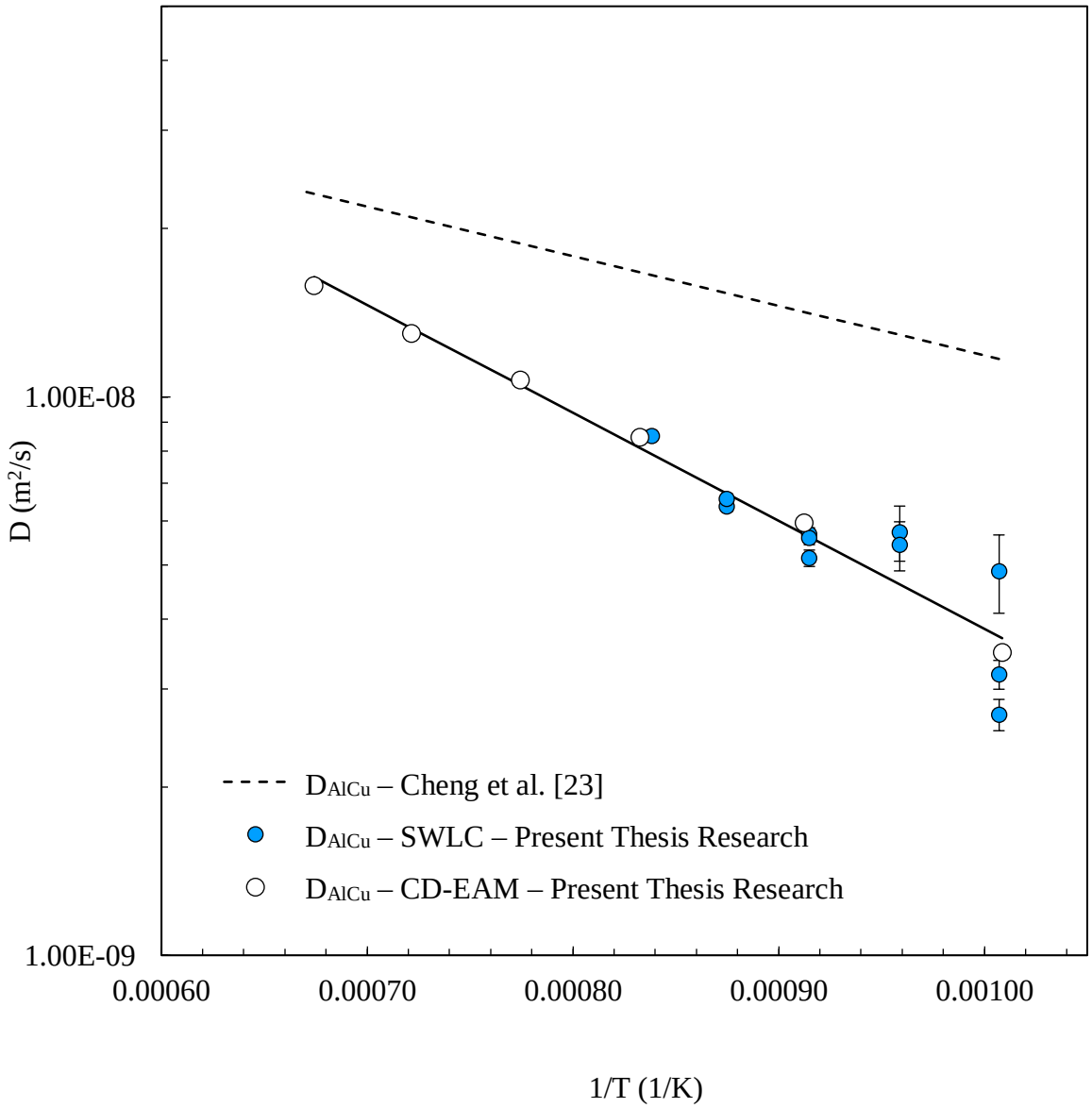

Figure 27 - Arrhenius plot of interdiffusion in liquid $Al_{60}Cu_{40}$. In the figure, the ○ represents the interdiffusion coefficients D_{AlCu} determined in the present thesis research using MD simulation with the Al-Cu CD-EAM interatomic potential, and the solid black line — represents the best fit Arrhenius relationship. Also in the figure, the ● represents the experimental interdiffusion coefficients D_{AlCu} determined using the SWLC method in Chapter 3, and the dashed --- line represents the best fit Arrhenius relationship for interdiffusion D_{AlCu} from Cheng et al. [23].

Exploring the molecular dynamics simulation data further, Figure 28 shows the pair correlation function for the liquid at a temperature of 1393 K in $Al_{80}Cu_{20}$ obtained using the CD-EAM Al-Cu interatomic potential. The value of the first nearest neighbor peak is well defined in the figure, and is located at a radial distance of 2.65 Å. This value agrees with the value reported in Brillo et al. [29] for the eutectic composition $Al_{83}Cu_{17}$ at 2.66 Å at a temperature of 1463 K. Brillo et al. [29] also report that the value of the first coordination number is 10.6 ± 0.5, which is in keeping with the value of the present simulation at 11.6. Also in the figure, the second and third nearest neighbour peaks are well defined, indicating the presence of short-range order within the liquid. In Figure 29 the partial radial distribution functions are shown for the $Al_{80}Cu_{20}$ at the same temperature, and the nature of ordering in the liquid can be inferred. For atom pairs Al-Al, Cu-Al, Cu-Cu, the ensemble average interatomic distances are 2.56 Å, 2.68 Å, and 2.94 Å. This can be interpreted as evidence of clustering phenomena within the melt, where within the statistical fluctuations, the Cu atoms remain within closer proximity to each other and are surrounded by Al atoms that are less close packed. The minimum value in the excess Gibbs free energy occurs at a composition that corresponds to the ε_1 intermetallic phase peritectic [30, 31, 32] at approximately 60 at% Cu, implying order within the liquid increases with increasing concentration. In the context of Darken's equation, the molecular dynamics simulation data supports the theory that clustering phenomena within the liquid enhances the rate of interdiffusion in liquid Al-Cu.

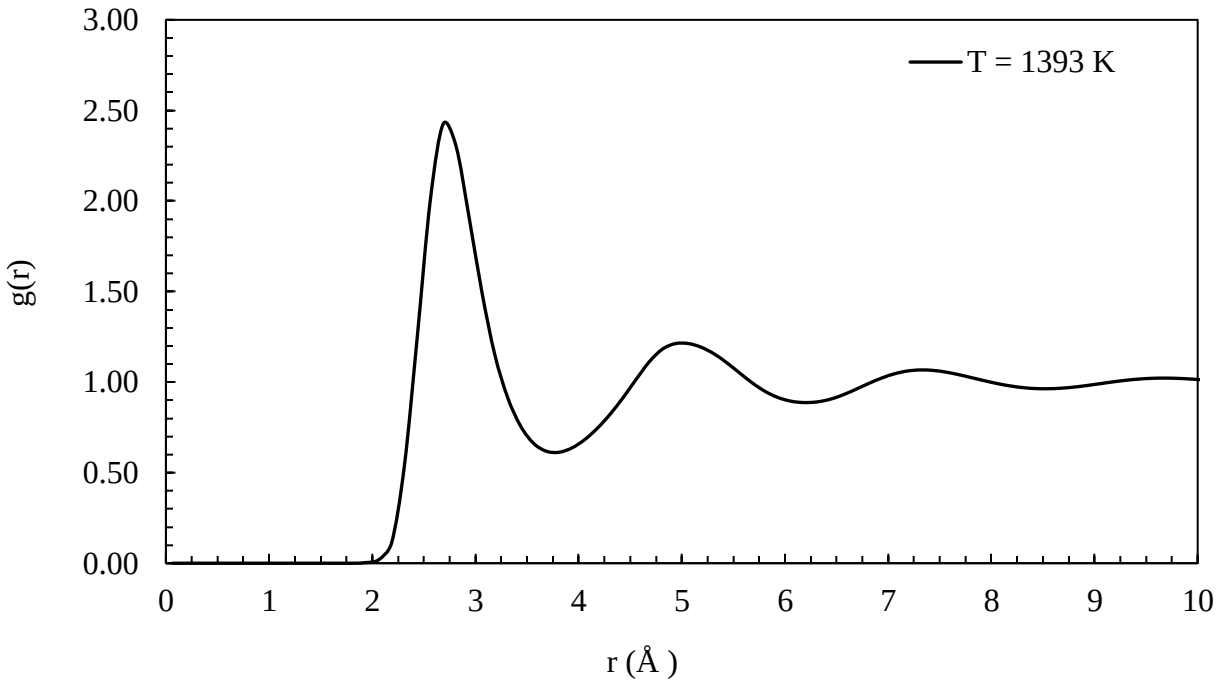

Figure 28 – The radial distribution function g(r) for liquid $Al_{80}Cu_{20}$ at T = 1393 K produced using molecular dynamics simulation with the Al-Cu CD-EAM potential.

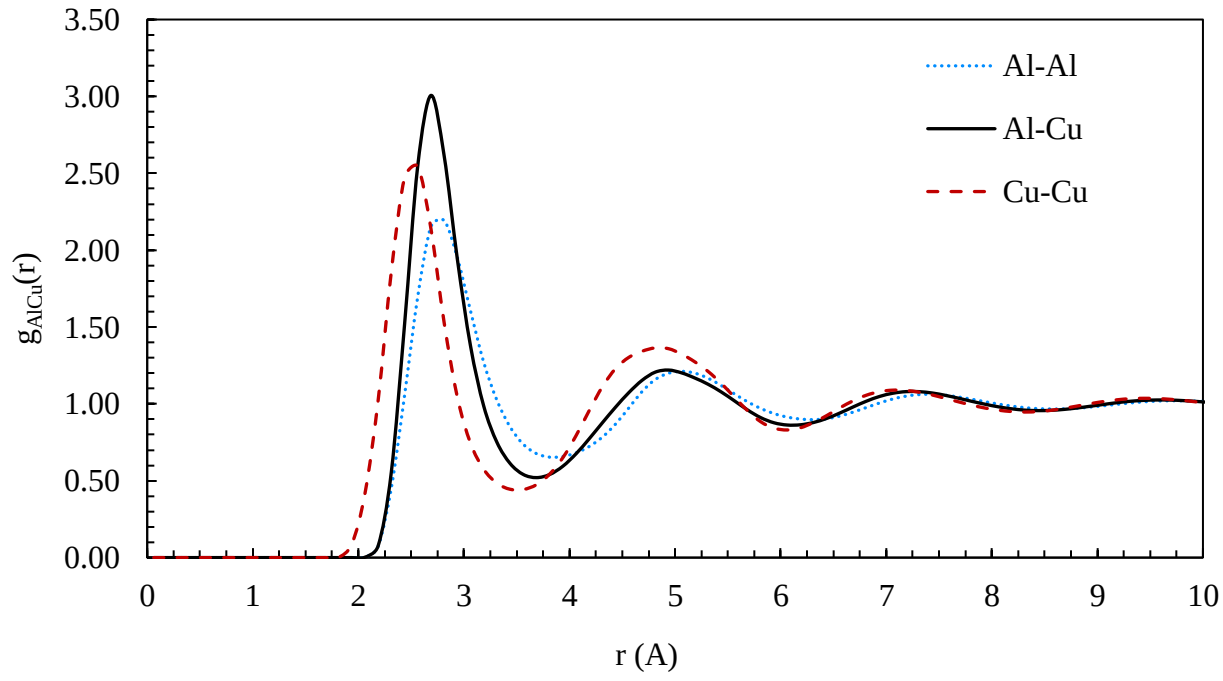

Figure 29 - The partial radial distribution functions $g_{AlCu}(r)$ for liquid$Al_{80}Cu_{20}$ at T = 1393 K produced using molecular dynamics simulation with the Al-Cu CD-EAM potential.

The interdiffusion results obtained using molecular dynamics simulation with the newly developed Al-Cu CD-EAM interatomic potential in Chapter 4 in general, agree with the interdiffusion data of Chapter 3 obtained using the SWLC method at the concentration of $Al_{\sim 100}Cu_{\sim 0}$ and $Al_{80}Cu_{20}$, and $Al_{60}Cu_{40}$. The molecular dynamics simulation results show that the temperature dependence of the liquid interdiffusion coefficient is well described by the Arrhenius relationship at constant concertation, over the temperature range of 993 K to 1493 K, at concentrations of $Al_{99.999}Cu_{0.001}$, $Al_{80}Cu_{20}$, and $Al_{60}Cu_{40}$. The best fit Arrhenius parameter values for the activation energy Q_0 and frequency factor D_0 are both found to increase with the concentration of Cu in the liquid, again reinforcing that the relationship between concentration, temperature, and the atomic dynamics that determine the rate of diffusion in the liquid metal is a complex and highly cooperative phenomenon [1].

4.5. SUMMARY

In this chapter diffusion in the liquid Al-Cu binary system was studied using molecular dynamics simulation. A new interatomic potential that is optimized for the Al-Cu liquid system (Al-Cu CD-EAM) was developed using the concentration-dependent embedded atom method. Self-diffusion and interdiffusion coefficients were determined at temperatures of 993 K, 1093 K, 1193 K, 1293 K, 1393 K, and 1493 K, for concentrations of $Al_{99.999}Cu_{0.001}$, $Al_{80}Cu_{20}$, and $Al_{60}Cu_{40}$.

The MD simulation results show that interdiffusion is well described by the Arrhenius relationship over the temperature interval considered at a given concentration. At the tracer concentration $Al_{99.999}Cu_{0.001}$, the best fit Arrhenius parameters were determined to have an activation energy of Q_0 = 22.81 $\pm$ 0.27 kJ/mol and frequency factor of D_0 = 1.04 (+0.03, -0.03) x 10^{-7} m^2/s. For $Al_{80}Cu_{20}$, the best fit Arrhenius parameters are Q_0 = 30.15 $\pm$ 0.49 kJ/mol and D_0 = 1.78 (+0.08, -0.08) x 10^{-7} m^2/s, and for $Al_{60}Cu_{40}$ Q_0 = 37.01 $\pm$ 1.48 kJ/mol and D_0 = 3.29 (+0.52, -0.45) x 10^{-7} m^2/s. In general, the simulation results at concentrations of $Al_{99.999}Cu_{0.001}$, $Al_{80}Cu_{20}$, and $Al_{60}Cu_{40}$ agree with the results obtained in Chapter 3 using the solid wire long capillary (SWLC) technique. In addition, the value of the self-diffusion coefficients D_{Cu} are in good agreement with experimental results obtained using quasielastic neutron scattering in the $Al_{80}Cu_{20}$. At the $Al_{60}Cu_{40}$ concentration, the MD simulation values for the interdiffusion are more accurate than those obtained using the SWLC, with similar average values for the best fit Arrhenius parameters but with lower standard deviations.

5. CONCLUSION

5.1. OVERVIEW

The objective of this thesis research was: 1. To obtain accurate interdiffusion coefficients for the binary liquid Al-Cu system over a range of temperature and concentrations, and 2. To investigate the concentration dependence of the interdiffusion coefficient in the binary liquid Al-Cu system and the effect of liquid structure on the interdiffusion coefficient. Two distinct approaches to obtaining liquid diffusion coefficients were presented. Chapter 3 utilized a traditional long capillary experimental method to accurately determine the concentration dependence interdiffusion coefficient across a concentration range limited by the liquidus concentration of the binary phase diagram, over a temperature interval of 993 K to 1193 K. Chapter 4 conducted a molecular dynamic (MD) simulation with a newly developed concentration-dependent embedded atom method (CD-EAM) interatomic potential. From the simulation, self-diffusion coefficients were calculated and the interdiffusion coefficient was determined using Darken's equation over a temperature interval of 993 K to 1493 K at concentrations of $Al_{99.999}Cu_{0.001}$, $Al_{80}Cu_{20}$, and $Al_{60}Cu_{40}$.

Chapter 2 provided an overview of the theoretical and experimental background necessary for this research, including a review of thermodynamics and diffusion theory for binary liquid mixtures. In addition, Chapter 2 reviewed literature specific to the Al-Cu system. A summary of Chapters 3 and 4 are presented next.

5.1.1. CHAPTER 3: REACTIVE INTERDIFFUSION IN THE AL-CU SYSTEM

Chapter 3 used the reactive diffusion long capillary method (solid wire technique) to obtain interdiffusion coefficients in the liquid Al-Cu melt. Quantitative chemical analysis was performed

using a scanning electron microscope equipped with an energy dispersive spectrometer. The concentration profiles of the diffusion specimens exhibited minimal scatter, indicating that interdiffusion coefficients were accurate and were not inflated through buoyancy driven convective mixing within the capillary. A mathematical model was developed utilizing the existing framework of the Variable Space Network (VSN) method that was modified to account for a concentration-dependent interdiffusion coefficient, and the change in volume of the diffusion couple that occurs upon solidification from the liquid state. The best-fit function describing the concentration dependence of the interdiffusion coefficient was determined by an F-test of nested candidate polynomial functions. Overall, the interdiffusion coefficient was determined at temperatures of 993 K, 1043 K, 1093 K, 1143 K, and 1193 K, across a range limited by the liquidus of the binary phase diagram of approximately 0 to 50 at% Cu in Al.

The results showed that interdiffusion is well described by the Arrhenius relationship over the temperature interval considered at a given concentration. For then tracer concentration of $Al_{\sim 100}Cu_{\sim 0}$, the best fit Arrhenius parameters were determined as Q_0 = 20.85 $\pm$ 4.49 kJ/mol and frequency factor D_0 = 8.21 (+5.4, -3.26) x 10^{-8} m^2/s. For $Al_{80}Cu_{20}$, the best fit Arrhenius parameters were determined as Q_0 = 34.41 $\pm$ 3.71 kJ/mol and D_0 = 2.84 (+1.47, -0.97) x 10^{-7} m^2/s, and for $Al_{60}Cu_{40}$ Q_0 = 38.74 $\pm$ 8.01 kJ/mol and D_0 = 4.03 (+5.89, -2.39) x 10^{-7} m^2/s. From the Arrhenius relationship, the activation energy and frequency factor were found to both increase significantly with increasing concentration, suggesting a nonlinear relationship between concentration, temperature, and interdiffusion coefficient due to chemical order within the melt.

5.1.2. CHAPTER 4: MOLECULAR DYNAMICS SIMULATION OF DIFFUSION IN THE AL-CU SYSTEM USING AN EMBEDDED ATOM METHOD INTERATOMIC POTENTIAL

Chapter 4 used molecular dynamic (MD) simulation to determine self- and interdiffusion coefficients for the binary Al-Cu system. A concentration-dependent embedded atom method (CD-EAM) interatomic potential was created for this research that was optimized for the liquid state. The self-diffusion coefficients and thermodynamic factor were calculated separately, and from this the interdiffusion coefficient was determined using Darken's equation. Further, the liquid structure was examined in terms of coordination number and nearest neighbor distance, as determined from the radial distribution function. Overall, the interdiffusion coefficient was determined at temperatures of 993 K, 1093 K, 1193 K, 1293 K, 1393 K, and 1493 K, for tracer concentrations in $Al_{99.999}Cu_{0.001}$, $Al_{80}Cu_{20}$, and $Al_{60}Cu_{40}$. In addition, it was shown that ordering or clustering phenomena within the liquid enhanced the value of the interdiffusion coefficient.

The results showed that the temperature dependence of the interdiffusion coefficient for the tracer concentration of $Al_{99.999}Cu_{0.001}$ obtained using the Al-Cu CD-EAM potential are well described by the Arrhenius relationship with best fit parameter values of Q_0 = 22.81 $\pm$ 0.27 kJ/mol and D_0 = 1.04 (+0.03, -0.03) x 10^{-7} m^2/s. For $Al_{80}Cu_{20}$, the best fit parameter values are Q_0 = 30.15 $\pm$ 0.49 kJ/mol and D_0 = 1.78 (+0.08, -0.08) x 10^{-7} m^2/s, and for $Al_{60}Cu_{40}$ the best fit parameter values are Q_0 = 37.01 $\pm$ 1.48 kJ/mol and D_0 = 3.29 (+0.52, -0.45) x 10^{-7} m^2/s. The results obtained in this chapter were found to be consistent with those obtained using the solid wire long capillary (SWLC) technique in Chapter 3 at concentrations of $Al_{99.999}Cu_{0.001}$, $Al_{80}Cu_{20}$, and $Al_{60}Cu_{40}$, confirming the accuracy of these data.

5.2. LIMITATIONS OF THE CURRENT WORK AND RECOMMENDATIONS FOR FUTURE RESEARCH

Developing a comprehensive theory of diffusion in liquid metals remains a complex and challenging problem. Two distinct approaches for examining liquid diffusion in the Al-Cu system was examined in thesis, including the traditional long capillary experimental method, as well as molecular dynamic (MD) simulation with a concentration-dependent embedded atom method (CD-EAM) interatomic potential. There are several possible limitations and constraints of these approaches, which are briefly outlined next. In addition, the implications of these limitations are discussed in terms of future research.

In Chapter 3, improvement can be made in the numerical framework developed in this thesis to analyze the solid wire technique. The method developed in this thesis used an explicit numerical solution with a truncation error of $\mathcal{O}(\Delta x^2) + \mathcal{O}(\Delta t)$ that is subject to a constraint in the size of the time step. The accuracy and speed of computation could be improved in future work through development of an implicit numerical solution with a smaller truncation error and temporal stability. In addition, the numerical framework could be modified to account for diffusion of mass into the solid across the interface. Another possible limitation of the analysis in Chapter 3 is regarding the ex-situ analysis of the diffusion couple after solidification that is modeled using molar volume data from previous research studies. An extension of this research could be to analyze the concentration in the sample in-situ using x-ray radiography methods, and therefore remove possible error due to volume correction.

In Chapter 4, further refinement of the Al-Cu CD-EAM interatomic potential is possible. For example, the cross-pair potential could be specifically fit to more experimental data, such as the concentration-dependent values of liquid density, and the radial distribution function (rdf). Further, the thermodynamic factor could be calculated directly from the simulation data using the

partial structure factors, and the velocity cross-correlation functions could be quantified from the simulation data. Both features are not currently supported in LAMMPS.

6. REFERENCES

[1] P. Kuhn, J. Horbach, F. Kargl, A. Meyer and T. Voigtmann, "Diffusion and interdiffusion in binary metallic melts," *Physical Review B,* vol. 90, no. 2, p. 024309, Jul 2014.

[2] R. W. Smith, P. J. Scott and B. Szpunar, "Soulte diffusion in nonionic liquids - effects of gravity," *Annals of the New York Academy of Sciences ,* vol. 1161, no. 1, pp. 526-536, 2009.

[3] A. Meyer and F. Kargl, "Diffusion of Mass in Liquid Metals and Alloys – Recent Experimental Developments and New Perspectives," *International Journal of Microgravity Science and Application,* vol. 30, no. 1, pp. 30-35, 2013.

[4] N. Armour, S. Dost and B. Lent, "Effect of free surface and gravity on silicon dissolution in germanium melt," *Journal of Crystal Growth,* vol. 299, no. 1, pp. 227-233, 2007.

[5] N. Armour and S. Dost, "Diffusion limited silicon dissolution in germanium melt," *Journal of Physics: Conference Series,* vol. 327, no. 1, p. 012016, 2011.

[6] R. A. Swalin, "On the theory of self-diffusion in liquid metals," *Acta Metallurgica,* vol. 7, no. 11, pp. 736-740, 1959.

[7] J. Cahoon, "A modified “Hole” theory for solute impurity diffusion in liquid metals," *Metallurgical and Materials Transactions A,* vol. 28, no. 3, pp. 583-593, 1997.

[8] R. A. Swalin and V. G. Leak, "Diffusion of heterovalent solutes in liquid silver," *Acta Metallurgica,* vol. 13, no. 5, pp. 471-478, 1965.

[9] A. Bruson and M. Gerl, "Diffusion coeffecient of 113Sn, 124Sb, 110mAg, and 195Au in liquid Sn," *Physical Review B,* vol. 21, no. 12, pp. 5447-5454, 1980.

[10] W. Sutherland, "LXXV. A dynamical theory of diffusion for non-electrolytes and the molecular mass of albumin," *Philosophical Magazine Series 6,* vol. 9, no. 54, pp. 781-785, 1905.

[11] M. Klassen and J. R. Cahoon, "Interdiffusion of Sn and Pb in liquid Pb-Sn alloys," *Metallurgical and Materials Transactions A,* vol. 31A, no. 5, pp. 1343-1352, 2000.

[12] Y. Geng, C. Zhu and B. Zhang, "A sliding cell technique for diffusion measurements in liquid metals," *AIP Advances,* vol. 4, no. 3, p. 037102, 2014.

[13] G. Mathiak, A. Griesche, K. H. Kraatz and G. Frohberg, "Diffusion in liquid metals," *Journal of Non-Crystalline Solids,* vol. 205, pp. 412-416, 1996.

[14] A. Meyer, "Self-diffusion in liquid copper as seen by quasielastic neutron scattering," *Physical Review B,* vol. 81, no. 1, p. 012102, Jan 2010.

[15] N. Lee and J. R. Cahoon, "Interdiffusion of copper and iron in liquid aluminum," *Journal of Phase Equilibria and Diffusion,* vol. 32, no. 3, pp. 226-234, 2011.

[16] T. Itami, S. Munejiri, T. Masaki, H. Aoki, Y. Ishii, T. Kamiyama, Y. Senda, F. Shimojo and K. Hoshino, "Structure of liquid Sn over a wide temperature range from neutron scattering experiments and first-principles molecular dynamics simulation: A comparison to liquid Pb," *Physical Review B,* vol. 67, p. 064201, 2003.

[17] C. B. Porth and J. R. Cahoon, "Interdiffusion of Bi in Liquid Sn," *Journal of Phase Equilibria and Diffusion,* vol. 31, no. 2, pp. 149-156, 2010.

[18] J. -H. Lee, S. Liu, H. Miyahara and R. Trivedi, "Diffusion-coefficient measurements in liquid metallic alloys," *Metallurgical and Materials Transactions B,* vol. 35, no. 5, pp. 909-917, 2004.

[19] J. Horbach, S. K. Das, A. Griesche, M. Macht, G. Frohberg and A. Meyer, "Self-diffusion and interdiffusion in Al80Ni20 melts: Simulation and experiment," *Physical Review B,* vol. 75, no. 17, p. 174304, 5 2007.

[20] M. Asta, D. Morgan, J. J. Hoyt, B. Sadigh, J. D. Althoff, D. de Fontaine and S. M. Foiles, "Embedded-atom-method study of structural, thermodynamic, and atomic-transport properties of liquid Ni-Al alloys," *Physical Review B,* vol. 59, no. 22, pp. 14271--14281, Jun 1999.

[21] B. Zhang, A. Griesche and A. Meyer, "Diffusion in Al-Cu Melts Studied by Time-Resolved X-Ray Radiography," *Physical Review Letters,* vol. 104, no. 3, p. 035902, 2010.

[22] B. Zhang, A. Griesche and A. Meyer, "Relation between self diffusion and interdiffusion in Al-Cu melts," *diffusion-fundamentals.org,* vol. 11, no. 100, pp. 1-8, 2009.

[23] H. Cheng, Y. J. Lü and M. Chen, " Interdiffusion in liquid Al–Cu and Ni–Cu alloys," *The Journal of Chemical Physics*, vol. 131, no. 4, p. 044502, 2009.

[24] Y. Tanaka and M. Kajihara, "Evaluation of interdiffusion in liquid phase during reactive diffusion between Cu and Al," *Materials Transactions*, vol. 47, no. 10, pp. 2480-2488, 2006.

[25] Y. Tanaka and M. Kajihara, "Numerical analysis for migration of interface between liquid and solid phases during reactive diffusion in binary Cu-Al system," *Materials Science and Engineering A,* vol. 459, no. 1-2, pp. 101-110, 2007.

[26] T. Ejima, T. Yamamura, N. Uchida, Y. Matsuzaki and M. Nikaido, "Impurity Diffusion of Fourth Period Solutes (Fe, Co, Ni, Cu and Ga) and Homovalent Solutes (In and Tl) into Molten Aluminum," *Journal of the Japan Institute of Metals,* vol. 44, no. 3, pp. 316-323, 1980.

[27] J. Cai and Y. Y. Ye, "Simple analytical embedded-atom-potential model including a long-range force for fcc metals and their alloys," *Phys. Rev. B,* vol. 54, no. 12, pp. 8398-8410, Sep 1996.

[28] C. A. Becker, F. Tavazza, Z. T. Trautt and R. A. Buarque de Macedo, "Considerations for choosing and using force fields and interatomic potentials in materials science and engineering," *Current Opinion in Solid State and Materials Science,* vol. 17, no. 6, pp. 277 - 283, 2013.

[29] J. Brillo, A. Bytchkov, I. Egry, L. Hennet, G. Mathiak, I. Pozdnyakova, D. Price, D. Thiaudere and D. Zanghi, "Local structure in liquid binary Al-Cu and Al-Ni Alloys," *Journal of Non-Crystalline Solids,* vol. 352, pp. 4008-4012, 2006.

[30] V. Witusiewicz, U. Hecht, S. Frie and S. Rex, "The Ag–Al–Cu system: Part I: Reassessment of the constituent binaries on the basis of new experimental data," *Journal of Alloys and Compounds,* vol. 385, no. 1-2, pp. 133-143, December 2004.

[31] H. Flandorfer, M. Rechchach, A. Elmahfoudi, L. Bencze, A. Popovic and H. Ipser, "Enthalpies of mixing of liquid systems for lead free soldering: Al–Cu–Sn system," *The Journal of Chemical Thermodynamics,* vol. 43, no. 11, pp. 1612-1622, 2011.

[32] I. Ansara, A. Dinsdale, G. Effenberg and M. Rand, COST 507, Definition of Thermochemical and Thermophysical Properties to Provide a Database for the Development of New Light Alloys: Thermochemical database for light metal alloys, Luxembourg: Office for Official Publications of the European Communities, 1998, p. 396.

[33] W. D. Murray and F. Landis, "Numerical Machine Solutions of Transient Heat-Conduction Problems Involving Melting or Freezing," *Journal of Heat Transfer,* vol. 81, pp. 106-112, 1959.

[34] S. Kutluay, A. Bahadir and A. Ozdes, "The numerical solution of one-phase classical Stefan problem," *Journal of Computational and Applied Mathematics,* vol. 81, no. 1, pp. 135-144, 1997.

[35] B. Karlsson and L. Larsson, "Homogenization by two-phase diffusion," *Materials Science and Engineering,* vol. 20, pp. 161-170, 1975.

[36] A. Caro, D. A. Crowson and M. Caro, "Classical Many-Body Potential for Concentrated Alloys and the Inversion of Order in Iron-Chromium Alloys," *Phys. Rev. Lett.,* vol. 95, no. 7, p. 075702, 2005.

[37] S. Plimpton, "Fast Parallel Algorithms for Short-Range Molecular Dynamics," *Journal of Computational Physics,* vol. 117, no. 1, pp. 1-19, 1995.

[38] P. Shewmon, Diffusion in Solids, 2nd ed., Warrendale: The Minerals, Metals and Materials Society, 1989.

[39] W. Schirmacher, Theory of Liquids and Other Disordered Media: A Short Introduction, Heidelberg New York Dordrecht London: Springer International Publishing Switzerland, 2015, pp. 5-26.

[40] M. S. Shell, Thermodynamics and Statistical Mechanics: An Intergrated Approach, Cambridge: Cambridge University Press, 2015, pp. 375, 445-459.

[41] A. Einstein, Investigations on the Theory of the Brownian Movement, R. Furth, Ed., Mineola, NY: Dover Publications Inc., 1956, pp. 1-18.

[42] A. Bruson and M. Gerl, "Diffusion coefficient of 113Sn, 124Sb, 110mAg, and 195Au in liquid Sn," *Physical Review B,* vol. 21, no. 12, pp. 5447-5454, 1980.

[43] P. J. Scott and R. W. Smith, "Solute mass diffusion coefficient: Comparison of microgravity experiments with molecular dynamic simulation and Enskog hard sphere corrected estimates," *Journal of Applied Physics,* vol. 104, no. 4, p. 043706, 2008.

[44] D. Lazarus, "Effect of screening on solute diffusion in metals," *Physical Review,* vol. 93, no. 5, pp. 973-976, 1954.

[45] L. Claire and A. D., "On the theory of impurity diffusion in metals," *Philosophical Magazine,* vol. 7, no. 73, pp. 141-167, 1962.

[46] W. Hume-Rothery, "The Engle-Brewer Theory of Metals and Alloys," *Materials Science,* vol. 13, no. 5, pp. 231-264, 1967.

[47] J. R. Cahoon and O. D. Sherby, "The activation energy for lattice self-diffusion and the engel-brewer theory," *Metallurgical and Materials Transactions A,* vol. 23, no. 9, pp. 2491-2500, 1992.

[48] V. Burachynsky and J. R. Cahoon, "A theory for solute impurity diffusion, which considers engel-brewer valences, balancing the fermi energy levels of solvent," *Metallurgical and Materials Transactions A,* vol. 28, no. 3, pp. 563-582, 1997.

[49] B. J. Alder, W. E. Alley and J. H. Dymond, "Studies in molecular dynamics. XIV. Mass and size dependence of the binary diffusion coefficient," *Journal of Chemical Physics,* vol. 61, no. 4, pp. 1415-1420, 1974.

[50] L. S. Darken, "Diffusion, mobility and their interrelation through free energy in binary metallic systems.," *Trans. AIME,* vol. 175, no. 1, pp. 184-194, 1948.

[51] D. B. Boercker and E. L. Pollock, "Interdiffusion in binary ionic mixtures," *Physical Review A,* vol. 36, no. 4, pp. 1779-1785, August 1987.

[52] T. Haxhimali, R. E. Rudd, W. H. Cabot and F. R. Graziani, "Diffusivity in asymmetric Yukawa ionic mixtures in dense plasmas," *Pysical Review E,* vol. 90, no. 2, p. 023104, 2014.

[53] A. B. Bhatia and D. E. Thorton, "Structural aspects of the electrical resistivity of binary alloys," *Physical Review B,* vol. 2, no. 4, pp. 3004-3012, 15 October 1970.

[54] U. Dahlborg, M. Besser, M. Calvo-Dahlborg, S. Janssen, F. Juranyi, M. J. Kramer, J. R. Morris and D. J. Sordelet, "Diffusion of Cu in AlCu alloys of different composition by quasielastic neutron scattering," *Journal of Non-Crystalline Solids,* vol. 353, no. 32-40, pp. 3295-3299, 2007.

[55] B. Szpunar and R. W. Smith, "A molecular dynamics simulation of the diffusion of the solute (Au) and the self-diffusion of the solvent (Cu) in a very dilute liquid Cu–Au solution," *Journal of Physics: Condensed Matter,* vol. 22, no. 3, p. 035105, 2010.

[56] S. Y. Wang, M. J. Kramer, M. Xu, S. Wu, S. G. Hao, D. J. Sordelet, K. M. Ho and C. Z. Wang, "Experimental and ab initio molecular dynamics simulation studies of liquid Al60Cu40 alloy," *Physical Review B,* vol. 79, p. 144205, Apr 2009.

[57] U. Dahlborg, M. Besser, M. Kramer, J. Morris and M. Calvo-Dahlborg, "Atomic dynamics in molten AlCu alloys of different compositions and at different temperatures by cold neutron scattering," *Physica B,* vol. 412, pp. 50-60, March 2013.

[58] F. Kargl, H. Weis, T. Unruh and A. Meyer, "Self diffusion in liquid aluminium," in *Journal of Physics: Conference Series* , 2012.

[59] J. Brillo, S. M. Chathoth, M. M. Koza and A. Meyer, "Liquid Al80Cu20: Atomic diffusion and viscosity," *Applied Physics Letters,* vol. 93, no. 12, p. 121905, 2008.

[60] J. Roszmann, M. Sekhon and S. Dost, "Measurement of the diffusivity of CdTe in liquid Te at crystal growth temperatures," *Journal of Crystal Growth,* vol. 411, no. 1, pp. 30-33, 2015.

[61] E. Javierre, C. Vuik, F. Vermolen and S. v. d. Zwaag, "A comparison of numerical models for one-dimensional Stefan problems," *Journal of Computational and Applied Mathematics,* vol. 192, pp. 445-459, 2006.

[62] D. Turnbull, "The gram-atomic volumes of alloys of transition metals with Al and Si," *Acta Metallurgica Materialia,* vol. 38, no. 2, pp. 243-249, 1990.

[63] J. Brillo, I. Egry and J. Westphal, "Density and thermal expansion of liquid binary Al-Ag and Al-Cu alloys," *International Journal of Materials Research,* vol. 99, no. 2, pp. 162-167, 2008.

[64] D. Bates and D. Watts, Nonlinear Regression Analysis and Its Applications, New York: Wiley, 2007.

[65] P. R. Bevington and D. K. Robinson, Data Reduction and Error Analysis for the Physical Sciences, New York: McGraw-Hill, 2003, pp. 161-163.

[66] J. E. Morral, "Chemical diffusivities and their hidden concentraion units," *Journal of Phase Equilibria and Diffusion,* vol. 35, no. 5, pp. 581-586, 2014.

[67] J. L. Murray, Binary Alloy Phase Diagrams, vol. 1, T. B. Massaiski, Ed., Ohio: American Society for Metals, 1986.

[68] J. R. Davis, Ed., Copper and Copper Alloys, Materials Park, OH: ASM International, 2001, p. 447.

[69] D. A. Jones, Principles and Prevention of Corrosion - Second Edition, Upper Saddle River, NJ: Prentice Hall, 1996, p. 411.

[70] M. Mendelev, M. Kramer, C. Becker and M. Asta, "nalysis of semi-empirical interatomic potentials appropriate for simulation of crystalline and liquid Al and Cu," *Philosophical Magazine,* vol. 88, no. 12, pp. 1723-1750, 2008.

[71] K. Furukawa, B. R. Orton, J. Hamor and G. I. Williams, "The structure of liquid tin," *Philosophical Magazine,* vol. 8, no. 85, pp. 141-155, 1962.

[72] S. Hosokawa, J. Greif, F. Demmel and W.-C. Pilgrim, "Quasielastic lineshape of liquid Sn studied by inelastic X-ray scattering," *Chemical Physics,* vol. 292, pp. 253-261, 2003.

[73] N. Isono, P. M. Smith, D. Turnbull and M. J. Aziz, "Anomalous diffusion of Fe in liquid Al measured by the pulsed laser technique," *Metallurgical and Materials Transactions A,* vol. 27A, no. 3, pp. 725-730, 1996.

[74] P. Kubicek and T. Peprica, "Diffusion in molten metals and melts: application to diffusion in molten iron," *International Metals Reviews,* vol. 28, no. 3, pp. 131-157, 1983.

[75] J. R. Cahoon, "The first coordination number for liquid metals," *Canadian Journal of Physics,* vol. 82, pp. 291-301, 2004.

[76] S. Suzuki, K. Helmut, G. Frohberg, R. Rosu, W. Wendel and G. Muller-Vogt, "Preflight diffusion experiments on liquid metals under 1g conditions for the FOTON-M2 mission," *Ann. N.Y. Acad. Sci.,* vol. 1077, pp. 380-394, 2006.

[77] X. Zhu and R. W. Smith, "Impurity diffusion of gold in liquid lead," *Adv. Space Res.,* vol. 22, no. 8, pp. 1253-1256, 1998.

[78] M. S. Daw and M. I. Baskes, "Embedded-atom method: Derivation and application to impurities, surfaces, and other defects in metals," *Phys. Rev. B,* vol. 29, no. 12, pp. 6443-6453, Jun 1984.

[79] X. W. Zhou, R. A. Johnson and H. N. G. Wadley, "Misfit-energy-increasing dislocations in vapor-deposited CoFe/NiFe multilayers," *Phys. Rev. B,* vol. 69, no. 14, p. 144113, Apr 2004.

[80] X. W. Zhou, H. N. G. Wadley, R. A. Johnson, D. J. Larson, N. Tabat, A. Cerezo, A. K. Petford-Long, G. D. W. Smith, P. H. Clifton, R. L. Martens and T. F. Kelly, "Atomic scale structure of sputtered metal multilayers," *Acta Materialia,* vol. 49, no. 19, pp. 4005-4015, 14 11 2001.

[81] R. A. Johnson, "Alloy models with the embedded-atom," *Phys. Rev. B,* vol. 39, no. 17, pp. 12554-12559, Jun 1989.

[82] The National Institute of Standards and Technology (NIST), "Interatomic Potentials Repository Project," 27 7 2016. [Online]. Available: http://www.ctcms.nist.gov/potentials/. [Accessed 18 11 2016].

[83] A. Stukowski, B. Sadigh, P. Erhart and A. Caro, "Efficient implementation of the concentration-dependent embedded atom method for molecular-dynamics and Monte-Carlo simulations," *Modelling and Simulation in Materials Science and Engineering,* vol. 17, no. 7, p. 07005, 2009.

[84] G. J. Ackland and V. Vitek, "Many-body potentials and atomic-scale relaxations in noble-metal alloys," *Physical Review B,* vol. 41, no. 15, p. 10324, 1990.

[85] G. Bonny, R. Pasianot and L. Malerba, "Interatomic potentials for alloys: Fitting concentration dependent properties," *Philosophical Magazine,* vol. 89, no. 8, pp. 711-725, 2009.

[86] Sandia Corporation, "pair_style eam command — LAMMPS documentation," 2013. [Online]. Available: http://lammps.sandia.gov/doc/pair_eam.html. [Accessed 18 11 2016].

[87] W. Humphrey, A. Dalke and K. Schulten, "VMD: Visual molecular dynamics," *Journal of Molecular Graphics,* vol. 14, no. 1, pp. 33-38, 196.

[88] M. E. Tuckerman, Statistical Mechanics: Theory and Molecular Simulation, Oxford: Oxford University Press, 2010.

7. APPENDIX A – NONLINEAR REGRESSION ANALYSIS

The general nonlinear regression model [64] is given by

$$y = m(\boldsymbol{x}, \boldsymbol{a}) + \varepsilon \tag{A-109}$$

where $m(\boldsymbol{x}, \boldsymbol{a})$ is the mean function, $\boldsymbol{x}$ is the predictor with one or more components, $\boldsymbol{a}$ is the parameter vector with one or more components, and ε are assumed to be independent errors with variance w/σ^2. The weight w may be related to the experimental observation, while the variance σ^2 is generally unknown and estimated from the data. The estimate of the parameter vector $\boldsymbol{a}$ attempts to minimize the residual sum of squares

$$S(\boldsymbol{a}) = \sum w\big(y - m(\boldsymbol{a}, \boldsymbol{x})\big)^2. \tag{A-110}$$

The likelihood function for a nonlinear function with normally distributed errors is

$$L(\boldsymbol{a}, \sigma^2) = \prod \left(\frac{w}{\sigma\sqrt{2\pi}}\right) exp\left(-\frac{1}{2\sigma^2} S(\boldsymbol{a})\right) \tag{A-111}$$

where the product is over n observations, and is maximized at the minimum value of $S(\boldsymbol{a})$. For the residual vector $r(\boldsymbol{a}) = \sqrt{w}\big(y - m(\boldsymbol{a}, \boldsymbol{x})\big)$, the minimum of $S(\boldsymbol{a})$ is given by

$$\frac{\partial S(\boldsymbol{a})}{\partial \boldsymbol{a}} = -2 \sum r(\boldsymbol{a}) \frac{\partial m(\boldsymbol{a}, \boldsymbol{x})}{\partial \boldsymbol{a}}. \tag{A-112}$$

Linearizing Equation (A-112) gives

$$F_{i,j} = \frac{\partial m(\boldsymbol{a}, \boldsymbol{x}_i)}{\partial \boldsymbol{a}_j}. \tag{A-113}$$

with i and j index the observation and parameter vectors, respectively. The covariance matrix of the regression parameters is then given by

$$\hat{v}(\hat{\boldsymbol{a}}) = \hat{\sigma}^2 (\boldsymbol{F}^T \boldsymbol{F})^{-1}. \tag{A-114}$$

where the hat denotes the minimized value. The square roots of the diagonal elements of the covariance matrix are the minimized parameter error estimates. If the mean function $m(\boldsymbol{x}, \boldsymbol{a})$ does

not have an analytical solution, a finite difference approximation can be used to approximate the partial derivatives in Equation (A-113). The minimized value of the of the parameter vector $\widehat{\boldsymbol{a}}$ is determined using an algorithm that expands $S(\boldsymbol{a})$ about a local minimum by an increment of the parameter vector, and iteratively arrives at a solution [65].